ACCEPTED MANUSCRIPT

Journal of Rheology

This is the author's peer reviewed, accepted manuscript. However, the online version of record will be different from this version once it has been copyedited and typeset.
PLEASE CITE THIS ARTICLE AS DOI: 10.1122/8.0000280

Entangled linear polymers in fast shear flows: comparison of tube-model predictions and experimental data

Hamid Taghipour[1], Salvatore Costanzo[2,3], Dimitris Vlassopoulos[3,4], Evelyne van Ruymbeke[1], and Laurence G. D. Hawke[1,]*

[1]Bio-and Soft Matter, Institute of Condensed Matter and Nanosciences, Université catholique de Louvain, Croix du Sud 1, B-1348 Louvain-la-Neuve, Belgium.

[2]Department of Chemical, Materials and Industrial Production Engineering (DICMaPI), University of Naples, P.le Tecchio 80, 80125 Naples, Italy.

[3]Institute of Electronic Structure and Laser, FORTH, Heraklion 70013, Crete Greece

[4]Department of Materials Science & Technology, University of Crete, Heraklion 70013, Crete Greece

*Corresponding author: laurence.hawke@uclouvain.be.

Abstract

This work addresses the shear response of entangled linear polymers by assessing the current state-of-the-art model and proposing alternative directions. In particular, we examine the performance of the Graham-Likhtman-McLeish-Milner (GLaMM) nonlinear tube model in fast shear flows. Predictions are compared against experimental data for well-characterized, monodisperse, entangled linear polystyrene (PS) chains. Unlike previous works using the GLaMM model, finite extensibility (FENE) is accounted for. Comparison of model predictions

ACCEPTED MANUSCRIPT
Journal of Rheology
This is the author's peer reviewed, accepted manuscript. However, the online version of record will be different from this version once it has been copyedited and typeset.
PLEASE CITE THIS ARTICLE AS DOI: 10.1122/8.0000280

and data reveals an overall reasonable performance but also highlights limitations. For example, the predictions significantly depend on whether the contribution of contour length fluctuations (CLF) to the retraction rate is accounted for or not. This specific sensitivity of the model is enhanced as the Rouse Weissenberg number increases. Possible improvement of the model by modification of the existing mechanisms/model assumptions and/or by incorporation of overlooked mechanisms such as chain tumbling and CCR-driven disentanglement (CCR-D) is discussed. As a possible way to overcome the existing limitations, we propose an alternative approach based on the time marching algorithm (TMA) and focus at the description of the steady-state regime. Compared to the GLaMM model, this approach allows to keep track of the relaxation state of each entanglement segment in a simple way while ensuring consistency between chain stretch and constraint release mechanisms. Moreover, it accounts for CCR-D in an indirect manner. A key ingredient is the use of the recently advanced concept of shear blob and its dependence on shear rate. Our simple modification of TMA reproduces the experimental steady-state viscosities accurately for all samples and for all shear rates examined.

I. INTRODUCTION, BACKGROUND AND OBJECTIVES

The accurate prediction of both linear and nonlinear viscoelasticity of macromolecular fluids plays a significant role in many fields of science and engineering including polymer physics, rheology, and polymer processing. Today, "Tube-model Theory" is widely considered to be the standard predictive tool for the viscoelastic response of entangled polymer chains. In its original version, the seminal contribution of de Gennes [1], and critical improvements by Doi and Edwards (DE) [2], the model confines a linear polymer chain in a virtual tube, to represent the effects of entanglements, and allows chain reorientation by means of curvilinear diffusion along the tube which is fixed in space. This process is termed reptation and for monodisperse linear chains is described by a single relaxation time, the so-called reptation time, τ_d. Despite its inspirational influence to generations of researchers in the field, several predictions of the

ACCEPTED MANUSCRIPT
Journal of Rheology
This is the author's peer reviewed, accepted manuscript. However, the online version of record will be different from this version once it has been copyedited and typeset.
PLEASE CITE THIS ARTICLE AS DOI: 10.1122/8.0000280

DE model do not comply with experimental findings. To overcome limitations in linear viscoelasticity, refined versions of the model incorporate non-reptative reorientation mechanisms such as contour length fluctuations (CLF), and thermal constraint release (CR) (or dynamic tube dilution, DTD) [3, 4, 5, 6, 7]. Concerning nonlinear shear flows, whereas several discrepancies between DE model predictions and experimental data have been identified and remain by large debatable [8], the most important deficiency concerns the steady state flow. The flow curve, represented as a steady state shear stress (σ_{xy}^{st}) vs shear rate ($\dot{\gamma}$) plot, exhibits a maximum at $\dot{\gamma} = 1/\tau_d$, followed by excessive thinning (with a slope of about -1.5) at high Weissenberg numbers based on terminal time (Wi_d) [2]. This behavior suggests the occurrence of instabilities and is in sharp contrast with the majority of the available experimental data, which manifest a monotonically increasing behavior of stress versus rate [9, 10, 11]. It partially arises from the erroneous assumption of instantaneous chain retraction.

To circumvent this drawback, Pearson *et al*. [12] and later Mead *et al*. [13, 14] considered a finite retraction rate, associated with the inverse Rouse relaxation time ${\tau_R}^{-1}$, allowing for accumulation of stretch. The latter is defined by $\lambda = L(t)/L_0$ with $L(t)$ and L_0 being the current (at time *t*) and equilibrium contour lengths of the chain, respectively. However, although the inclusion of stretch improves the excessive thinning predictions at Wi_R>1, it does not remove the non-monotonic behavior of the shear stress in the intermediate flow regime $1/\tau_d < \dot{\gamma} < 1/\tau_R$ [12]. In a conceptual breakthrough, Marrucci [15] pinpointed that chain segments can renew their orientation at a rate faster than $1/\tau_d$ owing to the fact that they are convected by the flow. This reorientation process is known as convective constraint release (CCR) and can be thought of as the nonlinear counterpart of thermal CR. In his work, Marrucci [15] implemented CCR to the entire chain, whose reptation time speeded-up. In this empirical treatment, the CCR effect is localized at the chain ends. Although originally Marrucci did not combine CCR and stretch to investigate the performance of his dumbbell model quantitatively,

ACCEPTED MANUSCRIPT
Journal of Rheology
This is the author's peer reviewed, accepted manuscript. However, the online version of record will be different from this version once it has been copyedited and typeset.
PLEASE CITE THIS ARTICLE AS DOI: 10.1122/8.0000280

his work formed the basis of more sophisticated nonlinear tube-model theories as discussed below.

A first example is the work of Mead, Larson and Doi [16], the so-called MLD model, which considers the effects of both CCR and stretch on the dynamics of the primitive path. The latter is defined as a coarse-grained chain that has the same topology as the tube itself. Unlike Marrucci [15], Mead *et al*. implemented the CCR effect in a uniform manner along the primitive path. Furthermore, they included elements of CCR relaxation in both tube orientation and stretch. The transition from CCR relaxation of orientation to CCR relaxation of stretch was materialized semi-phenomenologically by means of the so-called switch function. The latter depends on stretch; at fast rates it prescribes stretch relaxation whereas at low and intermediate rates it favors orientation relaxation. With these modifications, the MLD model predicts three regimes in the flow curve [16]: At $\dot{\gamma} < 1/\tau_d$ the stress increases linearly with $\dot{\gamma}$. At intermediate shear rates, the stress exhibits a plateau or a very weak overshoot, depending on the ratio τ_d/τ_R. Finally, at fast shear rates ($\dot{\gamma} > 1/\tau_R$) it rises again. At a qualitative level, this behavior is consistent with experimental findings. The elimination of the profound σ_{xy}^{st} overshoot of the DE model is attributed to the combined effect of two factors. At intermediate rates, the increase of the S_{xy} component of the orientation tensor and at fast rates, the stretch, i.e., the effective increase of the tube length. Despite these promising features however, a comprehensive comparison of model predictions and data, especially in the transient regime, is lacking. Due to the fact that the original model is computationally demanding, subsequent works focused on evaluating the performance of a simplified (toy) version of the full model [10, 16, 17, 18]. At fast rates, the toy model underpredicts the experimental stress overshoot and overpredicts its steady-state value [10, 19].

Apart from quantitative disagreement with data at large shear rates, another shortcoming of the MLD model is the lack of an explicit microscopic description of CCR. The first work to

ACCEPTED MANUSCRIPT
Journal of Rheology
This is the author's peer reviewed, accepted manuscript. However, the online version of record will be different from this version once it has been copyedited and typeset.
PLEASE CITE THIS ARTICLE AS DOI: 10.1122/8.0000280

address this challenge was that of Milner *et al*. [20], where the microscopic description of CCR is based on the conjecture that, like in CR, the primitive chain undertakes local hops of order a, the tube confinement length, thereby renewing its orientation locally. Apart from the usual three parameters used in linear viscoelastic (LVE) predictions, namely the entanglement molecular weight, M_e, the entanglement relaxation time, τ_e, and the entanglement plateau modulus, G_e, the model of Milner, McLeish and Likhtman (MML) contains a fourth parameter, namely c_ν, which controls the strength of the CCR effect. A c_ν value greater than 0.06 was found to be sufficient to remove the shear stress maximum in the intermediate flow regime where CCR acts (with $c_\nu = 0.1$ being the optimum value). Despite its aforementioned success in the intermediate flow regime, the MML model does not apply to the fast flow regime because undermines the role of stretch (it considers an instantaneous retraction rate).

It should be noted that in the MLD and MML models, as well as in the GLaMM model which is discussed below, CCR is thought to affect chain orientation and stretch only. It does not influence the confinement length (tube diameter) which is assumed to be constant. In other words, despite the local configuration renewal of the chains via CCR relaxation of orientation and/or stretch, the effective entanglement density of the system in question is always preserved. As detailed below, this assumption contradicts the more recent works [21, 22, 23, 24, 25, 26, 27, 28, 29] where CCR is thought to release some entanglement constraints at fast flow rates.

In a revised version of the MML, known as GLaMM model, Graham *et al*. [30] maintained the aforementioned treatment of CCR and additionally implemented a finite retraction rate to account for tube stretch. From a qualitative standpoint, the GLaMM and MLD predictions share similar characteristics, i.e., the steady-state flow curve exhibits the aforementioned three distinct regimes. Quantitatively, the GLaMM model has been assessed thoroughly [30] and compared against systematic experiments [31]. In the former case, the number of entanglements, Z, of the investigated samples, ranged from 8 to 31. The Rouse-Weissenberg

ACCEPTED MANUSCRIPT
Journal of Rheology
This is the author's peer reviewed, accepted manuscript. However, the online version of record will be different from this version once it has been copyedited and typeset.
PLEASE CITE THIS ARTICLE AS DOI: 10.1122/8.0000280

number Wi_R at the fastest rate typically ranged from 6 to 45, though a single measurement apparently achieved $Wi_R = 92$. The model appeared to perform satisfactorily at low and intermediate rates. However, in some cases, as for example the two PS solutions investigated in Ref. [10] too, no firm conclusion can be drawn about the nonlinear predictions due to the overestimation of the LVE response. Focusing on fast rates only, especially for $Wi_R > 15$, the model exhibited some systematic disagreement: it moderately overpredicted the stress maximum as well as the broadness and size of the stress overshoot (hereafter, the term overshoot size/magnitude is referred to as the ratio of peak to steady-state viscosity). It should be mentioned that the aforementioned conclusions are drawn based on $c_\nu = 0.1$ and $R_s = 2$, where R_s is the order one prefactor arising from the decoupling approximation in the model's retraction term [30].

Auhl *et al*. [31] compared GLaMM predictions (using $c_\nu = 0.1, R_s = 2$) with experimental data on six, monodisperse, polyisoprene (PI) melts. Z ranged from 0.5 to 47 while Wi_R ranged from 4 to 22. The comparison revealed that the model performed rather poorly for the three marginally entangled PI samples, whereas conclusions similar to the one of Ref. [30] were drawn for the well-entangled samples at fast shear rates. As is typically the case in measurements, the experimental rates studied in both Refs. [30] and [31] are below $1/\tau_e$, meaning that the fundamental assumption of a constant tube diameter is unaffected from this perspective. Recently, GLaMM shear viscosity predictions at fast shear rates were compared against non-equilibrium molecular dynamics (NEMD) results of Kremer–Grest (KG) chains [32]. Compared to GLaMM predictions, the simulation results exhibited a smoother behavior near the viscosity maxima but overall slightly larger overshoots. The disagreement between the two methods was attributed to the fact that, unlike simulations, the model is insensitive to possible changes in the friction coefficient due to flow. Another possible explanation for the disagreement was proposed to be the inhomogeneities in the entanglement density along the

ACCEPTED MANUSCRIPT
Journal of Rheology
This is the author's peer reviewed, accepted manuscript. However, the online version of record will be different from this version once it has been copyedited and typeset.
PLEASE CITE THIS ARTICLE AS DOI: 10.1122/8.0000280

chain contour. Such inhomogeneities call into question the GLaMM assumption of a constant tube diameter [30].

It is worth emphasizing that tube model predictions are extremely sensitive to changes in the tube properties upon deformation in response to stretch, as pointed out by Read [33]. Such properties are, for example, the tube diameter, the CCR hop length, and the persistence length of the tube, with the latter being the distance along the tube contour beyond which the orientation correlation due to a CCR hop decays.

Unlike the above "classical" tube models, more advanced simulation methods can directly address the question of whether tube properties change with flow or not. This is because they track the spatial correlation between the chains. Concerning the possibility of tube diameter changes, the primitive chain network (PCN) simulation results of Yaoita *et al*. [34] support the idea that entanglement density becomes inhomogeneous at large shear rates. The NEMD atomistic simulations of Baig *et al.* [21] on monodisperse linear PE chains lend support to the same notion as well. Specifically, Baig *et al.* investigated the conformational and topological properties of moderately entangled $C_{400}H_{802}$ chains over a broad range of Wi_R values and reported that shear induces disentanglement, the onset of which occurs at relatively small rates ($Wi_R > 2$). The level of disentanglement increased as the shear rate increased, with rates in the $Wi_R \gtrsim 10$ range causing the most significant impact. Similar findings were reported in the more recent NEMD studies of Nafar Sefiddashti *et al*. [26] on the same system as well as for longer chains, i.e., $C_{700}H_{1402}$ and $C_{1000}H_{2002}$ [29]. Moderate disentanglement in the $\tau_d{}^{-1} < \dot{\gamma} < \tau_R{}^{-1}$ regime was also reported in the PCN simulations of Masubuchi and Watanabe [35]. Importantly, the viscosity (stress) overshoot in this intermediate flow regime was solely attributed to orientation dynamics. The discrete slip-link model of Andreev *et al.* [23] also implies that, at fast shear flow, CCR events cause strong disentanglement of the chains. There, disentanglement is more important than finite extensibility (FENE) and/or chain ends

ACCEPTED MANUSCRIPT
Journal of Rheology
This is the author's peer reviewed, accepted manuscript. However, the online version of record will be different from this version once it has been copyedited and typeset.
PLEASE CITE THIS ARTICLE AS DOI: 10.1122/8.0000280

stretching in determining the overshoot size and thus the viscosity steady state. Note that early ideas of flow-induced disentanglement can be traced by to the work of Graessley [36].

Stimulated by such evidence, Ianniruberto and Marrucci [22], implemented a CCR-driven disentanglement process in an integro-differential version of the tube model for linear chains. Note that in the literature, CCR events that eventually lead to disentanglement are commonly referred to as flow-induced disentanglement (FID), entanglement dynamics (ED) or entanglement kinetics. As the key underlying mechanism of entanglement loss is CCR we have chosen not to use such terms. Therefore, hereafter, CCR-driven disentanglement will be referred to as CCR-D for the sake of simplicity. With the aforementioned modification, the model of Ianniruberto and Marrucci predicts that time-strain separability becomes valid at a time considerably longer than the expected Rouse time, in qualitative accordance with stress relaxation measurements following large step strains [22]. This behavior is due to disentanglement/re-entanglement kinetics; the amount as well as the time evolution of disentanglement depends on the applied strain therefore time-strain separability is reached at times of the order of the equilibrium reptation time when the equilibrium entanglement network is restored. Implementations of CCR-D in the tube model framework are also found in Ref. [24], where a multimode variant of the pom-pom model is utilized to enable viscosity overshoots at uniaxial elongation, and in Ref. [27] where a Rolie-Poly (RP) variant is used in the context of 3D printing modelling of linear chains. Nevertheless, this RP version overlooks FENE. Along with an advanced treatment of the coupling between CCR and stretch in the context of polydisperse melts, FENE has been implemented in the RP version of Boudara *et al*. [37]. The significance of entanglement loss has been also recognized by Mead and coworkers [25, 38] in revised versions of the toy MLD model.

Apart from CCR-D, another important mechanism for fast flows appears to be chain tumbling, whereby chains experience periods of high extension followed by short excursions

ACCEPTED MANUSCRIPT
Journal of Rheology
This is the author's peer reviewed, accepted manuscript. However, the online version of record will be different from this version once it has been copyedited and typeset.
PLEASE CITE THIS ARTICLE AS DOI: 10.1122/8.0000280

of rapid rotation (resembling a yo-yo type of response). This mechanism was noticed in the NEMD simulations of Kim *et al*. [39] for barely entangled $C_{78}H_{158}$ polyethylene chains. For large shear rates, the distribution of the end-to-end vector, R, departed from its Gaussian behavior and became bimodal, with the low-R peak reflecting collapsed chain configurations and the high-R peak signifying enhanced extension. Similar findings were reported in the NEMD simulation study of Baig *et al.* [21] on the moderately entangled $C_{400}H_{802}$ melt. Note that tumbling was the dominant mechanism at rates at which severe disentanglement occurred, implying that tumbling is promoted in a disentangled state. The tumbling dynamics of this particular system ($C_{400}H_{802}$) was elucidated further by Nafar Sefiddashti *et al.* [26], who monitored the motions of individual polymer chains by means of NEMD simulations. The tumbling dynamics of individual chains has also been experimentally reported by direct visualization of the motions of fluorescently labeled DNA chains in both dilute and concentrated solutions undergoing shear [40, 41, 42, 43].

Recently, Costanzo *et al.* [44] implemented tumbling in the tube model using a semi-phenomenological approach inspired by the molecular dynamics simulations of Sefiddashi and Khomami [26]. To account for the rapid alternation between stretched and collapsed chain configurations, they introduced a damped oscillatory function in the differential equation for the stretch evolution. Regarding the orientation evolution equation, the authors employed a history integral formulation similar to previous works of Ianniruberto and Marrucci [45, 46] as well as the toy MLD model [10, 16]. Other ingredients of the model are FENE, friction reduction due to alignment, which is relevant for extensional flows [47] and CCR, which is viewed as a mechanism that speeds-up orientation and stretch relaxation times while preserving the entanglement density. In the absence of tumbling, this model fails when $Wi_R \gg 1$. In particular, the predicted peak and steady viscosities are largely overestimated, in contrast to other tube models. Moreover, this version of the model does not provide undershoots. With

ACCEPTED MANUSCRIPT
Journal of Rheology
This is the author's peer reviewed, accepted manuscript. However, the online version of record will be different from this version once it has been copyedited and typeset.
PLEASE CITE THIS ARTICLE AS DOI: 10.1122/8.0000280

tumbling included, the aforementioned deficiencies disappear and the model reproduces adequately the vast majority of the experimental features, including viscosity undershoots at large shear rates. Therefore, that work demonstrates the importance of tumbling in fast shear flow, especially in relation to viscosity undershoots. It also implies that chain tumbling is essential for capturing the overshoots and steady states at $Wi_R \gg 1$. Arguably however, the model overpredicts the polymer stress, likely due to an overlook of CCR-D, an effect which is counterbalanced by considering a strong influence of chain tumbling in the steady regime. The recent work of Masubuchi, Ianniruberto, and Marrucci [28], where the same PS data are modelled by means of PCN simulations rather than the tube variant of Ref. [44], supports this speculation: While tumbling is observed in the simulations and contributes to both segmental orientation and stress undershoot, it does not appear to influence the stress overshoot and steady state so severely as in Ref. [44]. Moreover, while Ref. [44] suggests that chain tumbling has a dominant impact in the entire $Wi_R > 1$ regime, NEMD and PCN simulations [21, 26, 28, 29] imply that tumbling dominates at larger Wi_R values, i.e. $Wi_R > 10$, where significant chain disentanglement also occurs.

Another modeling work linking tumbling to transient undershoots in fast shear is that of Stephanou *et al.* [48]. The complete tumbling-snake model of Curtiss and Bird (CB) [49] was solved by means of Brownian dynamics simulations. Model predictions were compared against transient shear data on concentrated PS and DNA solutions. The model was able to adequately quantify the data, including the undershoot at large shear rates. Central to the model's success in predicting stress undershoot is a rotational Brownian contribution in the governing Fokker-Planck (diffusion) equation for the chain configuration. Apart from curvilinear modes (reptation), this contribution features reorientational motions that are perpendicular to the tube axis, in a manner that resembles constraint release events [50].

ACCEPTED MANUSCRIPT
Journal of Rheology
This is the author's peer reviewed, accepted manuscript. However, the online version of record will be different from this version once it has been copyedited and typeset.
PLEASE CITE THIS ARTICLE AS DOI: 10.1122/8.0000280

In a recent contribution, Nafar Sefiddashti *et al.* [29] extended their NEMD studies to longer chains, a $C_{1000}H_{2002}$ PE melt ($Z \approx 13$). The NEMD data analysis indicates that, as a direct consequence of entanglement loss, the viscosity overshoot is determined by the tube orientation, i.e., S_{xy}, rather than the tube stretch, λ, over a wide range of flow rates (including the $Wi_R > 1$ regime). The viscosity undershoot is also governed by S_{xy} due to the reduction in entanglement density (CCR-D) and the subsequent enhancement of chain tumbling events. The onset of CCR-D and chain tumbling occurs in the ${\tau_d}^{-1} < \dot{\gamma} < {\tau_R}^{-1}$ regime, however, these molecular mechanisms have a more drastic impact within ${\tau_R}^{-1} < \dot{\gamma} < {\tau_e}^{-1}$. Concerning the overshoot origin, similar results have been reported in the molecular dynamics simulation study of Ref. [51].

A different approach was proposed recently by Xie and Schweizer [52] who implemented in the tube model framework the concept of a deformation-induced "grip force", first advanced by Wang *et al.* [53]. This force has an interchain topological entanglement origin and provides the microscopic source of affine deformation (stretching). In this molecular scenario chain retraction and in turn CCR are temporarily quenched until the (elastic) retraction force exceeds the magnitude of the grip force. When $Wi_R > 1$, this force imbalance typically occurs beyond the stress overshoot [52]. In this respect, chain retraction and CCR become effective beyond the overshoot. Compared to traditional tube models, the relevant timescale for chain retraction and CCR relaxation is that of an effective stretch relaxation time rather than the bare Rouse time of the chain, with the former being faster. Moreover, it decreases in a shear rate-dependent manner. This alternative description of retraction and CCR appears to overperform the classic tube models with respect to steady-state shear stress predictions as well as peak strain (γ_{max}) predictions [52]. Note that the model does not consider CCR-D. Also, it does predict stress undershoot, however its molecular origin is unclear and certainly does not relate to chain tumbling but presumably to the delayed onset of CCR [52]. A delayed retraction process is also

ACCEPTED MANUSCRIPT
Journal of Rheology
This is the author's peer reviewed, accepted manuscript. However, the online version of record will be different from this version once it has been copyedited and typeset.
PLEASE CITE THIS ARTICLE AS DOI: 10.1122/8.0000280

reported in simulation studies of highly elongated melts of linear chains, and it is attributed to long-lived clustering of entanglement points that leads to a metastable inhomogeneous melt [54, 55, 56].

From the above, it becomes apparent that to advance the state-of-the-art in terms of understanding the physics of transient shear response and achieving quantitative predictions in the (Z, Wi_R) parameter range, the various emerging theoretical approaches and concepts should be confronted with reliable experimental data. It is generally accepted that obtaining accurate nonlinear shear measurements at large Z and Wi_R values is a challenging task. This is because measurements at large shear rates are known to be very sensitive to artifacts, for example wall slip, possibly shear banding and edge fracture [31, 57]. Recently, significant progress in measuring the nonlinear startup shear of entangled fluids has been reported [58, 59]. Using a home-made cone-partitioned-plate (CPP) fixture for the ARES rheometer, we have generated a large set of data on model polymer melts and solutions [44, 58, 60], which we shall use as reference for further developments in molecular modeling.

The objective of our work is to thoroughly reassess the performance of the GLaMM model in light of this detailed experimental information. This model is selected for several reasons. First, it considers the dependence of orientation and stretch on the tube coordinate. Second, it provides a microscopic description of CCR and chain retraction at the level of the tube diameter, unlike other nonlinear tube models. Third, it accounts for FENE and in this respect its predictions can be compared against those of the Ianniruberto-Marrucci model [44]. Furthermore, the GLaMM model assumes that the tube diameter is independent of the shear rate and all CCR events are thought to contribute to orientation and stretch relaxation but not to entanglement loss. In this respect, comparison of model predictions against experimental data covering a broad Wi_R range can indirectly reveal the flow strength at which CCR-driven disentanglement becomes important.

ACCEPTED MANUSCRIPT
Journal of Rheology
This is the author's peer reviewed, accepted manuscript. However, the online version of record will be different from this version once it has been copyedited and typeset.
PLEASE CITE THIS ARTICLE AS DOI: 10.1122/8.0000280

A second objective of this work, is to develop an alternative nonlinear tube model, with reduced mathematical complexity and numerical cost compared to the GLaMM and MLD models. Such a model should preserve the dependence of orientation and stretch on the tube coordinate and the coupling between stretch and CCR, while it accounts for CCR-D. It is an extension of the TMA, the time marching algorithm [6], which successfully describes the linear rheology of entangled chains [61, 62, 63, 64]. As a first step towards the development of a model that is applicable to the entire transient regime, the current nonlinear TMA version will focus on steady state conditions only.

The remaining of the article is organized as follows: Section II reports the molecular characteristics of the investigated PS samples as well as the linear rheological parameterization, as inferred by the TMA. Section III recounts the basic features of the GLaMM model. It also presents comparisons of model predictions and data. Section IV presents the modified TMA model and assesses its performance with respect to the measured steady-state viscosities. Section V summarizes the main findings of this work. The supplementary material provides additional figures and analysis that strengthen the results and discussion presented in the main sections of the article.

II. MATERIALS AND LINEAR VISCOELASTIC CHARACTERIZATION

We examine in detail the rheological data obtained with four PS melts and solutions, which are reported in Ref. [44]. Here we recount the molecular characteristics of the samples and present the linear viscoelastic parametrization that will be used subsequently in the assessment of the nonlinear models. The two PS melts are coded as PS1 and PS2, having weight-average molar masses M_w = 133 and 185 kg/mol, respectively. The two PS solutions are referred to as PS3 and PS4, respectively. In these samples, long chains with M_w = 285 kg/mol are embedded in a matrix of unentangled chains (2 kg/mol), which acts as an ideal solvent. The volume

ACCEPTED MANUSCRIPT
Journal of Rheology
This is the author's peer reviewed, accepted manuscript. However, the online version of record will be different from this version once it has been copyedited and typeset.
PLEASE CITE THIS ARTICLE AS DOI: 10.1122/8.0000280

fraction (also mass fraction here), φ, of the long chains is 0.47 and 0.65, respectively. All four samples have very narrow polydispersity, PD < 1.1. The choice of reference temperature was such that both the terminal flow and the rubbery plateau regime of the linear data could be observed. Linear and nonlinear viscoelastic properties of the two solutions are reported at 140°C and 150°C, respectively, while a reference temperature of 160°C has been used for the melts [39].

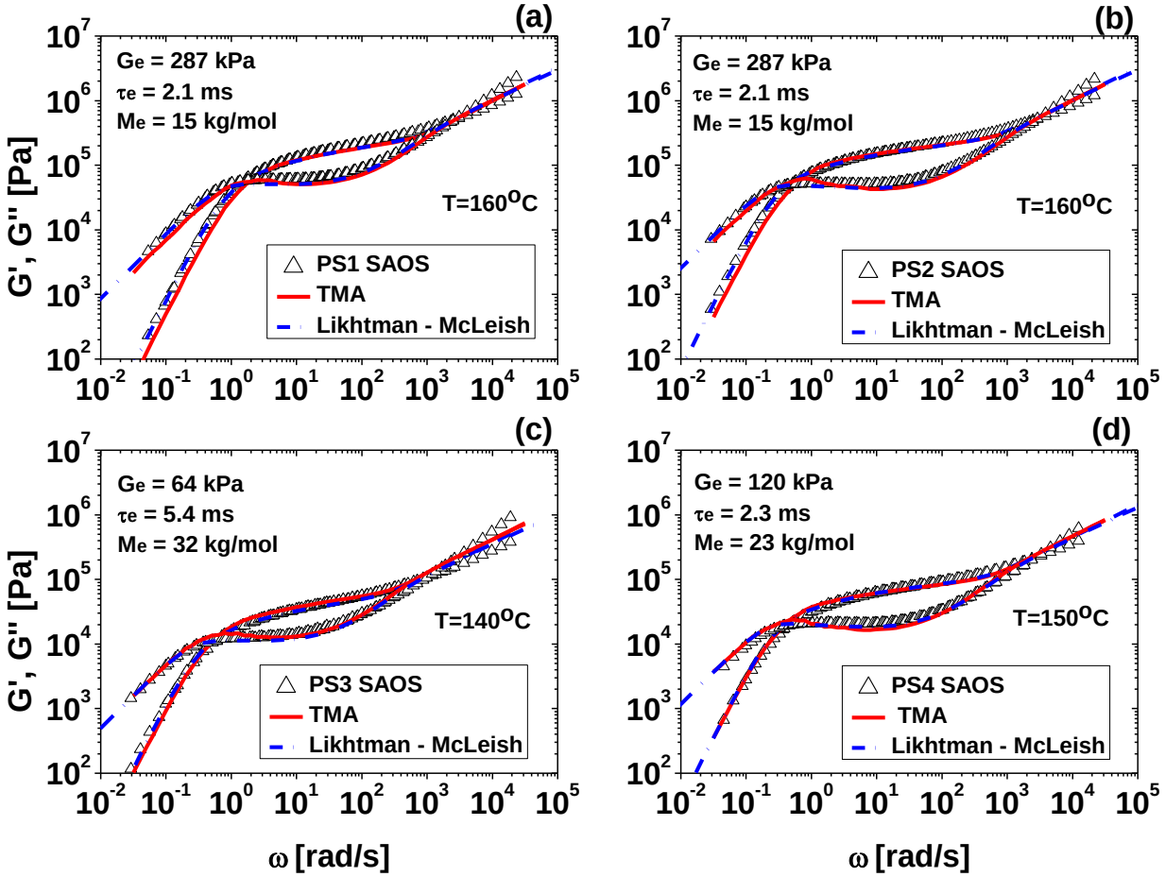

FIG. 1. Experimental and theoretical SAOS response of the PS samples (symbols and lines, respectively). T_{ref} = 160 °C, for the PS1 and PS2 melts. For the PS3 and PS4 solutions T_{ref} =140 °C and T_{ref} = 150 °C, respectively. In these two solutions, the volume fraction, φ, of polymer chains is 0.47 and 0.65, respectively. Solid lines refer to the TMA while dash-dotted lines refer to the Likhtman – McLeish (LM) theory [4]. For both models the parameterization is the same

ACCEPTED MANUSCRIPT
Journal of Rheology
This is the author's peer reviewed, accepted manuscript. However, the online version of record will be different from this version once it has been copyedited and typeset.
PLEASE CITE THIS ARTICLE AS DOI: 10.1122/8.0000280

and it is reported in panels (a) – (d) as well as in Table I. In addition, $c_v = 0.1$ for the LM theory [4]. The experimental data were first reported in Ref. [44].

Figure 1 depicts the linear viscoelastic response of all PS samples as measured by small amplitude oscillatory shear (SAOS). The solid lines are TMA predictions. The TMA requires three parameters, namely G_N^0 and M_e, and τ_e. The parameterization used is reported in panels (a) – (d) of Fig. 1 as well as in Table I. It is also discussed below. As readily seen from Fig. 1, the model reproduces the experimental data satisfactorily. Expected discrepancies are noted in the high-frequency regime ($\omega > 1/\tau_e$) but we do not discuss this further in the present study. Limitations of tube models in this regime are discussed in Ref. [65]. For the polymer melts, G_N^0 and M_e are fixed to 230 kPa and 15 kg/mol, respectively, in agreement with our previous works [66, 67]. For the solutions, the G_N^0 and M_e values correspond to those expected from the well-known scaling laws for dilution exponent of unity [66, 68] : $G_{N,sol}^0 = G_{N,melt}^0 \varphi^2$ and $M_{e,sol} = M_{e,melt}/\varphi$, with φ being the volume fraction of the polymer chains. Table I also reports the 'equilibrium' plateau moduli values at $t = \tau_e$, i.e., G_e. As discussed by Likhtman and McLeish [4], G_e and G_N^0 are related through $G_e = (5/4)G_N^0$. The physical explanation behind this relation is that a $1/5$ fraction of the initial stress at $t = \tau_e$ relaxes by fast longitudinal Rouse modes within the tube up to timescales of order τ_R [4]. Concerning the τ_e values, $\tau_e = 2.1X10^{-3}$ s for the PS1 and PS2 melts. As regards the PS3 and PS4 solutions, $\tau_e = 5.4X10^{-3}$ s and $\tau_e = 2.3X10^{-3}$ s, respectively. These τ_e values are slightly different from those expected from the $\tau_{e,sol} = \tau_{e,melt}/\varphi^2$ scaling law, which applies under *iso-*T_g conditions [66]. Since the data are not presented at such conditions the discrepancies from the aforementioned scaling law are justifiable.

The Likhtman – McLeish (LM) theory [4] contains the same parameters (G_e, M_e, τ_e, and c_v) as the GLaMM model. Thus, one can argue that it is a more natural choice to parameterize the

ACCEPTED MANUSCRIPT
Journal of Rheology
This is the author's peer reviewed, accepted manuscript. However, the online version of record will be different from this version once it has been copyedited and typeset.
PLEASE CITE THIS ARTICLE AS DOI: 10.1122/8.0000280

four PS samples. Using the open source Reptate rheology tool [69], it has been verified that the LM and TMA theories give very similar predictions for the same G_e, M_e, τ_e parameterization and $c_v = 0.1$. This result can be readily appreciated in Fig. 1 where LM predictions are included by dash-dotted lines.

For completeness, we note that analytical expressions for G' and G''exist in literature also [70]. Although they include the possibility of flow-induced alignment of chain ends, they disregard a detailed treatment of CR and CLF, unlike the TMA and LM approaches which have been preferred in this work for this reason. It is well known that, for monodisperse linear chains, the influence of CR and CLF increases with decreasing molecular weight [4]. Since the molecular weights examined in this work are relatively low, we anticipate flow-induced alignment of chain ends to be negligible. When studying more entangled systems, the alignment of chain ends might be important as CR and CLF are less effective in renewing orientation. In such a situation, the analytical equations of Ref. [70] could provide a means to quantify the degree of chain ends alignment and guide the boundary conditions for the GLaMM model. As will be discussed in more detail in Section III, chain ends are typically considered randomly orientated in the GLaMM model.

According to the TMA characterization, chains in the PS1 and PS3 samples are about nine entanglements long ($Z \simeq 9$) while in the PS2 and PS4 samples they are about twelve entanglements long ($Z \simeq 12$). In Table I, τ_d and $\tau_{d,CLF}$ are obtained according to $\tau_d = 3\tau_e Z^3$ and $\tau_{d,CLF} = 3\tau_e Z^3\left(1 - 3.38/\sqrt{Z} + 4.17/Z - 1.55/Z^{1.5}\right)$, respectively. The latter expression includes the CLF contribution in an approximate manner [4, 27]. While this is not used in the TMA model, which incorporates a detailed CLF treatment, it is involved in the estimation of the Wi_d numbers quoted in Tables II and AI. The respective Wi_R numbers are obtained based on the Rouse relaxation times $\tau_R = \tau_e Z^2$ (Table I). Table II refers to the fastest experimental shear rates achieved in Ref. [44] while Table S1 of the supplementary material

ACCEPTED MANUSCRIPT
Journal of Rheology
This is the author's peer reviewed, accepted manuscript. However, the online version of record will be different from this version once it has been copyedited and typeset.
PLEASE CITE THIS ARTICLE AS DOI: 10.1122/8.0000280

refers to all rates. In both Tables, $Wi_e(=\dot{\gamma}\tau_e)$ numbers are shown as well. Herein, rates for which $Wi_d < 1$ are referred to as slow and rates for which $Wi_d > 1$ and $Wi_R < 1$ as intermediate. For $1 < Wi_R < 10$ we have moderately fast and for $Wi_R > 10$ very fast rates.

Table I. Linear viscoelastic parameterization of the PS samples investigated [#]

Definition of TMA material parameters. Units are shown in brackets.
G_N^0: Entanglement plateau modulus. Units: [Pa]. M_e: Entanglement molecular weight. [g/mol].
τ_e: Entanglement relaxation time (relaxation time of a tube segment). [s].
In the TMA the aforementioned three material parameters are required only. The values of the remaining variables (except temperature) listed below are outcomes based on those three parameters. Note that these parameters are not arbitrary in the sense that, especially for monodisperse entangled linear chains, the range of their values is limited by the SAOS data, i.e. G_N^0 and M_e are correlated to the experimental plateau value of $G'(\omega)$ while τ_e is correlated to the high ω cross over point of $G'(\omega)$ and $G''(\omega)$.

Sample/ parameter	PS1	PS2	PS3	PS4
T [°C]	160	160	140	150
M_e $[\frac{kg}{mol}]$, Z	15, 8.9	15, 12.3	31.9, 8.9	23.1, 12.4
G_N^0 [Pa]	$2.3X10^5$	$2.3X10^5$	$0.51X10^5$	$0.97X10^5$
G_e [Pa]	$2.875X10^5$	$2.875X10^5$	$0.64X10^5$	$1.2X10^5$
τ_e [s]	0.0021	0.0021	0.0054	0.0023
τ_R [s]	0.17	0.32	0.44	0.35
τ_d [s]	4.59	11.72	11.80	12.84
$\tau_{d,CLF}$ [s]	1.21	4.02	3.21	4.42
φ	1.0	1.0	0.47	0.65

[#] For PS, $c_\infty = 9.6$ and $M_0 = 104.1$ [g/mol].

Table II. Fastest experimental shear rates and respective Weissenberg numbers.

ACCEPTED MANUSCRIPT
Journal of Rheology
This is the author's peer reviewed, accepted manuscript. However, the online version of record will be different from this version once it has been copyedited and typeset.
PLEASE CITE THIS ARTICLE AS DOI: 10.1122/8.0000280

Sample/ Parameter	PS1	PS2	PS3	PS4
$\dot{\gamma}$ [s^{-1}]	31.6	31.6	100	100
Wi_d	38.4	127	320.7	442.6
Wi_R	5.4	10	43.74	34.79
Wi_e	0.066	0.066	0.171	0.230

III. GLaMM MODEL ASSESSMENT

A. Mathematical formulation, assumptions, and parameters of the GLaMM model.

The complete mathematical formulation of the model is presented in Table III. The same table defines all the model variables. The model is formulated in terms of a time evolution equation for the (dimensionless) tube tangent correlation function, $\boldsymbol{f}(s,s',t) = \boldsymbol{f} = \langle \boldsymbol{R}'(s,t)\boldsymbol{R}'(s',t)\rangle/\alpha^2$, where α is the tube diameter. $\boldsymbol{f}$ is a second rank tensor. The model counts segments of size M_e along a chain that is enclosed in a tube comprising $Z = M/M_e$ entanglements. Therefore, s runs from 0 to Z. $\boldsymbol{R}(s,t)$ denotes the position vector of a chain segment s at time t, with $\boldsymbol{R}'(s,t) = \partial \boldsymbol{R}(s,t)/\partial s$ being its derivate with respect to contour position s. Physically $\boldsymbol{R}'(s,t)$ represents the tangent vector to the $\boldsymbol{R}(s,t)$ curve at segment s at time t. This tangent vector has length α. It must be emphasized that $\boldsymbol{f}$ carries information for both the orientation and stretch state of the tube segments, not only for the orientation state. As readily seen in Eq. (1) of Table III, the evolution equation comprises terms representing the dynamics of reptation, CLF, CR (both thermal and convective), chain stretch, and chain retraction down to the length scale of the tube diameter. Note that Eqs. (1a) and (11) incorporate FENE. Eq. (1) is not derived in this work. It is presented in the Reptate software (https://reptate.readthedocs.io/) [69]. The original GLaMM formulation is recovered when $\lambda_{max} \to \infty$ as $F(\lambda_s) = \lambda_s$. The stress is given by Eq. (1). The stress contribution of high

ACCEPTED MANUSCRIPT
Journal of Rheology
This is the author's peer reviewed, accepted manuscript. However, the online version of record will be different from this version once it has been copyedited and typeset.
PLEASE CITE THIS ARTICLE AS DOI: 10.1122/8.0000280

frequency Rouse modes is disregarded as it affects the very early time response of the model that is not of interest in this study. This contribution is also omitted in the open source GLAMM code developed by R. S. Graham. The code is available on Github (https://github.com/RichGraham/GLaMM_model).

Table III. Mathematical formulation of the GLaMM model

Evolution equation of the (dimensionless) tube tangent correlation function $\boldsymbol{f}(s,s',t)=\boldsymbol{f}(s,s')=\boldsymbol{f}$.

$$\frac{d\boldsymbol{f}}{dt}=\underbrace{\frac{d\boldsymbol{f}_{\text{flow}}}{dt}}_{\text{flow}}+\underbrace{\frac{d\boldsymbol{f}_{\text{rept-CLF}}}{dt}}_{\text{reptation and CLF}}+\underbrace{\frac{d\boldsymbol{f}_{\text{CR}}}{dt}}_{\text{CR and CCR}}+\underbrace{\frac{d\boldsymbol{f}_{retr}}{dt}}_{\text{retraction}} \quad (1a)$$

$$\frac{d\boldsymbol{f}_{\text{flow}}}{dt}=\boldsymbol{K}\cdot\boldsymbol{f}+\boldsymbol{f}\cdot\boldsymbol{K}^{\text{T}} \quad (1b)$$

$$\frac{d\boldsymbol{f}_{\text{rept-CLF}}}{dt}=\frac{1}{3\pi^2\tau_e}\frac{1}{\lambda_{s_{min}}}\left(\frac{\partial}{\partial s}+\frac{\partial}{\partial s'}\right)\left(\frac{D_{CLF}(s,s')}{\lambda_{s_{min}}}\left(\frac{\partial}{\partial s}+\frac{\partial}{\partial s'}\right)\boldsymbol{f}\right) \quad (1c)$$

$$\frac{d\boldsymbol{f}_{\text{CR}}}{dt}=\frac{3\nu}{2}\left[\frac{\partial}{\partial s}\left(\frac{F(\lambda_s)}{{\lambda_s}^2}\frac{\partial\boldsymbol{f}}{\partial s}\right)-\frac{\partial}{\partial s}\left(\frac{1}{\lambda_s}\frac{\partial\boldsymbol{f}^{eq}}{\partial s}\right)+\frac{\partial}{\partial s}\left(\frac{\boldsymbol{f}}{\lambda_s}\frac{\partial}{\partial s}\left(\frac{F(\lambda_s)}{\lambda_s}\right)\right)\right]$$
$$+\frac{3\nu}{2}\left[\frac{\partial}{\partial s'}\left(\frac{F(\lambda_{s'})}{{\lambda_{s'}}^2}\frac{\partial\boldsymbol{f}}{\partial s'}\right)-\frac{\partial}{\partial s'}\left(\frac{1}{\lambda_{s'}}\frac{\partial\boldsymbol{f}^{eq}}{\partial s'}\right)+\frac{\partial}{\partial s'}\left(\frac{\boldsymbol{f}}{\lambda_{s'}}\frac{\partial}{\partial s'}\left(\frac{F(\lambda_{s'})}{\lambda_{s'}}\right)\right)\right] \quad (1d)$$

$$\frac{d\boldsymbol{f}_{retr}}{dt}=\frac{R_s}{\pi^2\tau_e}\left[\frac{\partial}{\partial s}\left(\frac{\boldsymbol{f}}{\lambda_s}\frac{\partial F(\lambda_s)}{\partial s}\right)+\frac{\partial}{\partial s'}\left(\frac{\boldsymbol{f}}{\lambda_{s'}}\frac{\partial F(\lambda_{s'})}{\partial s'}\right)\right] \quad (1e)$$

$\boldsymbol{K}$ is the transported velocity gradient tensor. For constant shear, $\boldsymbol{K}=K_{xy}=\dot{\gamma}$ where $\dot{\gamma}$ is the shear rate. Thus, the shear component of the tube tangent correlation function is $f_{xy}(s,s',t)$.

Net constraint release rate at time t, $\nu(t)=\nu$. [s^{-1}].

$$\nu(t)=c_\nu\lambda(t) \quad (2a), \qquad \lambda(t)=\left(\underbrace{\lambda_{retr}(t)}_{\text{CCR from retraction}}+\underbrace{\lambda_{CLF}(t)}_{\text{CCR from CLF}}+\underbrace{\lambda_{tCR}(t)}_{\text{thermal CR}}\right) \quad (2b)$$

$$\lambda_{retr}(t)=\frac{-1}{2Z^*(t)}\int_0^Z\frac{1}{\lambda_s}\text{Tr}\left[\frac{d\boldsymbol{f}_{retr}}{dt}\right]ds \quad (3), \qquad \lambda_{CLF}(t)=\frac{-1}{2Z^*(t)}\int_0^Z\frac{1}{\lambda_s}\text{Tr}\left[\frac{d\boldsymbol{f}_{\text{rept-CLF}}}{dt}\right]ds \quad (4)$$

$$\lambda_{tCR}(t)=\frac{(1/3\beta_{rcr})}{Z^*(t)Z^2\tau_e} \quad (5a), \qquad \beta_{rcr}=(1+0.46\log_{10}c_\nu)\left(2.13-\frac{8.91}{\sqrt{Z}}+\frac{12.29}{Z}\right) \quad (5b)$$

Tr denotes matrix trace. Eq. (5b) holds in the ranges $Z=6-40$ and $c_\nu=0.1-1$ [30].

Position dependent diffusion coefficient for approximate CLF treatment. Dimensionless.

$$D_{CLF}(s,s')=\begin{cases}{a_d}^2/(s,min)^2 & s,min<a_d\sqrt{Z}\\ 1/Z & \text{otherwise}\end{cases} \quad s,min=\min(s,s',Z-s,Z-s'), \quad (6)$$

where $a_d=1.15$

ACCEPTED MANUSCRIPT
Journal of Rheology
This is the author's peer reviewed, accepted manuscript. However, the online version of record will be different from this version once it has been copyedited and typeset.
PLEASE CITE THIS ARTICLE AS DOI: 10.1122/8.0000280

$$\lambda_{s,min} = \sqrt{\mathrm{Tr}\boldsymbol{f}(s,min,s,min)} \quad (7) \quad \text{Units: Dimensionless. Range: } \lambda_{s,min} \geq 1$$

Effective number of entanglements, $Z^*(t)$, and local stretch at tube segment s, λ_s.

$$Z^*(t) = \int_0^Z \lambda_s \, ds \quad (8). \quad \text{[Dimensionless]. Range: } Z^*(t) \geq Z$$

$$\lambda_s = \sqrt{\mathrm{Tr}\boldsymbol{f}(s,s)} \quad (9). \quad \text{[Dimensionless]. Range: } 1 \leq \lambda_s \leq \lambda_{max}$$

GLaMM FENE function, referred to as FENE herein.

$$F(\lambda_s) = \lambda_s \left(\frac{{\lambda_{max}}^2 - \frac{{\lambda_s}^2}{3}}{{\lambda_{max}}^2 - {\lambda_s}^2} \right) \left(\frac{{\lambda_{max}}^2 - 1}{{\lambda_{max}}^2 - \frac{1}{3}} \right) \quad (10a). \text{ [Dimensionless]. Range: } F(\lambda_s) \geq 1$$

Kröger's FENE function [71], referred to as FENE 2 herein.

$$F(\lambda_s) = \lambda_s \left(\frac{1 - \left(\frac{1}{\lambda_{max}}\right)^2}{1 - \left(\frac{\lambda_s}{\lambda_{max}}\right)^2} \right) \left(\frac{2 + \left(\frac{1}{\lambda_{max}}\right)^2}{2 + \left(\frac{\lambda_s}{\lambda_{max}}\right)^2} \right) \quad (10b). \text{ [Dimensionless]. Range: } F(\lambda_s) \geq 1$$

Maximum stretch allowed, λ_{max}. [Dimensionless]. Constant per sample.

$$\lambda_{max} = 0.82 \sqrt{\frac{JM_e}{M_0 c_\infty}}. \text{ For PS, } J = 2, M_0 = 104.1 \frac{\mathrm{gr}}{\mathrm{mol}}, c_\infty = 9.6 \quad (10c)$$

Stress of the primitive chain (tube). [Pa]

$$\boldsymbol{\sigma} = \frac{12 G_e}{5Z} \int_0^Z \frac{F(\lambda_s)}{\lambda_s} \boldsymbol{f}(s,s) ds \quad (11)$$

Note that for the stress calculation only the diagonal components of $\boldsymbol{f}$ are required ($\boldsymbol{f}(s,s)$).

Initial conditions, i.e. equilibrium tube configuration. $\boldsymbol{f}^{eq}$ is dimensionless. $\boldsymbol{I}$ is the unit tensor.

$$\text{GLaMM paper (IC 1): } \boldsymbol{f}^{eq}(s,s',t=0) = \boldsymbol{f}^{eq} = \begin{cases} \boldsymbol{I}/3 & \text{for } |s-s'| < 0.5 \\ 0 & \text{otherwise} \end{cases} \quad (12a)$$

$$\text{Read } et\ al. \text{ (IC 2): } \boldsymbol{f}^{eq}(s,s',t=0) = \boldsymbol{f}^{eq} = (\boldsymbol{I}/3) e^{-2|s-s'|} \quad (12b)$$

The model requires five parameters, summarized in Table IV. Three of them, i.e. G_e, M_e, τ_e, are determined by matching tube model predictions and SAOS data (see Fig. 1 and Table I). The fourth parameter is the CCR parameter c_ν. According to Refs. [20, 30], $c_\nu = 1$ would mean that one retraction event results in one tube hop. This picture would hold if entanglements were purely binary events. Since in reality entanglements result from mutual interactions of many chains, several retraction events are required to produce a tube hop of length a. In this

ACCEPTED MANUSCRIPT
Journal of Rheology
This is the author's peer reviewed, accepted manuscript. However, the online version of record will be different from this version once it has been copyedited and typeset.
PLEASE CITE THIS ARTICLE AS DOI: 10.1122/8.0000280

respect, any choice in the range $0.1 < c_\nu < 1$ can be considered realistic. Here, following Refs. [20, 30, 31], $c_\nu = 0.1$. The fifth parameter is R_s. It is a prefactor of order unity that optimizes the decoupling approximation shown in Eq. (13) of Table IV. This decoupling approximation is required to obtain the $d\boldsymbol{f}_{retr}/dt$ term of Eq. (1a). Increases in R_s enhance chain retraction and thus stretch relaxation. By comparing model predictions and data, Graham *et al.* [30] found that $R_s = 2$ improves model performance. Hence, the same value is retained in this work.

Table IV. GLaMM model parameters.

Model parameters, determined from the linear viscoelastic response of the samples. τ_e: Entanglement relaxation time. [s^{-1}]. M_e: Molecular weight between entanglements. [gr/mol]. G_e: Plateau modulus at $t = \tau_e$. That is, $G_e = G'(\omega = {\tau_e}^{-1})$. [Pa]. c_ν: Dimensionless CCR parameter of order unity. It quantifies the retraction events that are necessary to impose a CCR hop on a tube segment. According to Refs. [20, 30, 31], $c_\nu = 0.1$.
R_s parameter. Order one prefactor arising from the following decoupling approximation [30]: $\langle\left(R'_i(s,t)R'_j(s',t)\right)\frac{\partial \ln\left(\boldsymbol{R}'(s,t)\cdot\boldsymbol{R}'(s',t)\right)}{\partial s}\rangle = R_s\langle R'_i(s,t)R'_j(s',t)\rangle\frac{\partial \ln\left(\langle\boldsymbol{R}'(s,t)\cdot\boldsymbol{R}'(s',t)\rangle\right)}{\partial s} =$ $R_s\boldsymbol{f}(\partial \ln \mathrm{Tr}\boldsymbol{f}/\partial s) = R_s\boldsymbol{f}\left(\partial \ln {\lambda_s}^2/\partial s\right) = 2R_s\frac{\boldsymbol{f}}{\lambda_s}\frac{\partial\lambda_s}{\partial s}$ (13) where i and j denote cartesian components, and $\langle\ldots\rangle$ an ensemble average. With FENE, Eq. (13) becomes $2R_s(\boldsymbol{f}/\lambda_s)\,\partial F(\lambda_s)/\partial s$, leading to the first term of Eq. (1e) after being multiplied by the operator $(1/2\pi^2\tau_e)\,\partial/\partial s$. The second term of Eq. (1e) is obtained in a similar manner. According to Ref. [30], $R_s = 2$ improves model performance.

At equilibrium the chain is assumed to obey random walk statistics, meaning that it comprises tube segments of constant length a, which, irrespective of the atomistic details of the chain (e.g. the value of the characteristic ratio c_∞) are uncorrelated to each other. The initial condition prescribed by Eq. (12a) reflects this idea. It prescribes a correlation that has a cutoff length-scale (width) of $|s - s'| < 0.5$, i.e. one tube segment, as measured in entanglement units. This cutoff width is essentially the tube persistence length, i.e. the length-scale below which CR

ACCEPTED MANUSCRIPT
Journal of Rheology
This is the author's peer reviewed, accepted manuscript. However, the online version of record will be different from this version once it has been copyedited and typeset.
PLEASE CITE THIS ARTICLE AS DOI: 10.1122/8.0000280

hops are not generated. In other words, CR hops cannot be generated within a tube segment; the latter undertakes a CR hop as a coherent unit.

The model retains the assumptions of constant tube diameter and persistence length even under strong deformation [30]. To do so, it assumes that the number of entanglements between successive tube segments (s and $s+1$) increases in proportion with the local stretch λ_s, defined by Eq. (9). Consequently, at time t, the chain experiences $Z^*(t)$ entanglements (Eq. (8) of Table III). As the chain portion between s and $s+1$ now comprises λ_s tube segments rather than one, Graham *et al*. [30] renormalize (reduce) the CCR magnitude by the factor λ_s. This renormalization of CCR weakens its effect on an extended chain. This feature of the model has a distinct impact on the obtained overshoots. In particular, the size of the overshoots grows as the shear rate increases, in agreement with experimental trends [30].

B. Numerical implementation of the model.

The mathematical formulation of Table III is solved numerically using a finite difference scheme as in the original GLaMM paper. Table V below summarizes the main features of the deployed numerical approach. Compared to the original paper, the only difference in the numerical implementation is the solution domain. Unlike Ref. [30], the present implementation makes use of the intrinsic symmetry of the RHS of Eq. (1a) and computes the solution in a single wedge quarter rather than the entire Z x Z square domain. The wedge domain is bounded by the lines $s=0$, $s=s'$ and $s=Z-s'$ as illustrated in Fig. S1 of the supplementary material. The boundary conditions are explained in the SI as well. The intrinsic symmetry of the RHS of Eq. (1a) can be realized by noting its invariance with respect to the $s=s'$ and $s=-s'$ substitutions. The advantage of the wedge approach is computational speed, in particular a factor of four gain compared to the square approach described in Ref. [30]. The authors are grateful to David. W. Mead for providing them a (FENE exclusive) code that implements the

ACCEPTED MANUSCRIPT
Journal of Rheology
This is the author's peer reviewed, accepted manuscript. However, the online version of record will be different from this version once it has been copyedited and typeset.
PLEASE CITE THIS ARTICLE AS DOI: 10.1122/8.0000280

aforementioned wedge quarter domain solution. It must be stressed that, as will be shown in the following section, the present code has been validated by comparing its predictions with those obtained from the open source GLaMM code. It should also be stressed that the wedge domain implementation has already been implemented in the GLaMM study of Auhl *et al.* [31]. However, it is not currently implemented in the open source GLaMM code (https://github.com/RichGraham/GLaMM_model).

Table V. Main features of the numerical implementation.

The chain is subdivided into $N_{mesh}+1$ points. According to Refs. [30, 31] the appropriate mesh selection is: $$N_{mesh} = 5Z, 3Z, Z \text{ for } Z < 5, 5 < Z < 13, Z > 13. \quad (14)$$
First order derivatives are calculated according to: $$\frac{\partial \boldsymbol{f}_{p,q}}{\partial s} = \frac{N_{mesh}}{2Z}\left(\boldsymbol{f}_{p+1,q} - \boldsymbol{f}_{p-1,q}\right), \qquad \frac{\partial \boldsymbol{f}_{p,q}}{\partial s'} = \frac{N_{mesh}}{2Z}\left(\boldsymbol{f}_{p,q+1} - \boldsymbol{f}_{p,q-1}\right) \quad (15a)$$ Second order derivatives are calculated according to: $$\frac{\partial^2 \boldsymbol{f}_{p,q}}{\partial s^2} = \left(\frac{N_{mesh}}{Z}\right)^2 \left(\boldsymbol{f}_{p+1,q} + \boldsymbol{f}_{p-1,q} - 2\boldsymbol{f}_{p,q}\right),$$ $$\frac{\partial^2 \boldsymbol{f}_{p,q}}{\partial s'^2} = \left(\frac{N_{mesh}}{Z}\right)^2 \left(\boldsymbol{f}_{p,q+1} + \boldsymbol{f}_{p,q-1} - 2\boldsymbol{f}_{p,q}\right) \quad (15b)$$ where p and q denote grid (mesh) points.
CLF derivatives are calculated according to: $$\left(\frac{\partial}{\partial s} + \frac{\partial}{\partial s'}\right) D_{CLF}(s, s') = \frac{1}{2\varepsilon}\left(D_{CLF\,p+\varepsilon,q+\varepsilon} - D_{CLF\,p-\varepsilon,q-\varepsilon}\right) \quad (16)$$ with $\varepsilon = 0.001$.
Integrals are calculated according to the trapezoidal rule: $$\int_0^Z F(s)ds = 0.5\frac{Z}{N_{mesh}}\left[F(0) + F(Z) + \sum_{p=2}^{N_{mesh}} F\left(\frac{pZ}{N_{mesh}}\right)\right] \quad (17)$$
Eq. (1a) is integrated forward in time using the Euler method. Chain ends are not updated. It is assumed that they always have their equilibrium configuration, $I/3$. Unless stated otherwise, the time step selection is as follows: $$\Delta t = 0.5\tau_e\left(\frac{Z}{N_{mesh}}\right)^2 \text{ for } Wi_R \le 2 \quad (18a), \qquad \Delta t = 0.1\tau_e\left(\frac{Z}{N_{mesh}}\right)^2 \text{ for } Wi_R > 2 \quad (18b)$$

ACCEPTED MANUSCRIPT
Journal of Rheology
This is the author's peer reviewed, accepted manuscript. However, the online version of record will be different from this version once it has been copyedited and typeset.
PLEASE CITE THIS ARTICLE AS DOI: 10.1122/8.0000280

C. CLF contribution to the retraction rate in the original GLaMM paper.

The accuracy of the wedge domain solution was verified by comparing model predictions of the current code with those obtained from the open source GLaMM implementation. Notice that the latter implementation incorporates FENE, i.e. Eqs. (1a), (10a), and (11). It also incorporates CLF contribution to the retraction rate, i.e. the contribution of Eq. (4) to Eq. (2b). Figure 2 presents this comparison for four samples studied in the original GLaMM paper. The comparison refers to the shear viscosity. The parameterization and the code name of the samples can be seen in the panels. Open circles refer to the open source code while lines refer to predictions of this work. As readily seen from Fig. 2 the predictions of the two codes coincide for all samples and rates. This excellent correspondence justifies the robustness of the numerical implementation used in this work. Open diamonds correspond to the original GLaMM predictions as extracted manually from Ref. [30]. They follow very closely the other curves confirming that the original predictions accounted for CLF contribution to the retraction rate. The discrepancy in Fig. 2(a) is a result of an error during the manual extraction of the curves. The N_{mesh} values were selected according to Eq. (14). In obtaining Fig. 2(a) FENE is disregarded, i.e. $\lambda_{max} = 10^{10}$ so that $F(\lambda_s) = \lambda_s$. Predictions of the open source GLaMM code and the current code in the presence of FENE are compared in Fig. S2 of the supplementary material. As readily seen from the latter figure, the current code reproduces the predictions of the open source code precisely.

ACCEPTED MANUSCRIPT
Journal of Rheology
This is the author's peer reviewed, accepted manuscript. However, the online version of record will be different from this version once it has been copyedited and typeset.
PLEASE CITE THIS ARTICLE AS DOI: 10.1122/8.0000280

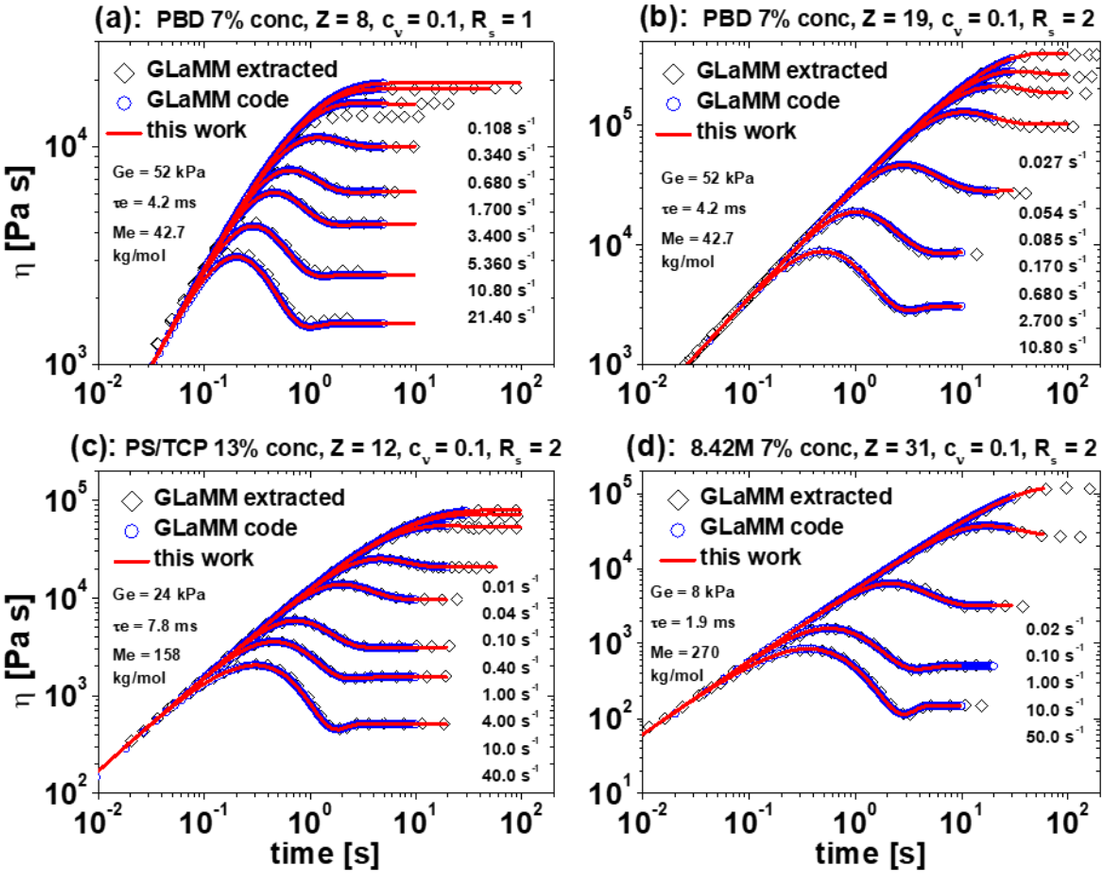

FIG. 2. Comparison of GLaMM predictions using the open source code available on GitHub (https://github.com/RichGraham/GLaMM_model) and the current code. The former predictions are shown by open circles while the latter predictions are shown by lines. Open diamonds are manually extracted predictions from the original GLaMM paper [30]. FENE is omitted. CLF contribution to $\nu(t)$ is included. Predictions refer to polymer solutions: (a.) and (b.) polybutadiene solutions of 7% polymer concentration in Flexon 391, a commercial hydrocarbon oil solvent [72]; (c.) and (d.) polystyrene solutions of 13% and 7% polymer concentration, respectively, in tricresyl phosphate (TCP) solvent [10].

D. Shear viscosity undershoot in the GLaMM model.

Figure 2 clearly shows that the GLaMM model predicts shear stress (viscosity) undershoots at the fastest shear rates. This behavior of the model is examined further in this section.

ACCEPTED MANUSCRIPT
Journal of Rheology
This is the author's peer reviewed, accepted manuscript. However, the online version of record will be different from this version once it has been copyedited and typeset.
PLEASE CITE THIS ARTICLE AS DOI: 10.1122/8.0000280

Attention focuses on the fastest rate of the PS/TCP sample where $\dot{\gamma} = 40$ s^{-1} ($Wi_R = 45$). To identify the cause of the undershoot two scenarios (options) are considered. In the first scenario, $\lambda_{tCR}(t)$ is accounted for by Eq. (5a). In the second option, $Z^*(t) = Z$ in Eq. (5a) therefore λ_{tCR} remains unchanged over time. Figure 3 presents various variables of the GLaMM predictions as a function of time for the aforementioned two options. As clearly seen from Fig. 3(c), $\lambda_{CLF}(t)$ goes only through an overshoot. On the other hand, $\lambda_{retr}(t)$ in option 1 goes through an undershoot at $t \approx 2$ s. This undershoot remains even when λ_{tCR} is considered constant implying that it is unrelated to the $\lambda_{tCR}(t)$ undershoot seen in option 1. Thus, the $\lambda_{tCR}(t)$ undershoot cannot be responsible for the viscosity undershoot seen in Fig. 3(a). Figure 3(b) reports the normalized stresses $(5Z/12G_e)\sigma_{xx}$, $(5Z/12G_e)\sigma_{yy}$ and $(5Z/12G_e)\sigma_{xy}$, i.e. the integrals of Eq. (11). Since $df_{\mathrm{yy,flow}}/dt = 0$ in shear flow, $(5Z/12G_e)\sigma_{yy}$ decays from its equilibrium value. In either option, it goes through an undershoot in the interval $1\text{ s} < t < 2$ s. This undershoot could in turn be responsible for the undershoot seen in $(5Z/12G_e)\sigma_{xy}$ at $t = 2$ s since $df_{\mathrm{xy,flow}}/dt = \dot{\gamma} f_{\mathrm{yy}}$, i.e. the evolution of f_{xy} depends on f_{yy}. Based on this finding, we speculate that the origin of the viscosity undershoot at fast rates is the undershoot of $(5Z/12G_e)\sigma_{yy}$ in the vicinity of its steady state. Although smaller in magnitude, the undershoot can also be seen in $(5Z/12G_e)\sigma_{xx}$. Presumably it is imposed by the flow term $df_{\mathrm{xx,flow}}/dt = 2\dot{\gamma} f_{\mathrm{xy}}$. For completeness, Fig. 3(d) presents $\lambda_{retr}(t) + \lambda_{CLF}(t)$ and the total retraction rate λ. Both go through an undershoot before their steady state.

To conclude this section, the following point should be emphasized. The analysis of this section suggests that the undershoot does not correspond to an underlying mechanism. Thus, the model would benefit from the incorporation of chain tumbling as it would provide a sound molecular mechanism for the viscosity undershoots at fast shear rates.

Journal of Rheology ACCEPTED MANUSCRIPT
This is the author's peer reviewed, accepted manuscript. However, the online version of record will be different from this version once it has been copyedited and typeset.
PLEASE CITE THIS ARTICLE AS DOI: 10.1122/8.0000280

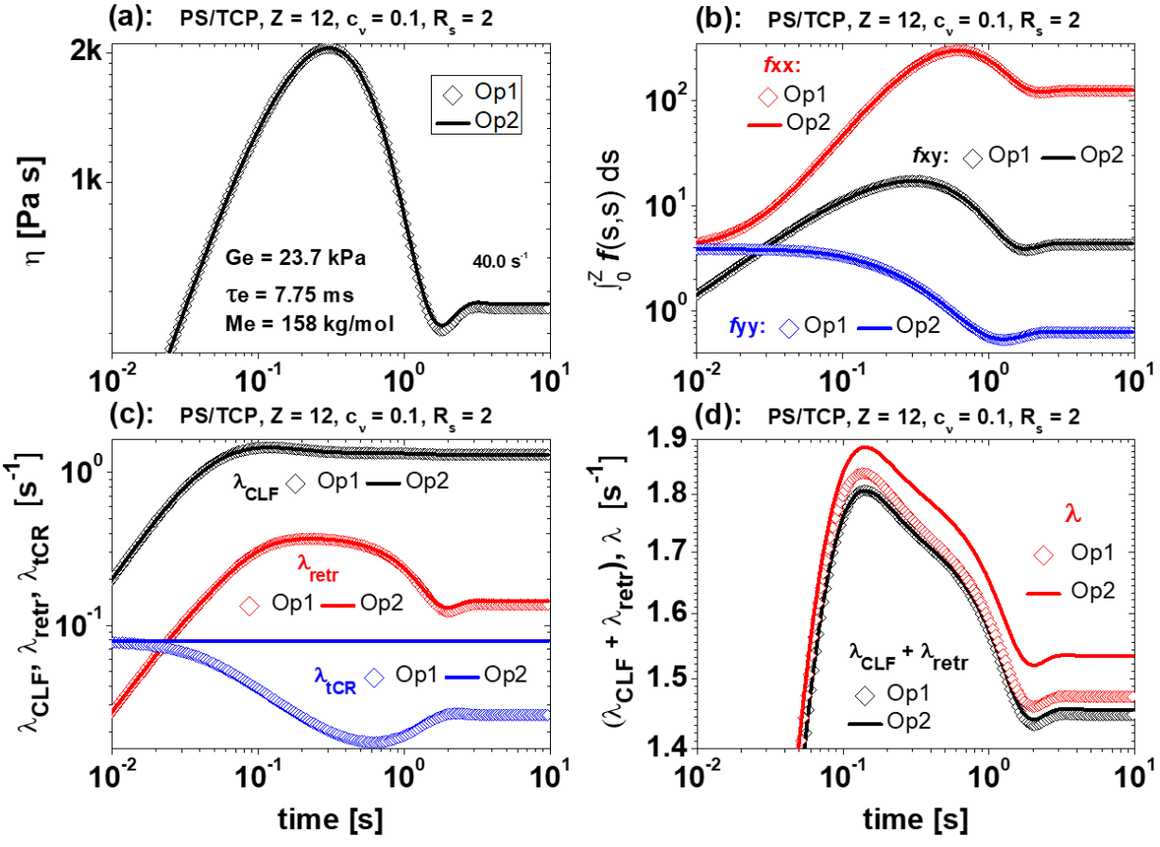

FIG. 3. (a.) Shear viscosity predictions for the PS/TCP material exhibiting an undershoot before steady state. (b.) $5Z/12G_e\,\boldsymbol{\sigma}$ vs time, i.e. the contribution of the integrals of Eq. (11) for the *xx*, *yy*, and *xy* components. (c.) $\lambda_{retr}(t)$, $\lambda_{CLF}(t)$, $\lambda_{tCR}(t)$, see Eq. (2b). (d.) $\lambda_{retr}(t) + \lambda_{CLF}(t)$ and $\lambda(t)$ outcomes. All model predictions omit FENE. In all panels, open symbols refer to option 1 while lines to option 2; see text for further explanation.

E. The significance of CLF contribution to retraction for numerical stability at high rates.

The section highlights the importance of CLF contribution to the retraction rate for overcoming numerical stability problems at fast shear rates. Figure 4 compares model predictions with and without CLF contribution to the retraction rate. Predictions neglect FENE. Figure 4(a) is obtained using the open source GLaMM code using a timestep of $0.1\tau_e(Z/N_{mesh})^2$ s. As readily seen predictions that disregard CLF contribution go through a profound minimum. At the highest rate, the code becomes unstable before the steady state is

ACCEPTED MANUSCRIPT
Journal of Rheology
This is the author's peer reviewed, accepted manuscript. However, the online version of record will be different from this version once it has been copyedited and typeset.
PLEASE CITE THIS ARTICLE AS DOI: 10.1122/8.0000280

achieved. Similar behavior is observed even if the timestep is reduced by a factor of 10 as clearly seen in Fig. 4(c). Figures 4(b) and 4(d) show the corresponding results using the current code. Results are identical to those of the open source code, except the long-time response at the highest rate; the current code cruses before the open source one. Notice that Eq. (12a) has been used as initial condition.

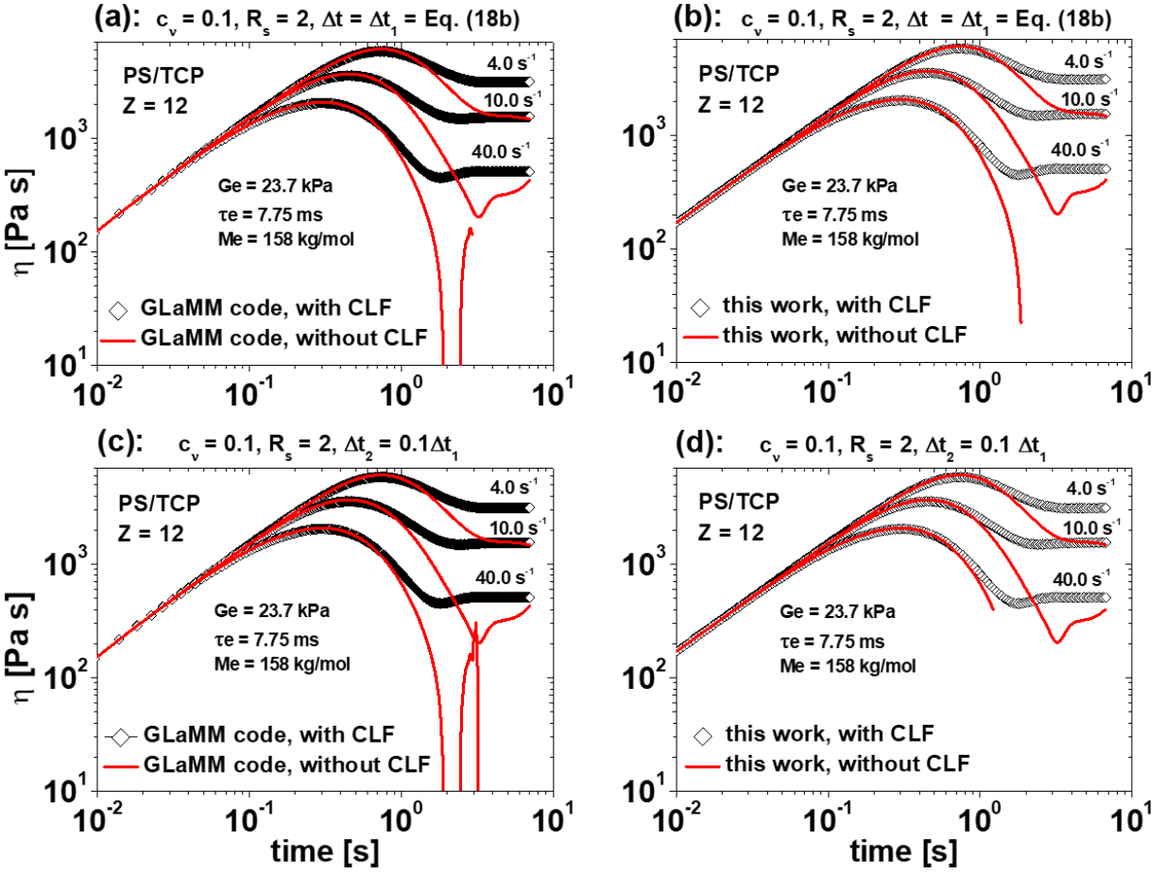

FIG. 4. (a.) and (c.) Viscosity predictions using the open source GLaMM code for two different timesteps. (b.) and (d.) Viscosity predictions using the current code. All predictions omit FENE. Symbols refer to model outcomes with CLF contribution to $\lambda(t)$ while lines to outcomes without.

ACCEPTED MANUSCRIPT
Journal of Rheology
This is the author's peer reviewed, accepted manuscript. However, the online version of record will be different from this version once it has been copyedited and typeset.
PLEASE CITE THIS ARTICLE AS DOI: 10.1122/8.0000280

To investigate further the instability origin attention now turns to the two highest rates, and model predictions obtained with a timestep of $0.01\tau_e(Z/N_{mesh})^2$ in the absence of CLF contribution to the retraction rate, i.e. Eq. (4) is set to zero. Figures 5(a) and 5(b) show the $(5Z/12G_e)\sigma_{xx}$, $(5Z/12G_e)\sigma_{yy}$ and $(5Z/12G_e)\sigma_{xy}$ outcomes for $\dot{\gamma}$ = 10 s^{-1} and 40 s^{-1}, respectively. $\lambda_{retr}(t)$, $\lambda_{tCR}(t)$ and $\lambda(t)$ outcomes are presented in Figs. 5(c) and 5(d). As in Fig. 3(b), $(5Z/12G_e)\sigma_{yy}$ goes through an undershoot before $(5Z/12G_e)\sigma_{xy}$. Similar to Figs. 3(c) and 3(d), $\lambda_{retr}(t)$ and $\lambda(t)$ exhibit an undershoot. In vast contrast to those cases, however, $\lambda_{retr}(t)$ becomes negative over time causing the overall retraction rate, $\lambda(t)$, to become negative. As a result, $\nu(t)$ becomes negative too, and the $d\boldsymbol{f}_{\mathrm{CR}}/dt$ terms (Eq. (1d)) change sign leading to oscillatory response until the numerical solution becomes totally unstable. The magnitude of this oscillations increases with increasing shear rate. In the next subsection we examine whether this instability is resolved when FENE is incorporated in the model.

Journal of Rheology ACCEPTED MANUSCRIPT
This is the author's peer reviewed, accepted manuscript. However, the online version of record will be different from this version once it has been copyedited and typeset.
PLEASE CITE THIS ARTICLE AS DOI: 10.1122/8.0000280

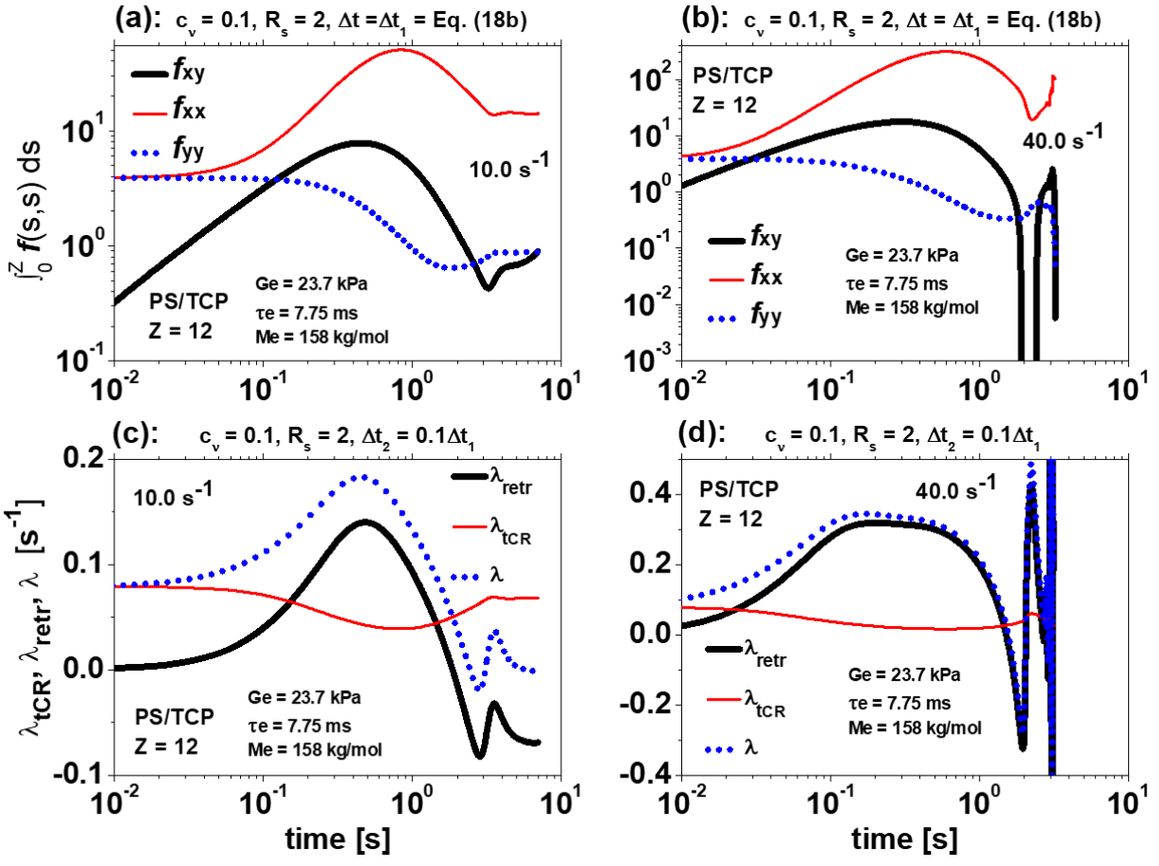

FIG. 5. (a.) and (b.) $5Z/12G_e\,\boldsymbol{\sigma}$ vs time GLaMM outcomes for $\dot{\gamma}$ = 10 s^{-1} and 40 s^{-1}, respectively. *xy*, *xx*, and *yy* components are shown by thick solid, solid, and dotted lines, respectively. (c.) and (d.) The corresponding $\lambda_{retr}(t)$, $\lambda_{tCR}(t)$, $\lambda(t)$ outcomes shown by thick solid, solid, and dotted lines, respectively. FENE is neglected. CLF contribution to the retraction rate is omitted, i.e. $\lambda_{CLF}(t) = 0$. Initial condition is prescribed by Eq. (12a).

F. Comparison of GLaMM predictions including FENE and PS experimental data.

Hereafter, model predictions are obtaining with FENE. Unless stated otherwise all predictions are obtained using Eq. (10a) for the FENE function and Eq. (12a) for initial condition. As Fig. 6 demonstrates FENE inclusion does not resolve the instability that occurs when CLF contribution to $\lambda(t)$ is omitted. Figure 6(a) shows that viscosity predictions do not attain a distinct steady state when $Wi_R \gtrsim 8$. As with the FENE exclusive scenario, we relate

ACCEPTED MANUSCRIPT
Journal of Rheology
This is the author's peer reviewed, accepted manuscript. However, the online version of record will be different from this version once it has been copyedited and typeset.
PLEASE CITE THIS ARTICLE AS DOI: 10.1122/8.0000280

the instability to the $(5Z/12G_e)\sigma_{yy}$ undershoot that "propagates" to the other $\boldsymbol{f}$ components through the flow term of the evolution equation. For $Wi_R = 25$, the $(5Z/12G_e)\boldsymbol{\sigma}$ undershoots can be seen in Fig. 6(b). Note that $(5Z/12G_e)\sigma_{yy}$ becomes negative at $t \approx 0.8$ s. The same applies to $\lambda_{retr}(t)$ and in turn to $\lambda(t)$ - see Fig. 6(c). As a result, the numerical solution becomes unstable. Figure 6(d) presents the $\lambda_{retr}(t)$ integrand as a function of the tube contour *s* at various times. At equilibrium, $\lambda_{retr,s}(t = 0)$ is zero in the entire *s* domain (not shown). As time goes on, $\lambda_{retr,s}$ becomes negative for inner segments meaning that their contribution to $\lambda_{retr}(t)$ is positive – see Eq. (3). In contrast, the contribution near chain ends is negative. Despite this, $\lambda_{retr}(t)$ remains positive up to $t \approx 0.7$ s. Then it becomes negative, and $\lambda_{retr,s}$ exhibits an oscillatory response with some segments having positive contribution to $\lambda_{retr}(t)$ and other segments negative. It is worth mentioning that if the $\lambda_{retr,s} > 0$ elements are set to zero the code becomes stable. Nevertheless, viscosity predictions at fast rates still manifest an undershoot. This shows that the undershoot origin does not arise from the $\lambda_{retr,s} > 0$ elements.

Journal of Rheology ACCEPTED MANUSCRIPT
This is the author's peer reviewed, accepted manuscript. However, the online version of record will be different from this version once it has been copyedited and typeset.
PLEASE CITE THIS ARTICLE AS DOI: 10.1122/8.0000280

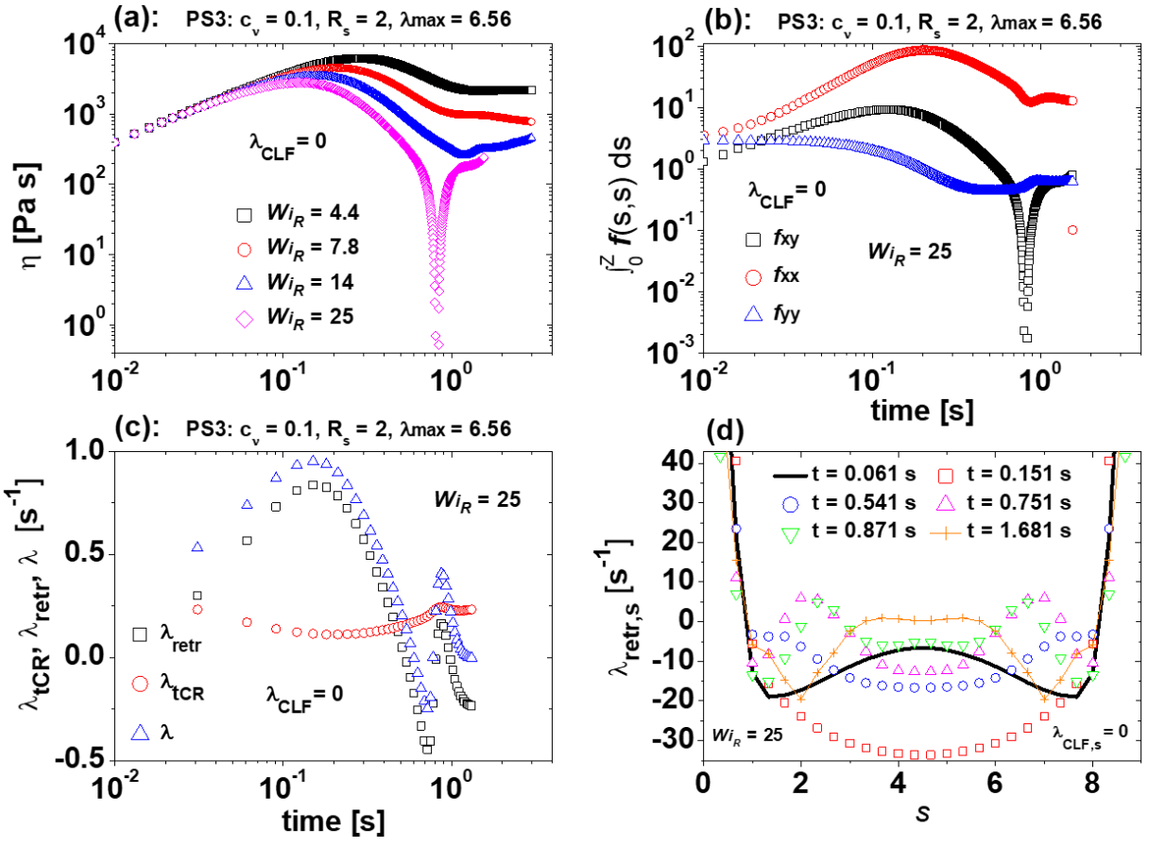

FIG. 6. (a.) Viscosity predictions for the fastest four rates of the PS3 sample. (b.) $5Z/12G_e\,\boldsymbol{\sigma}$ responses for the fastest rate ($Wi_R = 25$). (c.) The corresponding $\lambda_{retr}(t)$, $\lambda_{tCR}(t)$, $\lambda(t)$ outcomes. (d.) The $\lambda_{retr}(t)$ integrand, i.e. $\lambda_{retr,s}$, at various times. Predictions account for FENE, with $\lambda_{max} = 6.56$. CLF contribution to the retraction rate is omitted, i.e. $\lambda_{CLF}(t) = 0$. Initial condition is prescribed by Eq. (12a).

Attention now swifts to comparison with the experimental data of the four PS samples. Model predictions with FENE are obtained using $\lambda_{max} = 4.48$ for the two melts, $\lambda_{max} = 6.56$ for PS3, and $\lambda_{max} = 5.57$ for PS4. These values are determined from Eq. (10c) and the M_e values reported in Table I. Figure 7 compares the experimental data and model predictions with and without FENE. In either case, CLF contribution to $\nu(t)$ is accounted for. Figure 7 reveals several features. First, FENE incorporation has practically no effect in the $Wi_R \lesssim 20$ regime. Second, for $Wi_R > 20$ the overshoot size decreases when FENE is considered. This effect

ACCEPTED MANUSCRIPT
Journal of Rheology
This is the author's peer reviewed, accepted manuscript. However, the online version of record will be different from this version once it has been copyedited and typeset.
PLEASE CITE THIS ARTICLE AS DOI: 10.1122/8.0000280

becomes more pronounced as Wi_R increases. It is accompanied by the emergence of sharp peaks and a moderate increase of the steady state response. These features can be readily appreciated in Figs. 7(c) and 7(d) as well as in Fig. S4 of the supplementary material, which focuses on λ_{max} variations. Third, neither version faithfully reproduces the experimental results in the entire $Wi_R > 1$ range. For the PS1 and PS3 samples, where $Z = 9$, the model performs rather well for $Wi_R < 15$; at faster rates it captures the steady response but it overpredicts the peak viscosity. In contrast, for the longer chains ($Z = 12$) the model exhibits limitations when $Wi_R > 2$. At lower rates the limitation is the overprediction of the steady state. As Wi_R increases, both the peak and steady viscosities are overpredicted considerably.

Note that the FENE function of Eq. (10a) is an approximant of the inverse Langevin function. It is asymptotically wrong [71]. Thus, a second FENE function proposed by Kröger was also considered [71]. Its explicit formula is given by Eq. (10b). This function exhibits a more accurate asymptotic behavior of the inverse Langevin function. Nevertheless, as Fig. S3 of the supplementary material demonstrates, both FENE functions give in practice the same results, for the Wi_R range examined here. The superiority of Eq. (10b) over Eq. (10a) might be important at fast elongational flows.

ACCEPTED MANUSCRIPT
Journal of Rheology
This is the author's peer reviewed, accepted manuscript. However, the online version of record will be different from this version once it has been copyedited and typeset.
PLEASE CITE THIS ARTICLE AS DOI: 10.1122/8.0000280

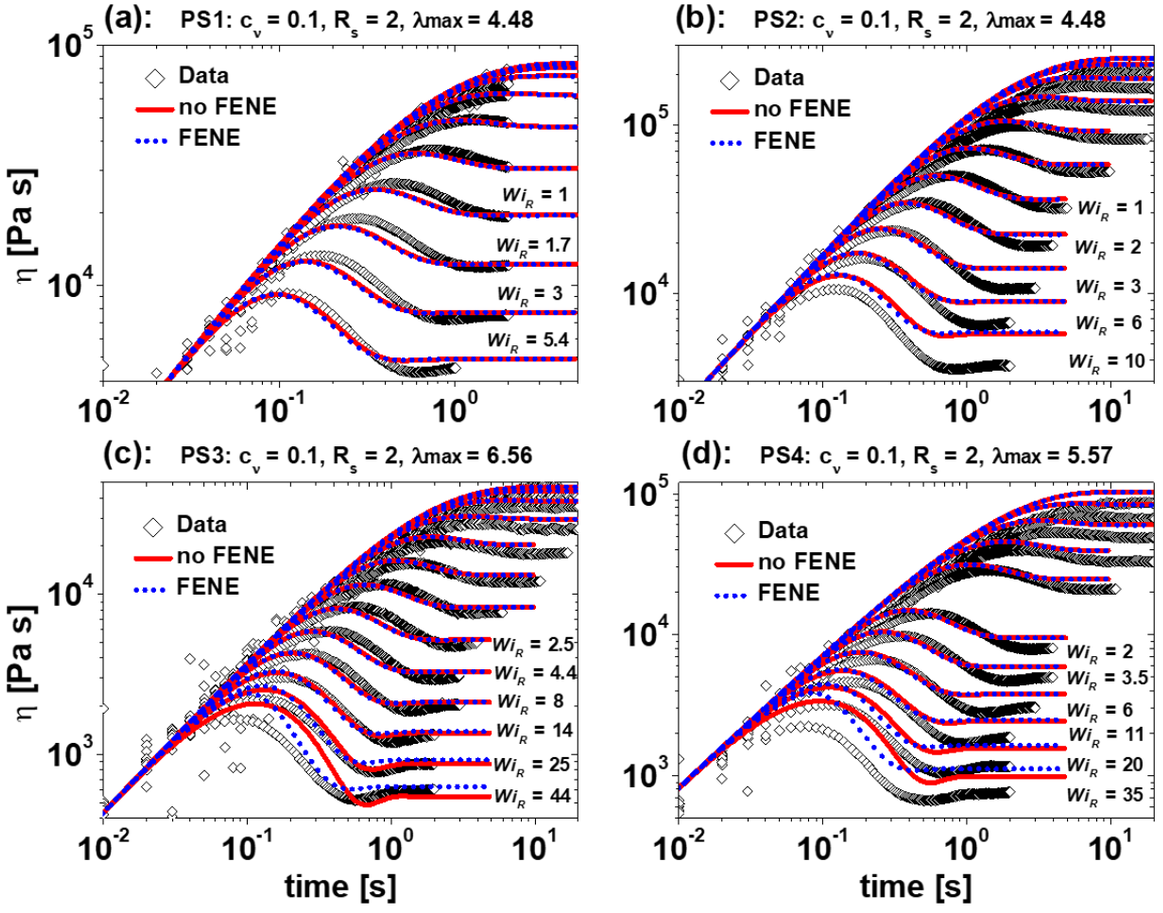

FIG. 7. Comparison of GLaMM predictions and experimental data (black squares), as indicated in the (a) - (d) legends. Model predictions include CLF contribution to $\nu(t)$. Solid lines omit FENE. Dotted lines include FENE.

To gain more insight into FENE effects on model predictions at fast rates, the s and t evolution of several molecular variables is examined. The molecular variables are $f_{xy}(s,s)$, the xy component of the $\boldsymbol{f}$ tensor, $\lambda_s(s)$, the stretch, $F\left(\lambda_s(s)\right)/\lambda_s(s)$, the FENE function, and $P_2(s)$, the average orientation along the chain in terms of the second Legendre polynomial $\langle 3\cos^2\theta_s - 1\rangle/2$, where θ_s is the average angle of segment s with the flow direction. According to Ref. [31], $\langle\cos^2\theta_s\rangle = f_{xx}(s,s)/\mathrm{Tr}\boldsymbol{f}(s,s)$. Note that $P_2(s)$ is not the usually measured or discussed flow-alignment angle $\chi = (90^\circ/\pi)\tan^{-1}\left[2\sigma_{xy}/\left(\sigma_{xx}-\sigma_{yy}\right)\right]$.

ACCEPTED MANUSCRIPT
Journal of Rheology
This is the author's peer reviewed, accepted manuscript. However, the online version of record will be different from this version once it has been copyedited and typeset.
PLEASE CITE THIS ARTICLE AS DOI: 10.1122/8.0000280

Attention focuses on the fastest PS3 rate where $Wi_R = 44$. Figures 8(a) and 8(b) show the s and t evolution of $f_{xy}(s,s)$ and $\lambda_s(s)$ without FENE. Figures 8(d) and 8(e) present the corresponding responses with FENE. As evidenced from those figures, FENE incorporation leads to moderately reduced responses along the chain for both $f_{xy}(s,s)$ and $\lambda_s(s)$, especially at early and intermediate timescales ($t \lesssim 0.2\ s$). At longer timescales, the discrepancies weaken. Despite the weaker f_{xy} and λ_s responses, the FENE inclusive viscosity predictions of Fig. 7(c) exhibit larger peak and steady state responses that the FENE exclusive outcomes. This behavior is attributed to the stress amplification achieved through the $F(\lambda_s)/\lambda_s$ factor in the stress definition – see Eq. (11). This amplification compensates for the lower f_{xy} and λ_s responses in the FENE inclusive results. As seen in Fig. 8(f), $F(\lambda_s)/\lambda_s$ values are larger than one whereas in the FENE exclusive case $F(\lambda_s)/\lambda_s = 1$. Concerning $P_2(s)$, the responses with and without FENE are practically identical; as Fig. 8(c) shows the entire chain is oriented in the flow direction, apart from the chain ends. All presented results are symmetric about the center of the chain. This is expected from the model assumption of the two chain ends being unstretched and randomly oriented at all times.

Journal of Rheology ACCEPTED MANUSCRIPT
This is the author's peer reviewed, accepted manuscript. However, the online version of record will be different from this version once it has been copyedited and typeset.
PLEASE CITE THIS ARTICLE AS DOI: 10.1122/8.0000280

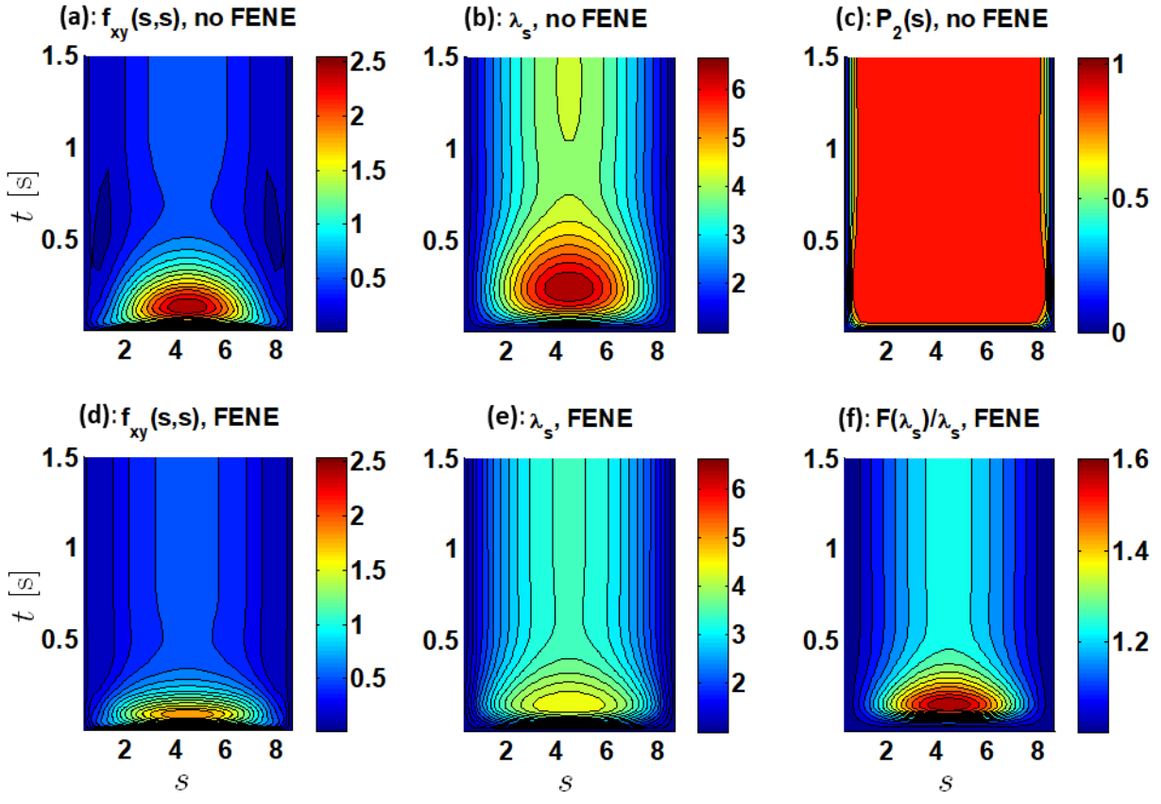

FIG. 8. (a.) - (c.) $f_{xy}(s,s)$, λ_s, and $P_2(s) = \left(1.5 f_{xx}(s,s)/\mathrm{Tr}\boldsymbol{f}(s,s)\right) - 0.5$ responses of the ($Wi_R = 44$) viscosity predictions shown in Fig. 7(c) as a function of time t and tube segment s. Responses neglect FENE. (d.) - (e.) $f_{xy}(s,s)$, λ_s, and $F(\lambda_s)/\lambda_s$ responses for the same shear rate that account FENE. In all panels, the right scale bars indicate the correspondence between $f_{xy}(s,s)$, $P_2(s)$, λ_s, $F(\lambda_s)/\lambda_s$ values and colors. $\lambda_{max} = 6.58$. (Color online.)

Next, the sensitivity of the model to the initial condition is examined. So far, all model predictions were obtained using Eq. (12a) that treats the chain as a smooth curve at length scales larger than a. As discussed by Read *et al.* [73], a more realistic description of tube dynamics requires a smooth, differentiable, $\boldsymbol{R}(s,t)$ curve at all length scales. Such a curve can be obtained by penalizing bending of the tube segments. As the authors demonstrated, at equilibrium, the tube tangent correlation function in the presence of a bending potential takes the form $(\boldsymbol{I}/3)e^{-2|s-s'|}$, i.e. Eq. (12b). By using the latter equation as initial condition we

ACCEPTED MANUSCRIPT
Journal of Rheology
This is the author's peer reviewed, accepted manuscript. However, the online version of record will be different from this version once it has been copyedited and typeset.
PLEASE CITE THIS ARTICLE AS DOI: 10.1122/8.0000280

hypothesize that the grid points representing the chain belong initially to a $\boldsymbol{R}(s,t)$ curve that it is smooth and differentiable at all length scales.

Figures 9(a) and 9(b) compare model predictions using Eqs. (12a) or (12b) as initial condition. These predictions are labeled as "IC 1" and "IC 2", respectively. In either case, parameterization, time step, and mesh discretization are identical. Also, CLF contribution to the constraint release rate is accounted for. Figures 9(a) and 9(b) refer to PS3 and PS4, respectively. These two figures reveal the model sensitivity on the initial condition. Predictions are affected at all rates. Overall, predictions using the Read *et al.* [73] initial condition (IC 2) manifest lower stress (viscosity) response than those using the original GLaMM condition (IC 1). Only the steady state response at very fast rates seems to be rather insensitive to the initial condition. As regards model performance, IC 1 predictions outperforms IC 2 predictions at intermediate rates. At slow and fast rates, the IC 2 outcomes describe the experimental response better than the IC 1 ones. The improvement at fast rates is to lessen the viscosity maximum overprediction.

ACCEPTED MANUSCRIPT
Journal of Rheology
This is the author's peer reviewed, accepted manuscript. However, the online version of record will be different from this version once it has been copyedited and typeset.
PLEASE CITE THIS ARTICLE AS DOI: 10.1122/8.0000280

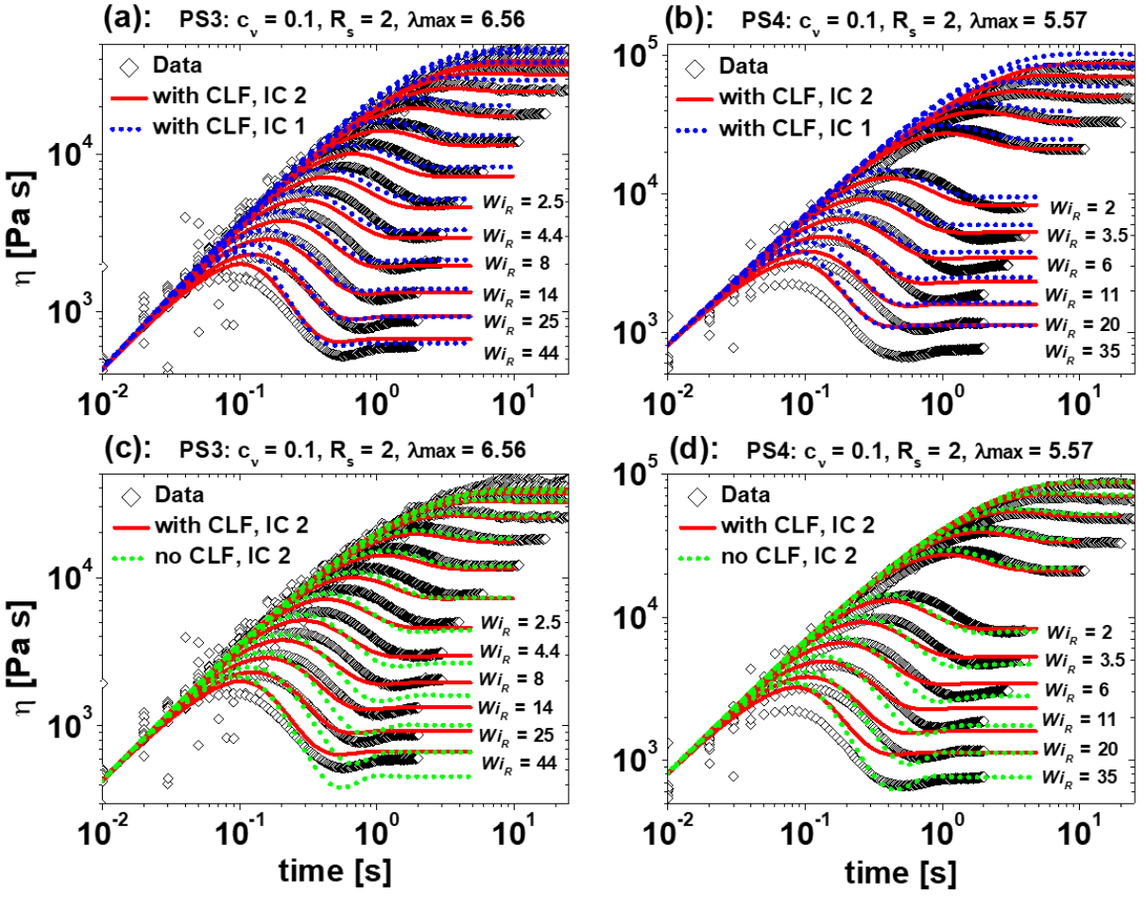

FIG. 9. Comparison of GLaMM predictions and experimental data (black squares). (a.) – (b.) Solid lines are obtained with Eq. (12b) as initial condition while dotted lines with Eq. (12a). Model predictions include CLF contribution to $\nu(t)$. (c.) – (d.) Model predictions are obtained with Eq. (12b) as initial condition. Solid lines include CLF contribution to $\nu(t)$ whereas dotted lines omit it.

Figures 9(c) and 9(d) compare model predictions with and without CLF contribution to the constraint release rate (or retraction rate). In either scenario Eq. (12b) prescribes the initial configuration (IC 2). In vast contrast with the predictions of Fig. 6(a), the numerical solution is stable even if CLF contribution is disregarded. Such a drastic difference is model outcomes by only changing the initial condition is remarkable. In our view, it highlights the model sensitivity on (1) the cutoff CR noise length scale (2) the $\boldsymbol{R}(s,t)$ curve coarse-graining, which

ACCEPTED MANUSCRIPT
Journal of Rheology
This is the author's peer reviewed, accepted manuscript. However, the online version of record will be different from this version once it has been copyedited and typeset.
PLEASE CITE THIS ARTICLE AS DOI: 10.1122/8.0000280

should actually be a continuous, smooth, differentiable curve at all length scales in order to define the tube tangent correlation function. In terms of model performance, the CLF exclusive outcomes describe much better the measured response of the longer chains (PS4) than the CLF inclusive outcomes. In fact, all steady states are nicely reproduced. On the other hand, the PS3 experimental response at fast rates is underpredicted.

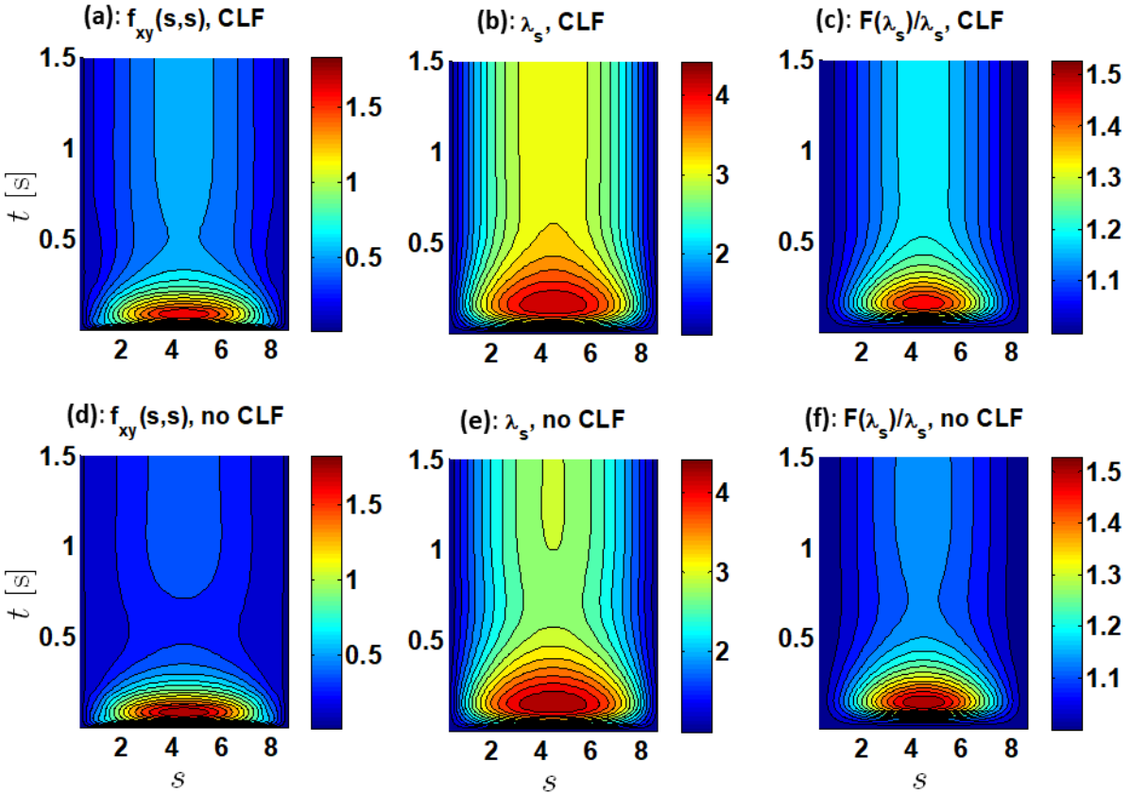

FIG. 10. $f_{xy}(s,s)$, λ_s, and $F(\lambda_s)/\lambda_s$ responses of the ($Wi_R = 44$) viscosity predictions shown in Fig. 9(c) as a function of time t and tube segment s. (a.) - (c.) CLF inclusive results. (d.) - (f.) CLF exclusive results. In either scenario, the initial condition corresponds to Eq. (12b). In all panels, the right scale bars indicate the correspondence between $f_{xy}(s,s)$, P_2, λ_s, $F(\lambda_s)/\lambda_s$ values and colors. $\lambda_{max} = 6.58$. (Color online.)

ACCEPTED MANUSCRIPT
Journal of Rheology
This is the author's peer reviewed, accepted manuscript. However, the online version of record will be different from this version once it has been copyedited and typeset.
PLEASE CITE THIS ARTICLE AS DOI: 10.1122/8.0000280

Figure 10 examines the s and t evolution of the molecular variables $f_{xy}(s,s)$, $\lambda_s(s)$, and $F\left(\lambda_s(s)\right)/\lambda_s(s)$ for the ($Wi_R = 44$) viscosity predictions of Fig. (9c). Figures 10(a) to 10(c) refer to CLF inclusive results whereas Figs. 10(d) to 10(e) present CLF exclusive results. According to these figures, CLF addition to $\nu(t)$ does not affect the responses at early and intermediate timescales ($t \lesssim 0.3$ s). At longer timescales CLF inclusion has the following effects. Compared to the CLF exclusive scenario, it gives a stronger $f_{xy}(s,s)$ response along the chain. This is because the enhanced retraction rate produces more CCR hops, thereby it tends to randomize the orientation of the tube segments. Such CCR hops or "kinks" along the tube are subsequently pulled by the flow and thus increase the $\lambda_s(s)$ response, especially for the inner tube segments. In turn, the $F\left(\lambda_s(s)\right)/\lambda_s(s)$ response is stronger in the CLF inclusive scenario. This behavior, combined with the enhanced $f_{xy}(s,s)$ response, lead to larger viscosity steady states when the CLF contribution to $\nu(t)$ is added.

G. Comparison of the GLaMM model and the Ianniruberto-Marrucci (IM) model [44].

We now compare the predictions of the GLaMM model to those of the Ianniruberto-Marrucci (IM) model presented in Costanzo *et al*. [44]. As mentioned in the introduction, the latter model incorporates chain tumbling which, apart from being the underlying mechanism of the viscosity undershoots at fast rates, appears to be essential for correctly predicting the steady-state viscosities throughout the entire nonlinear flow regime ($Wi_R > 1$). This feature can be readily appreciated in Fig. 11 where different (IM) model predictions are compared against the experimental data. To appreciate the effects of tumbling, IM model predictions are presented with (labeled "Cos2") and without tumbling (labeled "Cos1"), including CCR and FENE in either case. As observed in the figure, IM predictions that include chain tumbling capture the experimental steady viscosities nicely, but slightly overpredict the viscosity maxima at the fastest two rates. Notice that Fig. 11 refers to the PS1 melt for which the faster shear rate

ACCEPTED MANUSCRIPT
Journal of Rheology
This is the author's peer reviewed, accepted manuscript. However, the online version of record will be different from this version once it has been copyedited and typeset.
PLEASE CITE THIS ARTICLE AS DOI: 10.1122/8.0000280

corresponds to a relatively low Wi_R = 5.4. According to Ref. [44], the importance of chain tumbling in correctly determining the steady viscosities increases with increasing Wi_R.

On the other hand, predictions without chain tumbling severely overpredict the steady viscosities over the entire nonlinear flow regime. For comparison, Figure 11 also includes GLaMM predictions, labeled as "GLaMM 1" and "GLaMM 2". Both account for FENE and CLF contribution to the retraction rate. "GLaMM 1" predictions are actually those of Fig. 7(a), where $c_v = 0.1$ and $R_s = 2$. They provide a reasonable data description. This implies that the importance of chain tumbling is not as crucial as the IM model suggests. Even if a c_v and R_s parameterization that favors weak overshoots is considered, i.e. $c_v = 0.3$ and $R_s = 1$, the GLaMM viscosity predictions lie beneath the "Cos1" IM outcomes considerably. To avoid any misunderstanding, we do not claim that tumbling should not be implemented in the model to render it more realistic. As aforementioned, tumbling would provide a sound molecular mechanism for the viscosity undershoots and determine to some extent the steady state. What is actually claimed here, is that tumbling does not appear to have such a dramatic effect in determining the steady state as suggested by the IM model.

ACCEPTED MANUSCRIPT
Journal of Rheology
This is the author's peer reviewed, accepted manuscript. However, the online version of record will be different from this version once it has been copyedited and typeset.
PLEASE CITE THIS ARTICLE AS DOI: 10.1122/8.0000280

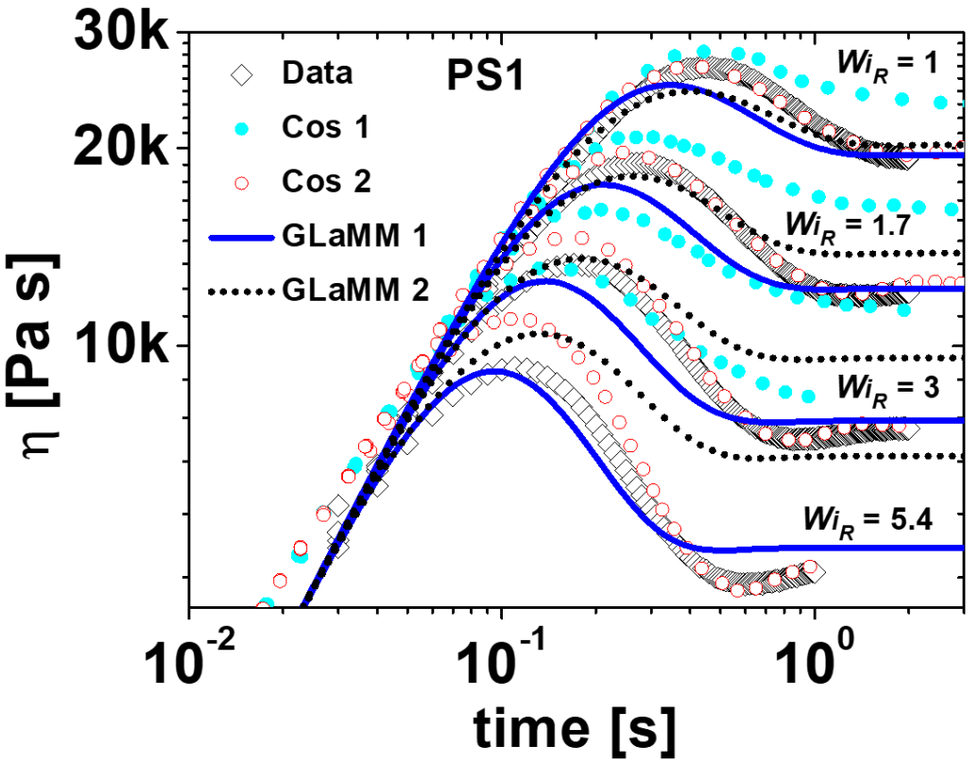

FIG. 11. Comparisons of the GLaMM and Ianniruberto-Marrucci (IM) [44] models' predictions for the fastest four rates of the PS1 melt. Diamonds represent the PS1 data. Open circles labeled as "Cos2" refer to IM outcomes including CCR, FENE, and chain tumbling. Filled symbols labeled as "Cos1" refer to IM predictions with CCR, FENE, but without tumbling. GLaMM outcomes for two c_ν and R_s combination are also included for comparison. Those labeled as "GLaMM 1" refer to $c_\nu = 0.1$ and $R_s = 2$ (solid lines). Those labeled as "GLaMM 2" refer to $c_\nu = 0.3$ and $R_s = 1$ (dotted lines). In either case, FENE as well as CLF addition to $\nu(t)$ are accounted for. The initial condition is prescribed by Eq. (12a).

At this point, we can only speculate on the reasons for which IM without tumbling predicts considerably higher viscosity response than the GLaMM even though the two models incorporate the same physics. The discrepancy might arise from the different way the two models implement the same physics. Unlike GLaMM, the IM formulation decouples stretch and orientation. Furthermore, it utilizes an integral equation for the orientation evolution.

ACCEPTED MANUSCRIPT
Journal of Rheology
This is the author's peer reviewed, accepted manuscript. However, the online version of record will be different from this version once it has been copyedited and typeset.
PLEASE CITE THIS ARTICLE AS DOI: 10.1122/8.0000280

Differences also arise in the way the two models implement CCR. In the IM model a semi-phenomenological, multimode treatment of CCR is employed. As regards orientation relaxation, CCR accelerates the reorientation time of each subchain (mode) by simply accelerating its reorientation time. Concerning stretch relaxation, CCR is thought to accelerate the Rouse relaxation time of the entire chain. The CCR effectiveness is controlled by β_{CCR}, a parameter analogous to c_v in the GLaMM model. A larger β_{CCR} value is used in the acceleration of the Rouse time as compared to the acceleration of the reorientation times ($\beta_{CCR} = 0.5$ and $\beta_{CCR} = 0.25$, respectively). Nevertheless, the fact that, unlike CCR driven stretch relaxation, CCR driven reorientation is prescribed to all subchains might impose a bias toward orientation relaxation in the model, leading to considerably higher S_{xy} and stretch values as compared to the GLaMM model. Finally, one should bear in mind that, despite its microscopic description as Rouse-like hops, the CCR treatment of the GLaMM model still strongly depends on the c_v parameter. In this respect, a detailed comparison between the two models would require the exact correspondence between β_{CCR} and c_v.

H. Assessment of the GLaMM model.

Although the overall model performance is acceptable, deviations from the experimental data mainly emerge when $Wi_R > 1$, and become more apparent as Wi_R increases further. Model limitations such as the peak and steady viscosity overestimation as well as the lack of a molecular mechanism for the undershoots, hint towards the omittance of molecular mechanisms such as CCR-D and chain tumbling. CCR-D challenges the validity of important model assumptions like those of a constant tube diameter and persistence length. Note in passing that the examined shear rates do not exceed the inverse of the entanglement relaxation time (τ_e), otherwise the assumption of constant tube diameter would have been surely questionable. The obvious statement to make here is that the lack of these mechanisms is

ACCEPTED MANUSCRIPT
Journal of Rheology
This is the author's peer reviewed, accepted manuscript. However, the online version of record will be different from this version once it has been copyedited and typeset.
PLEASE CITE THIS ARTICLE AS DOI: 10.1122/8.0000280

probably the primary source of error in the GLaMM model. Considering the fact that such mechanisms are widely observed in NEMD simulations, the incorporation of CCR-D and tumbling would indeed render the GLaMM model more realistic. Nevertheless, the finding of this work suggests that before looking at those aspects it is essential to resolve some other issues first. Resolving these issues will allow a more precise account of the missing physics of CCR-D and tumbling.

These issues are namely, (1) the assumption of isotropic and unstretched chain ends. This assumption affects the results significantly and it might be invalid at fast rates. It should be tested by NEMD simulations. (2) A more detailed description of CLF. As this work showed, the inclusion of CLF contribution to the retraction rate significantly influences the steady state response of the model. Considering that the CLF description of Eq. (1c) is approximate one may wonder what a difference a detailed CLF treatment can bring to the model. Actually, the fact that numerical stability is not an issue when the initial condition is given by Eq. (12b) rather than Eq. (12a) questions the physical importance of CLF addition to the retraction rate altogether. (3) Further validation of the $c_\nu = 0.1$ and $R_s = 2$ parameterization, which currently is taken for granted. Information from NEMD could be used for this purpose. For example, the closure approximation of Eq. (13) could be tested by examining NEMD atomistic trajectories with topological analysis codes such as the Z1 code [74, 75, 76], the CreTa code [77] and other techniques [78] as to extract the primitive paths and in turn enumerate the R_s prefactor of Eq. (13). There could be practical challenges in this task since such topological analysis codes are developed to study the equilibrium properties of polymer melts, where chain configurations are rather isotropic. We note however that the Z1 code has already been used to analyze NEMD results [29].

Moreover, (4) it seems important to consider a GLaMM variant that penalizes bending of the tube segments thus creating a smooth tube contour at all length scales. As Figs. 9(a) and 9(b)

ACCEPTED MANUSCRIPT
Journal of Rheology
This is the author's peer reviewed, accepted manuscript. However, the online version of record will be different from this version once it has been copyedited and typeset.
PLEASE CITE THIS ARTICLE AS DOI: 10.1122/8.0000280

showed, the model is sensitive to this change even at the level of the initial condition. In fact, Read *et al*. [73] have developed a GLaMM variant that substitutes Eq. (1d) with an equation that considers CR events in a tube with bending energy. They have actually shown that, for identical parameterization, shear viscosity predictions of their variant lie moderately below GLaMM outcomes. It would be worth to examine the performance of this GLaMM variant against actual data despite the increased computation cost of this variant. Note that Read *et al*. focused on CR only thus they ignored changes in reptation, CLF, and retraction due to the bending potential.

IV. NONLINEAR TMA

Whereas the overall performance of GLaMM presented above is reasonable, several aspects such as complexities in the numerical implementation of the models, ambiguity in model assumptions, and shortcomings for large Wi_R, raise the question of whether another, simpler approach could capture the essential physics and provide a quantitative account of the experimental findings on a wider range of Wi_R. One such approach is proposed in this section. It considers CCR-D in an indirect manner by accounting for the flow-induced disentanglement effect in the relaxation time of the chains, and by utilizing the dynamic tube dilution (DTD) concept [7, 79, 80] to account for constraint release. The approach uses the time marching algorithm (TMA) which provides an accurate description of the linear rheology of entangled polymers, as shown in Section II. In this work, the assessment of the proposed TMA modification focuses on the steady-state response.

More specifically, it is assumed that the shear deformation induces partial disentanglement of the chains, the latter being forced to move with the flow. Under high shear, these lost entanglements cannot be reformed if the (deeper) chain segments do not have time to diffuse against the flow, i.e. if their relaxation time is slower than the inverse shear rate. Consequently, in this case, once the chains are partially disentangled, they stay in their disentangled state as

ACCEPTED MANUSCRIPT
Journal of Rheology
This is the author's peer reviewed, accepted manuscript. However, the online version of record will be different from this version once it has been copyedited and typeset.
PLEASE CITE THIS ARTICLE AS DOI: 10.1122/8.0000280

long as the shear flow is maintained. In the following, we consider this partial disentanglement of the chains to determine the corresponding relaxation modulus and transient response of the samples (see Eq. (24a) of Table VII). While it allows us to correctly capture the steady-state viscosity of the samples, this approach is however not suitable for describing the viscosity at short times since at time *t=0* the chains are not yet deformed and are therefore fully entangled, contrary to our assumption. In order to correctly describe the short time response of the samples, one should therefore consider that a transition occurs between the initially fully entangled state of the chains and their partially entangled state, which would lead to the appearance of an overshoot in the transient predictions, as it is observed experimentally. This step being still under investigation, we only focus here on the long-time response of the samples, which allows us to fulfil our objective, i.e. to determine if assuming partial disentanglement of chains in addition to usual relaxation processes (reptation/CLF, CR) allows to correctly describe the steady viscosity.

To account for the nonlinear behavior of the samples under large shear, we propose two major modifications to the original TMA model. The starting point is the general expression of the stress relaxation modulus, used in the linear regime, see Eq. (19a) of Table VI. In Eq. (19a), $\Phi_{tube}(t)$ accounts for thermal constraint release. Since the latter mechanism, in principle, allows tube segments to explore a tube diameter that is larger than the initial tube diameter at $t = 0$, it can be thought of as DTD process. The corresponding tube diameter of this dilution process is equal to $a_0/{\Phi_{tube}}^{\alpha/2}$, with a_0 being the initial tube diameter. The scalar α is the so-called dilution exponent, which is taken equal to unity throughout this work. For monodisperse melts of linear chains, $\Phi_{tube}(t) = \varphi(t)$, where $\varphi(t)$ is the tube survival probability given by Eq. (20a) of Table VI. Note that in the original DE model, CR events are neglected and $\Phi_{tube}(t) = 1$. Usually, the reptation and CLF processes that determine $\varphi(t)$ are considered separately [6, 61]. Nevertheless, as a first minor modification to the original TMA, these two

ACCEPTED MANUSCRIPT
Journal of Rheology
This is the author's peer reviewed, accepted manuscript. However, the online version of record will be different from this version once it has been copyedited and typeset.
PLEASE CITE THIS ARTICLE AS DOI: 10.1122/8.0000280

reorientation mechanisms are merged into a single relaxation time, $\tau_d(x)$, as to simplify the $\varphi(t)$ expression. The $\tau_d(x)$ formula is given by Eq. (20b). x is a normalized curvilinear variable along half of the primitive path. A graphical representation of x can be seen in Fig. 12; CLF occur about the middle of the linear chain where $x = 1$. Importantly, the aforementioned minor modification does not alter the accuracy of the LVE TMA predictions shown in Fig. 1.

Table VI. Mathematical formalism and variables of the linear TMA.

Definition of model variables. If dimensional, units are shown in brackets.

$\eta(t)$: Shear viscosity. [Pa s]. $G(t)$: Relaxation modulus [Pa]. $G(t) \geq 0$.

$G_R(t)$: Contribution to $G(t)$ from Rouse motions. [Pa]. $G_R(t) \geq 0$.

$\varphi(t)$: Tube survival probability, i.e. the polymer fraction not relaxed by reptation and/or CLF at time *t*.

$\Phi_{tube}(t)$: Polymer fraction acting as constraint to CR/Rouse-like exploration of the tube at equilibrium. Essentially, it determines the width (lateral length) that a tube segment x can explore before its lateral motion is limited by entanglements. In general, $\Phi_{tube}(t) \neq \varphi(t)$ due to chain topology dependent CR dynamics. For linear monodisperse chains $\Phi_{tube}(t) \approx \varphi(t)$. $0 \leq \Phi_{tube}(t) \leq 1$.

$\tau_{rep}(x), \tau_{CLF}(x)$: Disentanglement time of tube segments x due to reptation and CLF, respectively. [s].

$\tau_d(x)$: Disentanglement time of tube segments x due to the combined actions of reptation and CLF. [s].

Z, N: The number of entanglements acting on the chain. The degree of polymerization of the chain.

$M_w, \tau_R(M)$: Molecular weight of the chain [g/mol]. Rouse relaxation time of the chain [s].

α: tube dilation parameter, $\alpha = 1$.

Equations:

$$G(t) = G_N^0 \varphi(t) \Phi_{tube}(t)^\alpha + G_R(t) \quad (19a), \qquad \Phi_{tube}(t) = \varphi(t) \quad (19b)$$

$$\varphi(t) = \int_0^1 \exp[-t/\tau_d(x)]\, dx \quad (20a), \qquad \tau_d(x) = \left(\tau_{CLF}(x)^{-1} + \tau_{rep}(x)^{-1}\right)^{-1} \quad (20b)$$

$$\tau_{rep}(x) = 3\, \tau_e (M_w/M_e)^3 \quad (21a)$$

$$\tau_{CLF}(x) = \begin{cases} \tau_{early}(x) = (9\pi^3/16)\, \tau_e\, [(M_w/2)/M_e]^4\, x^4, & x \leq x_{tr} \\ \tau_{CLF}(x - dx)\, \exp\left[3(M_w/2){M_e}^{-1}\, x\, (1-x)\, dx\right], & x > x_{tr} \end{cases} \quad (21b)$$

where x_{tr} is the tube coordinate where the retraction potential equals $k_B T$ [61], and $\boldsymbol{dx}$ is the increment along the tube coordinate in the code.

$$G_R(t) = (G_N^0/Z)\left[\frac{1}{4}\sum_{p=1}^{Z-1} \exp[-p^2 t/\tau_R(M_w)] + \frac{5}{4}\sum_{p=Z}^{N} \exp[-2p^2 t/\tau_R(M_w)]\right] \quad (22)$$

ACCEPTED MANUSCRIPT
Journal of Rheology
This is the author's peer reviewed, accepted manuscript. However, the online version of record will be different from this version once it has been copyedited and typeset.
PLEASE CITE THIS ARTICLE AS DOI: 10.1122/8.0000280

$$\eta(t) = \int_{-\infty}^{t} G(t')\,dt' \quad (23)$$

To describe the nonlinear shear response**,** a first major modification is proposed. As already mentioned, the underlying assumption behind the nonlinear TMA is that, in nonlinear shear flows the chains are forced to disentangle, and the molecular segments with a relaxation time $\tau_d(x)$ larger than $1/\dot{\gamma}$ are diffusing too slowly to create new entanglements. Therefore, once they are disentangled, they are moving with the flow. In this respect, their relaxation time $\tau_{rel}(x)$ must be of the order of $1/\dot{\gamma}$. Hence, $\tau_{rel}(x) = \min(\tau_d(x), \theta/\dot{\gamma})$, with θ being an unknown prefactor of order unity. Thus, in the nonlinear regime, only the chain segments close to the chain extremities are moving fast enough to relax and create new entanglements despite the shear flow. In this regime, the analogous to $\varphi(t)$ tube survival probability, $\varphi_{NLVE}(t)$, is given by Eq. (25a). The corresponding tube diameter or entanglement blob size at time *t*, a, is given by $a = a_0/\varphi_{NLVE}(t)^{\alpha/2}$. Although, Eq. (25a) encompasses the CCR idea of Marrucci [15], the present formulation implements CCR at each tube segment separately rather than at the global level of tube relaxation. From this perspective it resembles more the CCR implementation of the MLD and GLaMM models. A crucial difference with these models, however, is the assumption that not all segments that relax by CCR will be able to re-entangle, as explained above.

Table VII. Mathematical formalism and variables of the nonlinear TMA.

Definition of model variables. If dimensional, units are shown in brackets.
$G_{NLVE}(t)$: Nonlinear relaxation modulus [Pa]. $G(t) \geq 0$.
$\varphi_{NLVE}(t)$: Polymer fraction not relaxed by reptation/CLF or by the flow at time *t*. $0 \leq \varphi_{NLVE}(t) \leq 1$.
n_b: Number of shear blobs per chain. $\dot{\gamma}$ dependent.
M_b: Shear blob molecular weight, i.e. the chain molar mass enclosed within a shear blob. $\dot{\gamma}$ dependent.

ACCEPTED MANUSCRIPT
Journal of Rheology
This is the author's peer reviewed, accepted manuscript. However, the online version of record will be different from this version once it has been copyedited and typeset.
PLEASE CITE THIS ARTICLE AS DOI: 10.1122/8.0000280

ξ: The size of a shear blob. $\dot{\gamma}$ dependent. Under flow, it determines the (confinement) length-scale that a tube segment x can explore before its CR/Rouse-like motion is limited by the flow. [m]

Φ_{blob}: $\dot{\gamma}$-dependent function relating ξ to a_0, the equilibrium tube diameter: $\xi = a_0/\sqrt{\Phi_{blob}}$. $\Phi_{blob} > 0$.

$\Phi_{tube,NLVE}(t)$: Defined as the maximum value between $\varphi_{NLVE}(t)$ and Φ_{blob}. $\Phi_{tube,NLVE}(t) > 0$.

$\tau_{rel}(x)$: Relaxation time of tube segments x in the presence of flow. Defined as the minimum between the disentanglement time $\tau_d(x)$ and the inverse flow rate (approximately). [s].

M_0, τ_0, b: monomeric molar mass [g/mol], relaxation time [s] and size [m] of a Rouse (Kuhn) segment.

Equations:

$$G_{NLVE}(t) = G_N^0 \varphi_{NLVE}(t) \Phi_{tube,NLVE}(t) \quad (24a), \qquad \Phi_{tube,NLVE}(t) = \max[\, \varphi_{NLVE}(t), \Phi_{blob}\,] \quad (24b)$$

$$\varphi_{NLVE}(t) = \int_0^1 \exp[-t/\tau_{rel}(x)]\, dx \quad (25a), \qquad \tau_{rel}(x) = \min[\, \tau_d(x), \theta/\dot{\gamma}\,] \quad (25b)$$

with θ being an unknown prefactor of order unity.

$$n_b = \frac{M_w}{M_b} = \frac{\sqrt{\tau_R(M_w)/\tau_0}}{\sqrt{\tau_R(M_b)/\tau_0}} = \frac{\sqrt{\tau_R(M_w)}}{\sqrt{\tau_R(M_b)}} = \sqrt{\tau_R(M_w)\dot{\gamma}} \quad (26)$$

$$\Phi_{blob} = \frac{{a_0}^2}{\xi^2} = \frac{(M_e/M_0)b^2}{M_b b^2} = \frac{M_e}{M_b} = \frac{n_b M_e}{M_w} = \frac{\sqrt{\tau_R(M_w)\dot{\gamma}} M_e}{M_w} = \sqrt{\tau_o} M_e \sqrt{\dot{\gamma}} = \sqrt{\tau_e \dot{\gamma}} \quad (27)$$

$$\eta(t) = G_N^0 \int_{-\infty}^{t} G_{NLVE}(t')\, dt' = G_N^0 \int_{-\infty}^{t} \varphi_{NLVE}(t') \max(\, \varphi_{NLVE}(t'), \Phi_{blob}\,)\, dt' \quad (28)$$

The consequences of the first modification are illustrated in Fig. 12, where $\tau_{rel}(x)$ is plotted as a function of x. The solid line refers to $\tau_d(x)$, i.e. the LVE disentanglement time in the absence of modification, while the dashed curve represents $\tau_{rel}(x)$. This figure shows that, at this shear rate the first modification only speeds-up disentanglement of the deeper segments ($x > 0.3$) as chain extremities fluctuate fast enough to disentangle by tube escape modes (reptation, CLF) before being forced to disentangle by the flow. It is important to note that, after their relaxation, outer segments are able to re-entangle. The inner segments, i.e., $x > 0.3$ have thermal (LVE) disentanglement times that are slower than the flow time $1/\dot{\gamma}$ and therefore, once disentangled, they cannot re-entangle and are moving with the flow [80].

ACCEPTED MANUSCRIPT
Journal of Rheology
This is the author's peer reviewed, accepted manuscript. However, the online version of record will be different from this version once it has been copyedited and typeset.
PLEASE CITE THIS ARTICLE AS DOI: 10.1122/8.0000280

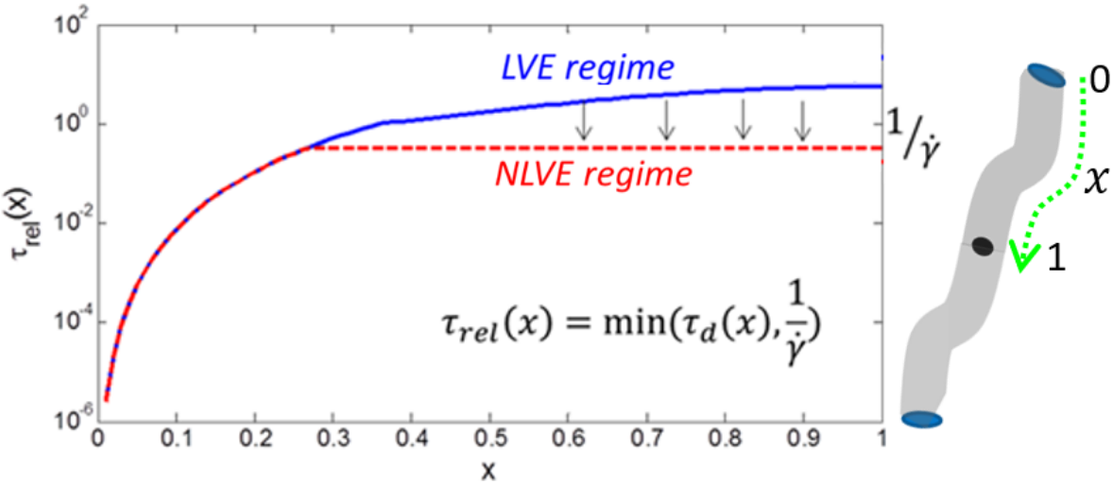

FIG. 12. Relaxation times $\tau_d(x)$ and $\tau_{rel}(x)$, given by Eqs. (20b) and (25b), respectively, plotted against the tube coordinate x. The solid line refers to $\tau_d(x)$, while the dashed curve depicts $\tau_{rel}(x)$. The model parameterization corresponds to PS2 (see Table I) and $\dot{\gamma}$ = 10 s^{-1} ($Wi_R = 3.2$). $\theta = 1$ in Eq. (25b). CLF occur about the middle of the linear chain, $x = 1$.

From Fig. 12 and Eq. (25b), i.e. $\tau_{rel}(x) = \min(\tau_d(x), \theta/\dot{\gamma})$, it becomes apparent that the chain portion which is affected by CCR increases with increasing shear rate. This behavior in turn affects the $\dot{\gamma}$ dependence of the steady-state shear viscosity. Actually, if all tube segments were relaxing at the same time, i.e., at $\theta/\dot{\gamma}$, then shear thinning would occur in the entire $\dot{\gamma}$ range and thus a power law with a slope of -1 would be always observed, i.e. $\eta_{st}(\dot{\gamma}) \propto \dot{\gamma}^{-1}$. On the contrary, by accounting for these fast relaxing chain extremities, it is expected that on lowering the shear rate, the relaxation of the chains will be more weakly accelerated, yielding a value of $\eta_{st}(\dot{\gamma})$ slightly lower than expected and consequently, a scaling $\eta_{st}(\dot{\gamma}) \propto \dot{\gamma}^{-c}$ with a smaller slope c, in agreement with experimental findings [44, 81]. It is therefore important to consider CCR for each chain portion in order to capture this effect. In literature, this is commonly accounted for by using a multimode CCR treatments as in the works of Marrucci and Ianniruberto [44, 82, 83, 84]. Notice that under fast flow, the relaxation time of the deeper segments, $\tau_{rel}(x)$, does not depend on the chain molar mass, as it is also observed

ACCEPTED MANUSCRIPT
Journal of Rheology
This is the author's peer reviewed, accepted manuscript. However, the online version of record will be different from this version once it has been copyedited and typeset.
PLEASE CITE THIS ARTICLE AS DOI: 10.1122/8.0000280

experimentally [44]: when plotted as a function of shear rate, the steady-state viscosities of monodisperse polymer melts superimpose at high $\dot{\gamma}$.

The modification discussed so far solely describes the CCR influence on chain disentanglement in the absence of stretch. However, since in the fast flow regime ($Wi_R > 1$) chains experience stretch, a second modification to the original TMA is required. Central to the second modification is the assumption that the effect of the flow is to prescribe relaxation of chain orientation at a particular length scale, ξ. ξ can be represented by a blob that depends on shear rate (which sets eventually the confinement length scale within which reorientation occurs). Hereafter, this blob will be referred to as the shear blob. This type of blob is inspired by that of Rabin and Öttinger discussed in the context of sheared dilute polymer solutions [85] and advanced by Rubinstein and Grosberg in the context of ring polymers [86]. It bears analogies to the tension or Pincus blob [68], implemented by Colby *et al.* for unentangled polymers [87].

In this respect, the flow imposes preferential orientation to a chain at length scales larger than ξ, whereas orientation of chain segments within each blob remains uncorrelated (and energy is dissipated at this length scale only). This preferential orientation is viewed herein as local stretch. Since stretch relaxation dynamics is dominated by Rouse modes, one can first estimate the size and the number of the respective shear blobs, borrowing scaling arguments from unentangled chains, and then incorporate entanglement effects into the emerging molecular picture. Following Ref. [87], n_b, the number of shear blobs per chain can be estimated according to Eq. (26) of Table VII, that is $n_b = \sqrt{\tau_R(M_w)\dot{\gamma}}$ where, $\tau_R(y)$ is the Rouse relaxation time of a chain portion having molar mass y, and. In deriving Eq. (26), the expression $\tau_R(M_b) = 1/\dot{\gamma}$ has been utilized following the aforementioned assumption, i.e., at steady state the flow prescribes orientation at the length scale of the shear blob and molecular strands within the shear blob are equilibrated (or isotopically oriented). In other words, molecular strands of

ACCEPTED MANUSCRIPT
Journal of Rheology
This is the author's peer reviewed, accepted manuscript. However, the online version of record will be different from this version once it has been copyedited and typeset.
PLEASE CITE THIS ARTICLE AS DOI: 10.1122/8.0000280

molar mass lower than M_b have Rouse relaxation times faster than $1/\dot{\gamma}$ and thus they have sufficient time to dissipate energy and equilibrate (reorient) within the shear blob. So, the Rouse time of the shear blob is simply $1/\dot{\gamma}$. From Eq. (26) it is evident that the number of shear blobs increases with increasing shear rate according to $n_b \propto \dot{\gamma}^{1/2}$. Moreover, the $\dot{\gamma}$ dependence of the blobs' size $\xi \propto {M_b}^{1/2}$ can be also estimated, $\xi \propto \dot{\gamma}^{-1/4}$.

Furthermore, ξ can be related to the equilibrium tube diameter, a_0, through $\xi = a_0/\sqrt{\Phi_{blob}}$. Using the latter expression, Φ_{blob} can be rewritten as $\Phi_{blob} = {a_0}^2/\xi^2$ or $\Phi_{blob} = M_e/M_b$ (see Eq. (27)). In this respect, Φ_{blob} is a flow rate dependent function (see Eq. (27)) that relates the size of the shear blob to the size of the (equilibrium) entanglement blob. In this representation, $\Phi_{blob} = 1$ corresponds to $M_b = M_e$ and a modulus equal to G_N^0.

To arrive to an expression for the nonlinear relaxation modulus, i.e. Eq. (24a) of Table XII, we first need to incorporate the tube notion in the shear blobs molecular picture. In the linear regime, the tube diameter defines the distance a chain can explore perpendicularly to its primitive path without feeling the entanglement effect. The effective tube diameter changes with time according to $a_0/\sqrt{\Phi_{tube}} = a_0/\sqrt{\varphi(t)}$. In the nonlinear regime, and without the stretch modification (shear blobs), the effective tube diameter would be $a = a_0/\sqrt{\varphi_{NLVE}(t)}$, where $\varphi_{NLVE}(t)$ accounts for tube escape occurred either by reptation/CLF or flow disentanglement (CCR-D). As aforementioned, an additional confinement length scale arises when considering the shear blobs, namely, the shear blob size ξ. Depending on the flow rate, three distinct cases are realized. They are illustrated schematically in Fig. 13, and are explained below.

ACCEPTED MANUSCRIPT
Journal of Rheology
This is the author's peer reviewed, accepted manuscript. However, the online version of record will be different from this version once it has been copyedited and typeset.
PLEASE CITE THIS ARTICLE AS DOI: 10.1122/8.0000280

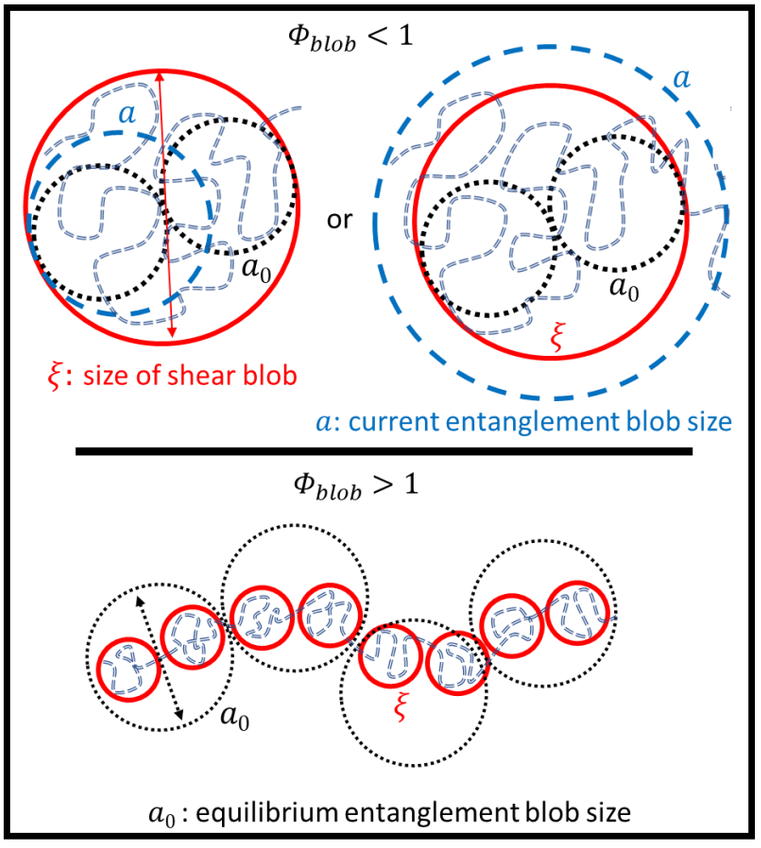

FIG. 13. Schematic illustration of the blob picture discussed in the context of stretch modification of the TMA model. Depending on $\dot{\gamma}$, three main cases are realized. At relatively low rates $\xi > a > a_0$ and Φ_{blob}<1 (upper, left). Here, a sets the DTD confinement length scale. At higher rates, but slower than $1/\tau_e$, $a > \xi > a_0$ and Φ_{blob}<1 (upper, right). Here, ξ sets the DTD confinement length scale. At $\dot{\gamma} > 1/\tau_e$, $a > a_0 > \xi$ and Φ_{blob}>1 (bottom). Although ξ sets the DTD confinement length scale, DTD is essentially suppressed.

The first case is realized at low shear rates. (See Fig. 13 upper left.) Since $\Phi_{blob} = \sqrt{\tau_e \dot{\gamma}}$, here, Φ_{blob} is less than one and relatively low, meaning that ξ is larger than a_0 (recall $\xi = a_0/\sqrt{\Phi_{blob}}$.) In this regime, ξ is also larger than the effective (time-dependent) tube diameter which varies due to chain disentanglement via reptation/CLF or the flow itself (i.e. CCR-D). That is, $\xi > a$, where $a = a_0/\sqrt{\varphi_{NLVE}(t)}$. Therefore, in the time interval $1/\dot{\gamma}$, the confinement

ACCEPTED MANUSCRIPT
Journal of Rheology
This is the author's peer reviewed, accepted manuscript. However, the online version of record will be different from this version once it has been copyedited and typeset.
PLEASE CITE THIS ARTICLE AS DOI: 10.1122/8.0000280

length within which the chain can renew its orientation via Rouse-like constraint release modes (DTD) is simply a; at low rates the stretch modification is irrelevant, as expected, therefore the shear blob does not impose any reorientation restriction.

The second case is realized as $\dot{\gamma}$ increases further but Φ_{blob} remains still below one. In this flow regime and above a certain $\dot{\gamma}$ value, the DTD confinement length imposed by a will surpass ξ (see Fig. 13 upper right.). This is because in such a situation more chain segments become disentangled by the flow (CCR-D). Here, the size of the shear blobs is larger than the size of the (equilibrium) entanglement blobs but smaller than that of the effective blobs a. Hence, the shear blobs set the limit of the DTD effect. In this flow regime, the stretch modification of the TMA is important. That is, depending on $\dot{\gamma}$, Φ_{blob} has a moderate to significant effect on the stress relaxation modulus. This molecular picture for this second regime is valid up to $\dot{\gamma} = 1/\tau_e$.

At even faster rates, i.e. $\dot{\gamma} > 1/\tau_e$, Φ_{blob} >1. Here, the flow-limited tube diameter (shear blob) is smaller compared to the initial tube diameter (i.e. $M_b < M_e$) (see Fig. 13 bottom). As in case two above, the shear blobs set the confinement length scale within which CR-Rouse reorientation (DTD) occurs. Nevertheless, CR-Rouse relaxation is essentially suppressed in this regime as the blob size is small; the chains are stretched even within the equilibrium entanglement blob. Nevertheless, it is important to note that this regime is typically not reached in experiments, and certainly not in the experimental data considered in this work.

The aforedescribed interdependence of dynamic tube dilution (DTD), flow-driven disentanglement (CCR-D) and chain stretch, can be cast into a single equation, namely $\Phi_{tube,NLVE}(t) = \max(\varphi_{NLVE}(t), \Phi_{\text{blob}})$, where $\Phi_{tube,NLVE}(t)$ is analogous to the constraint release function $\Phi_{tube}(t)$ in the nonlinear flow regime. Having defined $\Phi_{tube,NLVE}(t)$, the nonlinear stress relaxation modulus, $G_{NLVE}(t)$, can be defined by Eq. (24a) of Table VII. Equation (24a) accounts for both CCR-D and stretch in a consistent way. Using this equation,

ACCEPTED MANUSCRIPT
Journal of Rheology
This is the author's peer reviewed, accepted manuscript. However, the online version of record will be different from this version once it has been copyedited and typeset.
PLEASE CITE THIS ARTICLE AS DOI: 10.1122/8.0000280

the shear viscosity at time t (associated with dissipation up to t) can be calculated according to Eq. (28) of Table VII. Notice that the nonlinear TMA does not account for the Rouse contribution to the viscosity as it will affect the early time response of the predictions which is not of prime interest in this study.

Figure 14 compares the predictions of the modified TMA (Eq. (28)) and the experimental data. Model predictions without accounting for the existence of a maximum shear blob are obtained using $\Phi_{tube,NLVE}(t) = \varphi_{NLVE}(t)$ in Eq. (24a). Thus, the disparity between the predictions obtained with and without accounting for Φ_{blob} at $W_R > 1$ signifies the role of the stretch function in limiting the DTD effect with Φ_{blob}. In this respect, compared to its absence, predictions obtained by accounting for Φ_{blob} exhibit higher steady-state viscosities as a result of the smaller confinement length within which Rouse-like constraint release equilibration may occur (chain stretch is considered by the shrinking of the flow-limited tube diameter, i.e. an increase of Φ_{blob}). Focusing on the comparison of the latter against experimental data, it is observed that the steady state viscosities of all samples for all shear rates are well described. However, this is only possible if the θ value in Eq. (25b) is slightly larger than unity. In particular, all predictions displayed in Fig. 14 are obtained with $\theta = 1.45$. In fact, very similar steady-state predictions are obtained with θ values in the range 1.25 to 1.45. Nevertheless, it would not seem sensible to assign great significance to the exact θ values at present since polymer chains with a much larger range of molar masses should be tested. The important aspect here is that such prefactor should be close to unity for the (scaling) model to hold, which seems to be the case.

ACCEPTED MANUSCRIPT
Journal of Rheology
This is the author's peer reviewed, accepted manuscript. However, the online version of record will be different from this version once it has been copyedited and typeset.
PLEASE CITE THIS ARTICLE AS DOI: 10.1122/8.0000280

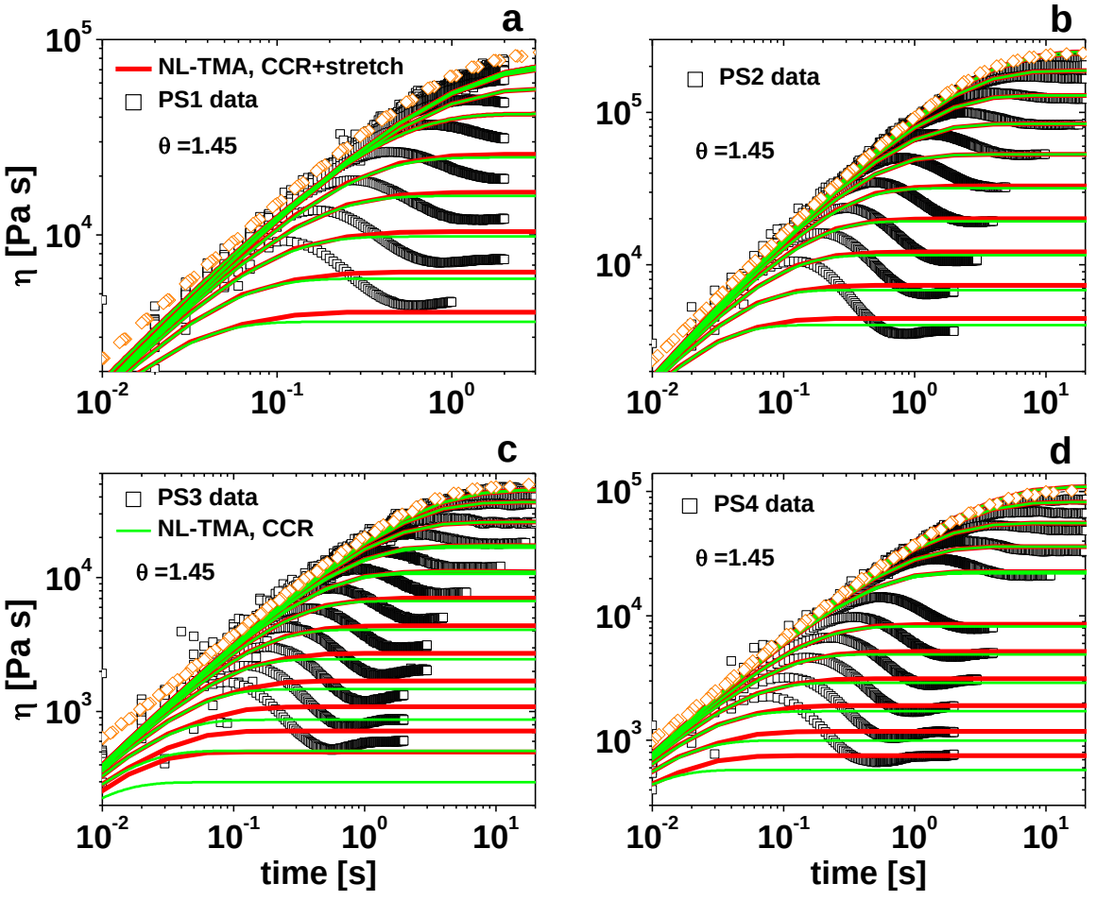

FIG. 14. Comparison of the nonlinear TMA predictions and the experimental data for PS melts and solutions (as identified in each panel). Red (thick) and green (thin) lines correspond to TMA predictions obtained with and without the stretch modification. In all cases, the θ value in Eq. (25b) is 1.45. Squares represent data. Diamonds are the SAOS PS data shown in Fig. 1, using the conversion $|\eta^*(\omega)| = \eta(\dot{\gamma} \to 0, t = 1/\omega)$. (Color online.)

The very satisfactory agreement between model predictions and data for steady-state shear viscosities at different shear rates points to the importance of accounting for the inter-dependence of constraint release and flow. Indeed, a specificity of the present model is the control of thermal constraint release in coordination with the stretch state of the chains, as achieved through Eq. (17). In other words, both the time (or thermal) and flow effects are accounted for in the same function, $\Phi_{tube,NLVE}(t)$, which determines the confinement length,

ACCEPTED MANUSCRIPT
Journal of Rheology
This is the author's peer reviewed, accepted manuscript. However, the online version of record will be different from this version once it has been copyedited and typeset.
PLEASE CITE THIS ARTICLE AS DOI: 10.1122/8.0000280

which is limited either by the time (with $\Phi_{tube,NLVE}(t) \geq \varphi_{NLVE}(t)$) or by the flow (with $\Phi_{tube,NLVE}(t) \geq \Phi_{blob}$).

As already mentioned, in the model, the viscosity overshoot at intermediate and moderately fast rates is viewed as a transition from a fully entangled state (corresponding to the linear envelop) to a partly entangled state (corresponding to the predictions obtained with Eq. (24a)). At faster rates, the same picture holds but the influence of the stretch function Φ_{blob} is more pronounced in the level of the steady viscosity. The current model version suffers of two drawbacks. First, it overlooks the fact that chain dynamics of entangled linear chains are not self-similar above the entanglement molecular weight [86]. In this respect, Eq. (26) for unentangled chains is utilized in the entire N regime, not only for $N < N_e$. The necessity to use a $\theta \neq 1$ value might originate from this limitation. Second, the model excludes the transient regime. Despite these limitations the good model performance lends support to the notion that a successfully description of the nonlinear shear dynamics of entangled linear chains can emerge from a shear blob molecular picture, as is the case for entangled rings [86].

V. CONCLUSIONS

We have systematically assessed the performance of the GLaMM model by comparing its predictions with experimental data on well characterized, nearly monodisperse, entangled solutions and melts of linear polystyrene. In this context, we have also incorporated FENE into the GLaMM model. Since nonlinear models require knowledge of linear viscoelastic parameters, the respective master curves of the used samples were first predicted by the time marching algorithm (TMA).

The findings of the current work confirm the good performance of the model in the $Wi_R < 10$ regime. They also highlight the limitations of the model at severely fast flows ($Wi_R > 10$). In this regime, FENE implementation benefits the model by narrowing the rather large

ACCEPTED MANUSCRIPT
Journal of Rheology
This is the author's peer reviewed, accepted manuscript. However, the online version of record will be different from this version once it has been copyedited and typeset.
PLEASE CITE THIS ARTICLE AS DOI: 10.1122/8.0000280

overshoots seen in FENE exclusive predictions. Model predictions are sensitive to the parameterization and the implementation of CLF contribution to the retraction rate. In this respect, the model overpredicts the overshoot and steady viscosities in several occasions. Such comparisons suggest that the model would benefit from the implementation of CCR-D. The model would also benefit from the incorporation of chain tumbling as it would provide a sound molecular mechanism for the viscosity undershoots at fast shear rates.

CCR-D is considered in a modified version of the TMA that is proposed for the steady-state regime. Our results show unequivocally that the nonlinear TMA model reproduces the experimental steady-state viscosities accurately for all samples and shear rates examined. The model builds-up on the concept of shear blobs and highlights its significance, in line with recent developments in the literature. Moreover, the modeling results emphasize the importance of coupling different relaxation mechanisms such as CCR, stretch, and DTD. As a future perspective, the nonlinear TMA approach will be extended to the transient regime.

SUPPLEMENTARY MATERIAL

The supplementary material contains Table S1 which reports the values of the experimentally achieved shear rates and the corresponding Weissenberg numbers. Moreover, it contains information about the boundary conditions treatment of the GLaMM numerical implementation. It also discusses aspects regarding the FENE outcomes of the GLaMM model.

ACKNOWLEDGMENTS

H.T., L.G.D.H, and E.v.R. thank the Fonds National de la Recherche Scientifique - FNRS for financial support. This work has benefited from useful discussions with R.S. Graham, H. Watanabe, J. D. Schieber, M. Rubinstein and A. Y. Grosberg. The authors are grateful to David. W. Mead for providing them with his GLaMM code that implements the wedge domain

ACCEPTED MANUSCRIPT
Journal of Rheology
This is the author's peer reviewed, accepted manuscript. However, the online version of record will be different from this version once it has been copyedited and typeset.
PLEASE CITE THIS ARTICLE AS DOI: 10.1122/8.0000280

solution. Computational resources were provided by the supercomputing facilities of the Université catholique de Louvain (CISM/UCL) and the Consortium des Équipements de Calcul Intensif (CECI).

References

[1] P. G. de Gennes, "Reptation of a polymer chain in the presence of fixed obstacles," *J. Chem. Phys.,* vol. 55, no. 2, p. 572–579, 1971.

[2] M. Doi and S. F. Edwards, The Theory of Polymer Dynamics, Oxford: Oxford University Press, 1986.

[3] S. T. Milner and T. C. B. McLeish, "Reptation and Contour-Length Fluctuations in Melts of Linear Polymers," *Phys. Rev. Lett. ,* vol. 81, no. 3, pp. 725-728, 1998.

[4] A. E. Likhtman and T. C. B. McLeish, "Quantitative Theory for Linear Dynamics of Linear Entangled Polymers," *Macromolecules,* vol. 35, no. 16, pp. 6332-6343, 2002.

[5] T. C. B. McLeish, "Tube theory of entangled polymer dynamics," *Adv. Phys.,* vol. 51, no. 6, p. 1379–1527, 2002.

[6] E. van Ruymbeke, R. Keunings and C. Bailly, "Prediction of linear viscoelastic properties for polydisperse mixtures of entangled star and linear polymers: Modified tube-based model and comparison with experimental results," *J. Non-Newton. Fluid Mech.,* vol. 128, no. 1, pp. 7-22, 2005.

[7] E. van Ruymbeke, Y. Masubuchi and H. Watanabe, "Effective Value of the Dynamic Dilution Exponent in Bidisperse Linear Polymers: From 1 to 4/3," *Macromolecules,* vol. 45, no. 4, p. 2085−2098, 2012.

[8] Wang and S, Nonlinear Polymer Rheology: Macroscopic Phenomenology and Molecular Foundation, Hoboken, NJ: Wiley, 2018.

[9] M. Bercea, C. Peiti, B. Simionescu and P. Navard, "Shear rheology of semidilute poly(methyl methacrylate) solutions," *Macromolecules,* vol. 26, no. 25, p. 7095–7096, 1993.

[10] C. Pattamaprom and R. G. Larson, "Constraint Release Effects in Monodisperse and Bidisperse Polystyrenes in Fast Transient Shearing Flows," *Macromolecules,* vol. 34, no. 15, pp. 5229-5237, 2001.

ACCEPTED MANUSCRIPT
Journal of Rheology
This is the author's peer reviewed, accepted manuscript. However, the online version of record will be different from this version once it has been copyedited and typeset.
PLEASE CITE THIS ARTICLE AS DOI: 10.1122/8.0000280

[11] P. Tapadia and S. Q. Wang, "Nonlinear flow behavior of entangled polymer solutions: Yieldlike entanglement-disentanglement transition," *Macromolecules,* vol. 37, no. 24, p. 9083–9095, 2004.

[12] D. Pearson, E. Herbolzheimer, N. Grizzuti and G. Marrucci, "Transient Behavior of Entangled Polymers at High Shear Rates," *J. Polym. Sci. B Polym. Phys. ,* vol. 29, no. 13, pp. 1589-1597, 1991.

[13] D. W. Mead and L. G. Leal, "The reptation model with segmental stretch," *Rheol. Acta,* vol. 34, no. 4, p. 339–359, 1995.

[14] D. W. Mead, D. Yavich and L. G. Leal, "The reptation model with segmental stretch," *Rheol Acta,* vol. 34, no. 4, p. 360–383, 1995.

[15] G. Marrucci, "Dynamics of entanglements: A nonlinear model consistent with the cox-merz rule," *J. Non-Newton. Fluid Mech.,* vol. 62, no. 2-3, pp. 279-289, 1996.

[16] D. W. Mead, R. G. Larson and M. Doi, "A Molecular Theory for Fast Flows of Entangled Polymers," *Macromolecules,* vol. 31, no. 22, p. 7895–7914, 1998.

[17] X. Ye, R. G. Larson, C. Pattamaprom and T. Sridhar, "Extensional properties of monodisperse and bidisperse polystyrene solutions," *J. Rheol.,* vol. 47, no. 2, pp. 443-468, 2003.

[18] T. Isaki, M. Takahashi and O. Urakawa, "Biaxial damping function of entangled monodisperse polystyrene melts: Comparison with the Mead–Larson–Doi model," *J. Rheol.,* vol. 47, no. 5, pp. 1201-1210, 2003.

[19] T. Schweizer, J. van Meerveld and H. C. Ottinger, "Nonlinear shear rheology of polystyrene melt with narrow molecular weight distribution-Experiment and theory," *J. Rheol.,* vol. 48, no. 6, pp. 1345-1363, 2004.

[20] S. T. Milner, T. C. B. McLeish and A. E. Likhtman, "Microscopic theory of convective constraint release," *J. Rheol.,* vol. 45, no. 2, pp. 539-563, 2001.

[21] C. Baig, V. G. Mavrantzas and M. Kroger, "Flow Effects on Melt Structure and Entanglement Network of Linear Polymers: Results from a Nonequilibrium Molecular Dynamics Simulation Study of a Polyethylene Melt in Steady Shear," *Macromolecules,* vol. 43, no. 16, p. 6886–6902, 2010.

[22] G. Ianniruberto and G. Marrucci, "Convective constraint release (CCR) revisited," *J. Rheol.,* vol. 58, no. 1, pp. 89-102, 2014.

[23] M. Andreev, R. N. Khaliullin, R. J. A. Steenbakkers and J. D. Schieber, "Approximations of the discrete slip-link model and their effect on nonlinear rheology predictions," *J. Rheol.,* vol. 57, no. 2, pp. 535-557, 2013.

Journal of Rheology ACCEPTED MANUSCRIPT
This is the author's peer reviewed, accepted manuscript. However, the online version of record will be different from this version once it has been copyedited and typeset.
PLEASE CITE THIS ARTICLE AS DOI: 10.1122/8.0000280

[24] L. G. D. Hawke, Q. Huang, O. Hassager and D. J. Read, "Modifying the pom-pom model for extensional viscosity overshoots," *J. Rheol.,* vol. 59, no. 4, pp. 995-1017, 2015.

[25] D. W. Mead, N. Banerjee and J. Park, "A constitutive model for entangled polymers incorporating binary entanglement pair dynamics and a configuration dependent friction coefficient," *J. Rheol.,* vol. 59, no. 2, pp. 335-363, 2015.

[26] M. H. Nafar Sefiddashti, B. J. Edwards and B. Khomami, "Individual chain dynamics of a polyethylene melt undergoing steady shear flow," *J. Rheol.,* vol. 59, no. 1, pp. 119-153, 2015.

[27] C. McIlroy and P. D. Olmsted, "Deformation of an amorphous polymer during the fused-filament-fabrication method for additive manufacturing," *J. Rheol.,* vol. 61, no. 2, p. 379, 2017.

[28] Y. Masubuchi, G. Ianniruberto and G. Marrucci, "Stress Undershoot of Entangled Polymers under Fast Startup Shear Flows in Primitive Chain Network Simulations," *Nihon Reoroji Gakk,* vol. 46, no. 1, pp. 23-28, 2018.

[29] M. H. Nafar Sefiddashti, B. J. Edwards and B. Khomani, "Elucidating the Molecular Rheology of Entangled Polymeric Fluids via Comparison of Atomistic Simulations and Model Predictions," *Macromolecules,* vol. 52, no. 21, p. 8124–8143, 2019.

[30] R. S. Graham, A. E. Likhtman, T. C. B. McLeish and S. T. Milner, "Microscopic theory of linear, entangled polymer chains under rapid deformation including chain stretch and convective constraint release," *J. Rheol.,* vol. 47, no. 5, pp. 1171-1200, 2003.

[31] D. Auhl, J. Ramirez, A. E. Likhtman, P. Chambon and C. Fernyhough, "Linear and nonlinear shear flow behavior of monodisperse polyisoprene melts with a large range of molecular weights," *J. Rheol.,* vol. 52, no. 3, pp. 801-835, 2008.

[32] M. Anwar and R. S. Graham, "Nonlinear shear of entangled polymers from nonequilibrium molecular dynamics," *J. Polym. Sci. Part B: Polym. Phys.,* vol. 57, no. 24, pp. 1692-1704, 2019.

[33] D. J. Read, "Convective constraint release with chain stretch: Solution of the rouse-tube model in the limit of infinite tubes," *J. Rheol.,* vol. 48, no. 2, p. 349–377, 2004.

[34] T. Yaoita, T. Isaki, Y. Masubuchi, H. Watanabe, G. Ianniruberto, F. Greco and G. Marrucci, "Statics, linear, and nonlinear dynamics of entangled polystyrene melts simulated through the primitive chain network model," *J. Chem. Phys.,* vol. 128, no. 15, p. 154901, 2008.

[35] Y. Masubuchi and H. Watanabe, "Origin of Stress Overshoot under Start-up Shear in Primitive Chain Network Simulation," *ACS Macro Lett.,* vol. 3, no. 11, pp. 1183-1186, 2014.

[36] W. W. Graessley, "Molecular Entanglement Theory of Flow Behavior in Amorphous Polymers," *J. Chem. Phys.,* vol. 43, no. 8, pp. 2696-2703, 1965.

ACCEPTED MANUSCRIPT
Journal of Rheology
This is the author's peer reviewed, accepted manuscript. However, the online version of record will be different from this version once it has been copyedited and typeset.
PLEASE CITE THIS ARTICLE AS DOI: 10.1122/8.0000280

[37] V. A. H. Boudara, J. D. Peterson, L. G. Leal and D. J. Read, "Nonlinear rheology of polydisperse blends of entangled linear polymers: Rolie-Double-Poly models," *J. Rheol.,* vol. 63 , no. 1, pp. 71-91, 2019.

[38] D. W. Mead, S. Monjezi and J. Park, "A constitutive model for entangled polydisperse linear flexible polymers with entanglement dynamics and a configuration dependent friction coefficient. Part I: Model derivation," *J. Rheol. ,* vol. 62, no. 1, pp. 121-134, 2017.

[39] J. M. Kim, B. J. Edwards, D. J. Keffer and B. Khomami, "Single-chain dynamics of linear polyethylene liquids under shear flow," *Phys. Lett. A ,* vol. 373, no. 7, p. 769–772, 2009.

[40] D. E. Smith, H. P. Babcock and S. Chu, "Single-Polymer Dynamics in Steady Shear Flow," *Science,* vol. 283, no. 5408, pp. 1724-1727, 1999.

[41] R. E. Teixeira, H. P. Babcock, E. S. G. Shaqfeh and S. Chu, "Shear Thinning and Tumbling Dynamics of Single Polymers in the Flow-Gradient Plane," *Macromolecules,* vol. 38, no. 2, p. 581–592, 2005.

[42] C. M. Schroeder, R. E. Teixeira, E. S. G. Shaqfeh and S. Chu, "Characteristic Periodic Motion of Polymers in Shear Flow," *Phys. Rev. Lett.,* vol. 95, no. 1, p. 018301, 2005.

[43] R. E. Teixeira, A. K. Dambal, D. H. Richter, E. S. G. Shaqfeh and S. Chu, "The Individualistic Dynamics of Entangled DNA in Solution," *Macromolecules,* vol. 40, no. 7, pp. 2461-2476, 2007.

[44] S. Costanzo, Q. Huang, G. Ianniruberto, G. Marrucci, O. Hassager and D. Vlassopoulos, "Shear and extensional rheology of polystyrene melts and solutions with the same number of entanglements," *Macromolecules,* vol. 49, no. 10, pp. 3925-3935, 2016.

[45] G. Ianniruberto and G. Marrucci, "On compatibility of the Cox-Merz rule with the model of Doi and Edwards," *J. Non-Newton. Fluid Mech.,* vol. 65, no. 2-3, pp. 241-246, 1996.

[46] G. Ianniruberto and G. Marrucci, "Convective orientational renewal in entangled polymers," *J. Non-Newton. Fluid Mech.,* vol. 95, no. 2-3, p. 363–374, 2000.

[47] G. Ianniruberto, " Extensional Flows of Solutions of Entangled Polymers Confirm Reduction of Friction Coefficient," *Macromolecules,* vol. 48, no. 17, p. 6306– 6312, 2015.

[48] P. S. Stephanou, T. Schweizer and M. Kröger, "Communication: Appearance of undershoots in start-up shear: Experimental findings captured by tumbling-snake dynamics," *J. Chem. Phys.,* vol. 146, no. 16, p. 161101, 2017.

[49] R. B. Bird, R. C. Armstrong and O. Hassager, Dynamics of Polymeric Liquids: Volume 2, Kinetic Theory, New York: John Wiley & Sons, 1987.

[50] P. S. Stephanou and M. Kröger, "Solution of the complete Curtiss-Bird model for polymeric liquids subjected to simple shear flow," *J. Chem. Phys.,* vol. 144, no. 12, p. 124905, 2016.

ACCEPTED MANUSCRIPT
Journal of Rheology
This is the author's peer reviewed, accepted manuscript. However, the online version of record will be different from this version once it has been copyedited and typeset.
PLEASE CITE THIS ARTICLE AS DOI: 10.1122/8.0000280

[51] J. Cao and A. E. Likhtman, "Simulating Startup Shear of Entangled Polymer Melts," *ACS Macro Lett.,* vol. 4, no. 12, p. 1376–1381, 2015.

[52] S. J. Xie and K. S. Schweizer, "Consequences of Delayed Chain Retraction on the Rheology and Stretch Dynamics of Entangled Polymer Liquids under Continuous Nonlinear Shear Deformation," *Macromolecules,* vol. 51, no. 11, p. 4185–4200, 2018.

[53] S. Wang, Y. Wang, S. Cheng, X. Li, X. Zhu and H. Sun, "New Experiments for Improved Theoretical Description of Nonlinear Rheology of Entangled Polymers," *Macromolecules,* vol. 46, no. 8, p. 3147–3159, 2013.

[54] H.-P. Hsu and K. Kremer, "Primitive Path Analysis and Stress Distribution in Highly Strained Macromolecules," *ACS Macro Lett.,* vol. 7, no. 1, pp. 107-111, 2018.

[55] H.-P. Hsu and K. Kremer, "Chain Retraction in Highly Entangled Stretched Polymer Melts," *Phys. Rev. Lett.,* vol. 121, no. 16, p. 167801, 2018.

[56] H.-P. Hsu and K. Kremer, "Clustering of Entanglement Points in Highly Strained Polymer Melts," *Macromolecules,* vol. 52, no. 17, pp. 6756-6772, 2019.

[57] S. Ravindranath and S. Q. Wang, "Steady state measurements in stress plateau region of entangled polymer solutions: Controlled-rate and controlled-stress modes," *J. Rheol.,* vol. 52, no. 4, pp. 957-980, 2008.

[58] F. Snijkers and D. Vlassopoulos, "Cone-partitioned-plate geometry for the ARES rheometer with temperature control," *J. Rheol.,* vol. 55, no. 6, p. 1167{1186, 2011.

[59] T. Schweizer and W. Schmidheiny, "A cone-partitioned plate rheometer cell with three partitions (CPP3) to determine shear stress and both normal stress differences for small quantities of polymeric fluids," *J. Rheol.,* vol. 57, no. 3, pp. 841-856, 2013.

[60] S. Costanzo, G. Ianniruberto, G. Marrucci and D. Vlassopoulos, "Measuring and assessing first and second normal stress differences of polymeric fluids with a modular cone-partitioned plate geometry," *Rheol. Acta,* vol. 57, no. 5, pp. 363-376, 2018.

[61] V. Shchetnikava, J. J. M. Slot and E. van Ruymbeke, "A comparison of tube model predictions of the linear viscoelastic behavior of symmetric star polymer melts," *Macromolecules,* vol. 47, no. 10, p. 3350–3361, 2014.

[62] C. H. R. M. Wilsens, L. G. D. Hawke, E. M. Troisi, D. Hermida-Merino, G. de Kort, N. Leoné, K. Saralidze, G. W. M. Peters and S. Rastogi, "Effect of Self-Assembly of Oxalamide Based Organic Compounds on Melt Behavior, Nucleation, and Crystallization of Isotactic Polypropylene," *Macromolecules,* vol. 51, no. 13, pp. 4882-4895, 2018.

[63] C. H. R. M. Wilsens, L. G. D. Hawke, G. W. de Kort, S. Saidi, M. Roy, N. Leoné, D. Hermida-Merino, G. W. M. Peters and S. Rastogi, "Effect of Thermal History and Shear on the

ACCEPTED MANUSCRIPT
Journal of Rheology
This is the author's peer reviewed, accepted manuscript. However, the online version of record will be different from this version once it has been copyedited and typeset.
PLEASE CITE THIS ARTICLE AS DOI: 10.1122/8.0000280

Viscoelastic Response of iPP Containing an Oxalamide-Based Organic Compound," *Macromolecules,* vol. 52, no. 7, p. 2789–2802, 2019.

[64] L. G. D. Hawke, D. Romano and S. Rastogi, "Nonequilibrium Melt State of Ultra-High-Molecular-Weight Polyethylene: A Theoretical Approach on the Equilibrium Process," *Macromolecules,* vol. 52, no. 22, p. 8849–8866, 2019.

[65] S. J. Park, P. S. Desai, X. Chen and R. G. Larson, "Universal Relaxation Behavior of Entangled 1,4-Polybutadiene Melts in the Transition Frequency Region," *Macromolecules,* vol. 48, no. 12, pp. 4122-4131, 2015.

[66] T. Shahid, Q. Huang, F. Oosterlinck, C. Clasen and E. Van Ruymbeke, "Dynamic dilution exponent in monodisperse entangled polymer solutions," *Soft Matter,* vol. 13, no. 1, pp. 269-282, 2017.

[67] H. Lentzakis, S. Costanzo, D. Vlassopoulos, R. H. Colby, D. J. Read, H. Lee and E. Van Ruymbeke, "Constraint release mechanisms for H-polymers moving in linear matrices of varying molar masses," *Macromolecules,* vol. 52, no. 8, pp. 3010-3028, 2019.

[68] M. Rubinstein and R. H. Colby, Polymer Physics, Oxford: Oxford University Press, 2003.

[69] V. A. H. Boudara, D. J. Read and J. Ramírez, "reptate rheology software: Toolkit for the analysis of theories and experiments," *J. Rheol.,* vol. 64, no. 3, pp. 709-722, 2020.

[70] M. Kröger and S. Hess, "Viscoelasticity of polymeric melts and concentrated solutions. The effect of flow-induced alignment of chain ends," *PHYSICA A,* vol. 195, no. 3–4, pp. 336-353, 1993.

[71] M. Kröger, "Simple, admissible, and accurate approximants of the inverse Langevin and Brillouin functions, relevant for strong polymer deformations and flows," *J. Non-Newton. Fluid Mech.,* vol. 223, pp. 77-87, 2015.

[72] E. V. Menezes and W. W. Graessley, "Nonlinear rheological behavior of polymer systems for several shear-flow histories," *J. Polym. Sci., Part B: Polym. Phys.,* vol. 20, no. 10, pp. 1817-1833, 1982.

[73] D. J. Read, K. Jagannathan and A. E. Likhtman, "Entangled Polymers: Constraint Release, Mean Paths, and Tube Bending Energy," *Macromolecules,* vol. 41, no. 18, pp. 6843-6853, 2008.

[74] M. Kröger, "Shortest multiple disconnected path for the analysis of entanglements in two-and three-dimensional polymeric systems.," *Comput. Phys. Commun.,* vol. 168, no. 3, p. 209−232, 2005.

[75] N. C. Karayiannis and M. Kröger, "Combined molecular algorithms for the generation, equilibration and topological analysis of entangled polymers: methodology and performance," *Int. J. Mol. Sci. ,* vol. 10, no. 11, p. 5054−5089, 2009.

ACCEPTED MANUSCRIPT
Journal of Rheology
This is the author's peer reviewed, accepted manuscript. However, the online version of record will be different from this version once it has been copyedited and typeset.
PLEASE CITE THIS ARTICLE AS DOI: 10.1122/8.0000280

[76] S. Shanbhag and M. Kröger, "Primitive path networks generated by annealing and geometrical methods: insights into differences," *Macromolecules,* vol. 40, no. 8, p. 2897−2903, 2007.

[77] C. Tzoumanekas and D. N. Theodorou, "Topological Analysis of Linear Polymer Melts: A Statistical Approach," *Macromolecules ,* vol. 39 , no. 13, p. 4592–4604, 2006 .

[78] R. Everaers, S. K. Sukumaran, G. S. Grest, C. Svaneborg, A. Sivasubramanian and K. Kremer, "Rheology and microscopic topology of entangled polymeric liquids," *Science,* vol. 303, no. 5659, pp. 823-826, 2004.

[79] S. T. Milner and T. C. B. McLeish, "Parameter-Free Theory for Stress Relaxation in Star Polymer Melts," *Macromolecules,* vol. 30, no. 7, p. 2159–2166, 1997.

[80] H. Watanabe, S. Ishida and Y. Matsumiya, "Rheodielectric Behavior of Entangled cis-Polyisoprene under Fast Shear," *Macromolecules,* vol. 35, no. 23, p. 8802–8818, 2002.

[81] F. Snijkers and D. Vlassopoulos, "Appraisal of the Cox-Merz rule for well-characterized entangled linear and branched polymers," *Rheol. Acta,* vol. 53, no. 12, p. 935–946, 2014.

[82] E. Somma, O. Valentino, G. Titomanlio and G. Ianniruberto, "Parallel superposition in entangled polydisperse polymer melts: Experiments and theory," *J. Rheol.,* vol. 51, no. 5, pp. 987-1005, 2007.

[83] G. Ianniruberto, "Quantitative appraisal of a new CCR model for entangled linear," *J. Rheol.,* vol. 57, no. 1, pp. 211-235, 2015.

[84] G. Ianniruberto and G. Marrucci, "Shear banding in Doi–Edwards fluids," *J. Rheol.,* vol. 61, no. 1, pp. 93-106, 2017.

[85] Y. Rabin and H. C. Öttinger, "Dilute Polymer Solutions: Internal Viscosity, Dynamic Scaling, Shear Thinning and Frequency-Dependent Viscosity," *EPL,* vol. 13, no. 5, pp. 423-428, 1990.

[86] D. Parisi, S. Costanzo, Y. Jeong, J. Ahn, T. Chang, D. Vlassopoulos, J. D. Halverson, K. Kremer, T. Ge, M. Rubinstein, G. S. Grest, W. Srinin and A. Y. Grosberg, "Nonlinear Shear Rheology of Entangled Polymer Rings," *Macromolecules,* vol. 54, no. 6, pp. 2811-2827, 2021.

[87] R. H. Colby, D. C. Boris, W. E. Krause and S. Dou, "Shear thinning of unentangled flexible polymer liquids," *Rheol. Acta,* vol. 46, no. 5, p. 569–575, 2007.

ACCEPTED MANUSCRIPT
Journal of Rheology
This is the author's peer reviewed, accepted manuscript. However, the online version of record will be different from this version once it has been copyedited and typeset.
PLEASE CITE THIS ARTICLE AS DOI: 10.1122/8.0000280

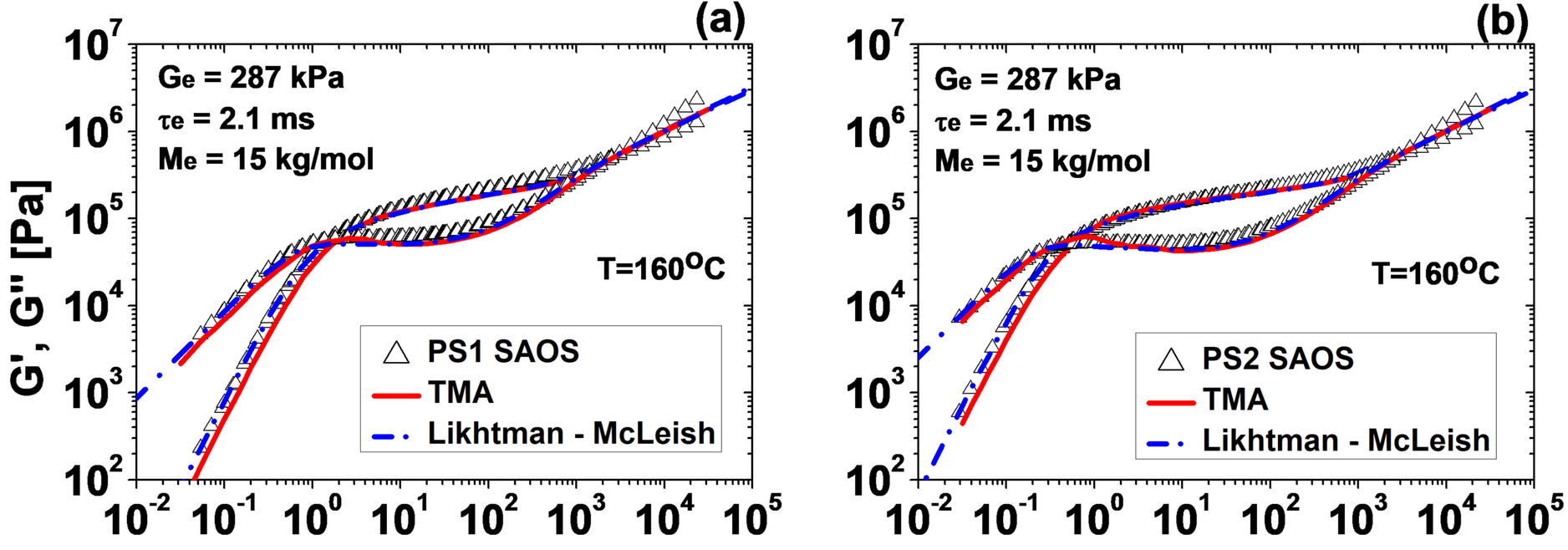

ACCEPTED MANUSCRIPT

Journal of Rheology

This is the author's peer reviewed, accepted manuscript. However, the online version of record will be different from this version once it has been copyedited and typeset.
PLEASE CITE THIS ARTICLE AS DOI: 10.1122/8.0000280

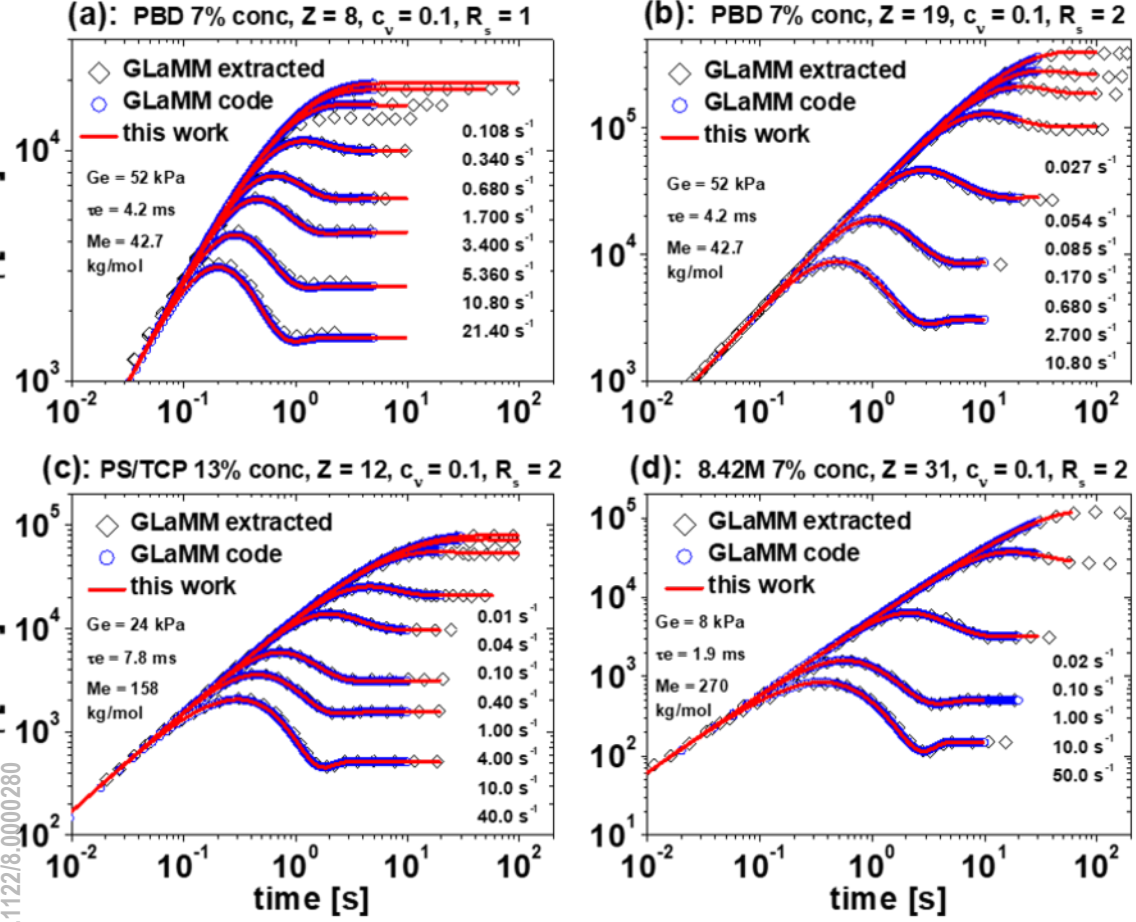

ACCEPTED MANUSCRIPT

Journal of Rheology

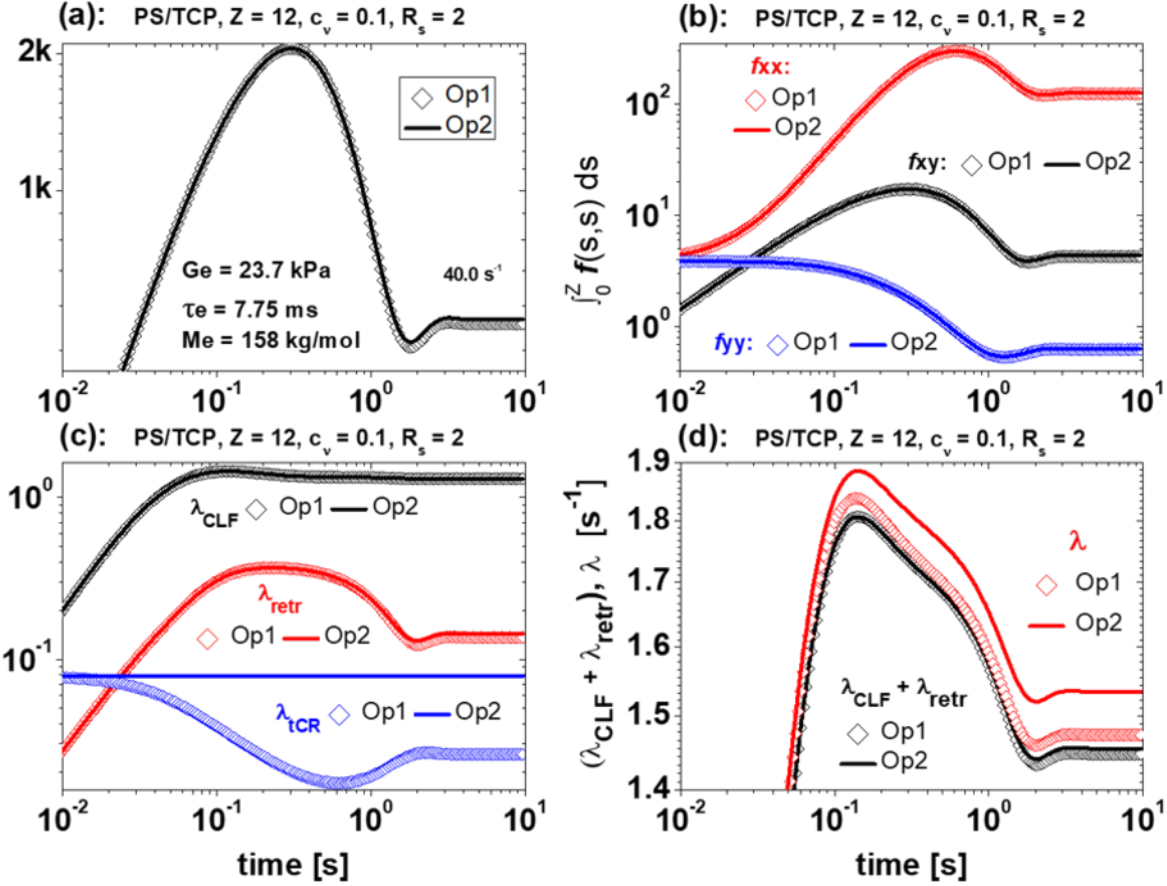

This is the author's peer reviewed, accepted manuscript. However, the online version of record will be different from this version once it has been copyedited and typeset.
PLEASE CITE THIS ARTICLE AS DOI: 10.1122/8.0000280

ACCEPTED MANUSCRIPT

Journal of Rheology

This is the author's peer reviewed, accepted manuscript. However, the online version of record will be different from this version once it has been copyedited and typeset.
PLEASE CITE THIS ARTICLE AS DOI: 10.1122/8.0000280

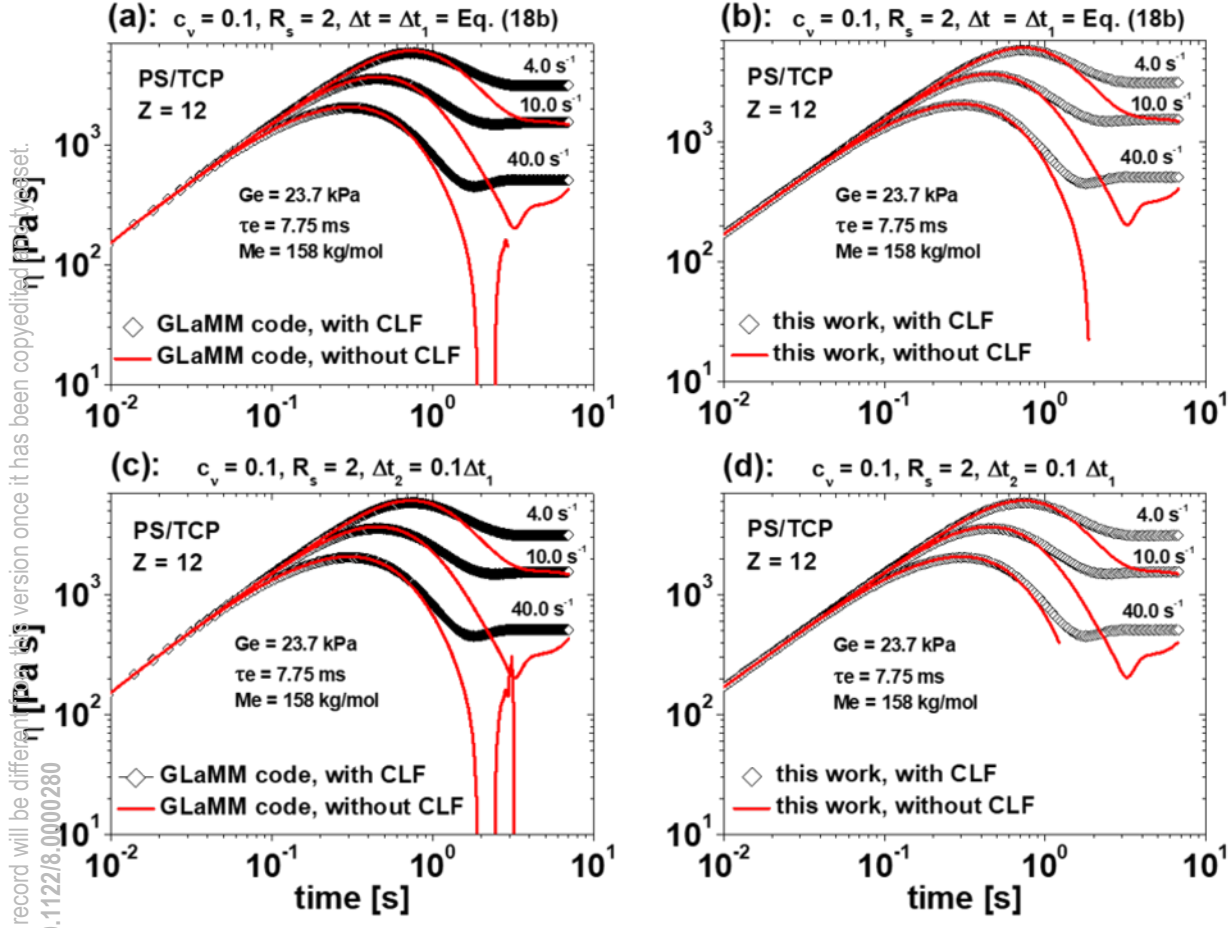

ACCEPTED MANUSCRIPT

Journal of Rheology

This is the author's peer reviewed, accepted manuscript. However, the online version of record will be different from this version once it has been copyedited and typeset.
PLEASE CITE THIS ARTICLE AS DOI: 10.1122/8.0000280

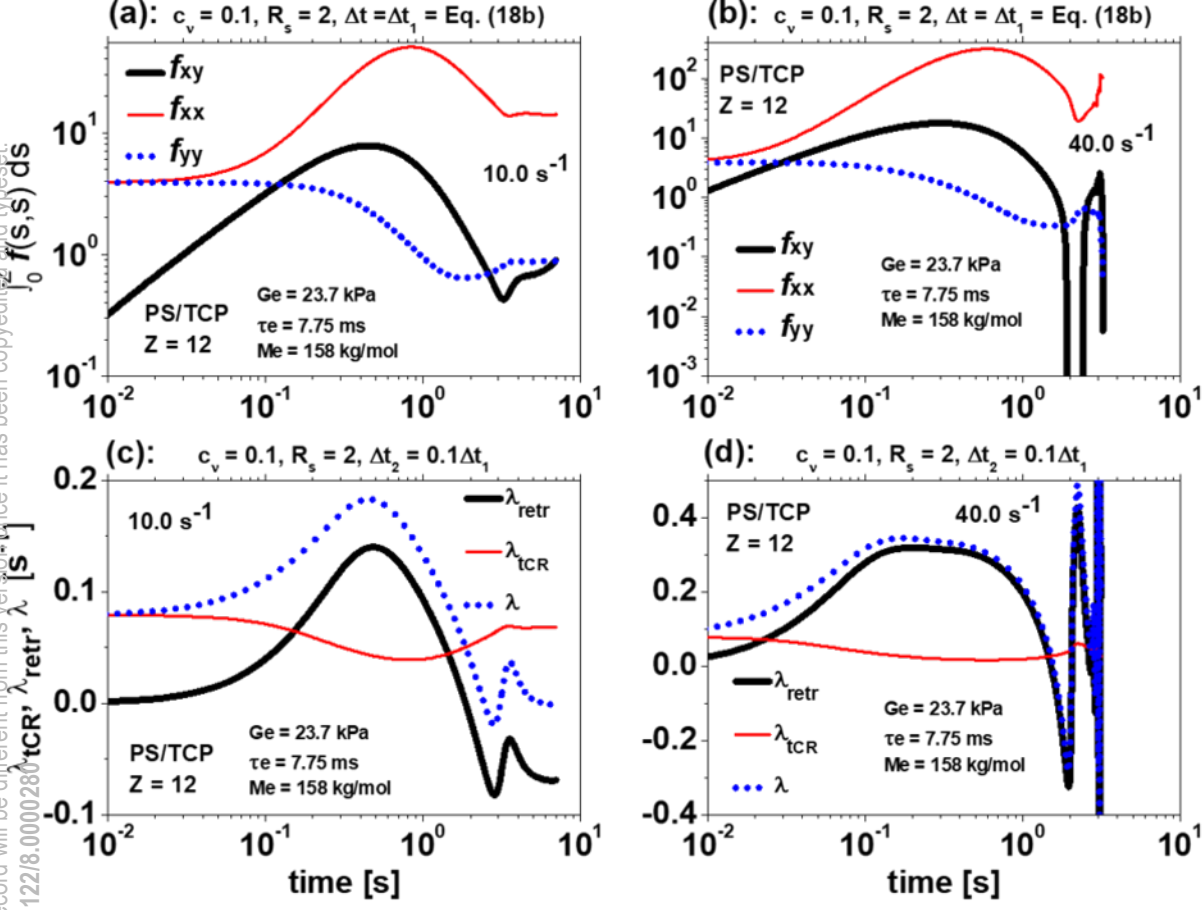

ACCEPTED MANUSCRIPT

Journal of Rheology

This is the author's peer reviewed, accepted manuscript. However, the online version of record will be different from this version once it has been copyedited and typeset.
PLEASE CITE THIS ARTICLE AS DOI: 10.1122/8.0000280

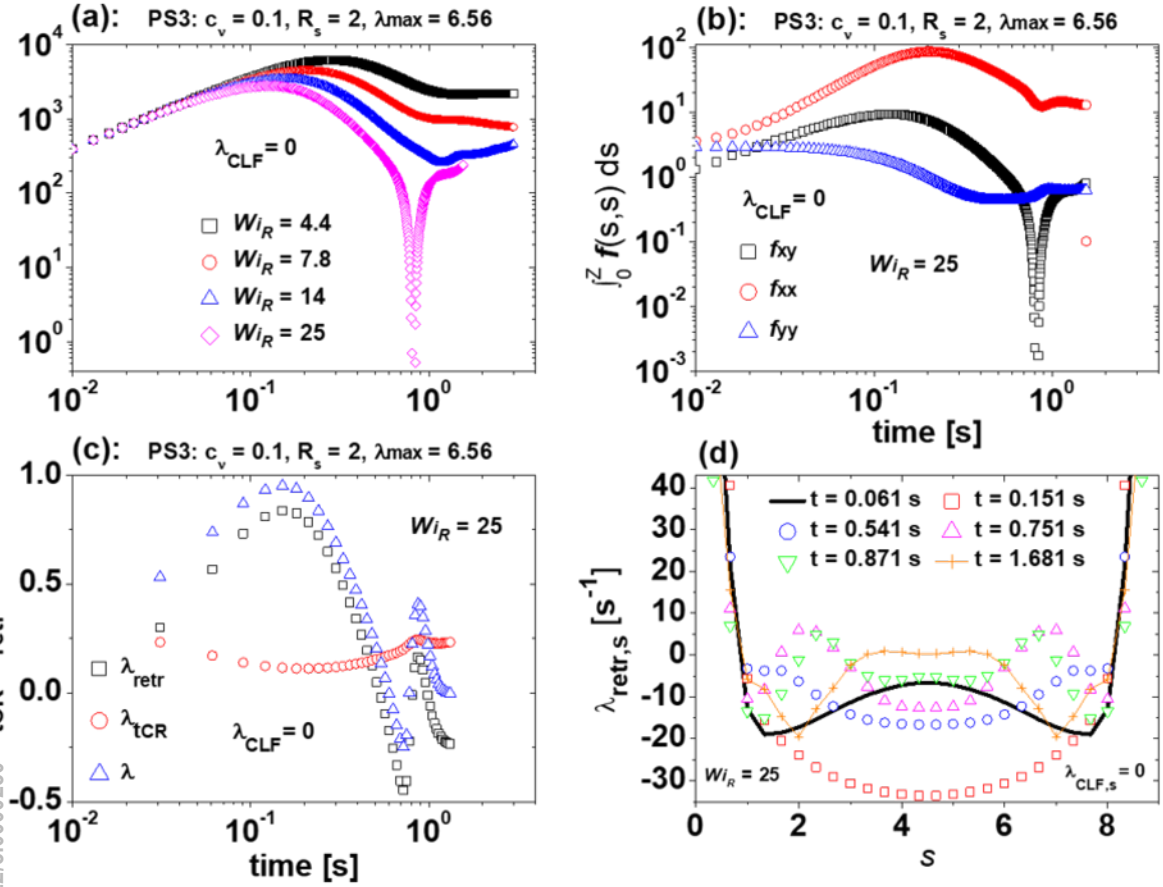

ACCEPTED MANUSCRIPT

Journal of Rheology

This is the author's peer reviewed, accepted manuscript. However, the online version of record will be different from this version once it has been copyedited and typeset.
PLEASE CITE THIS ARTICLE AS DOI: 10.1122/8.0000280

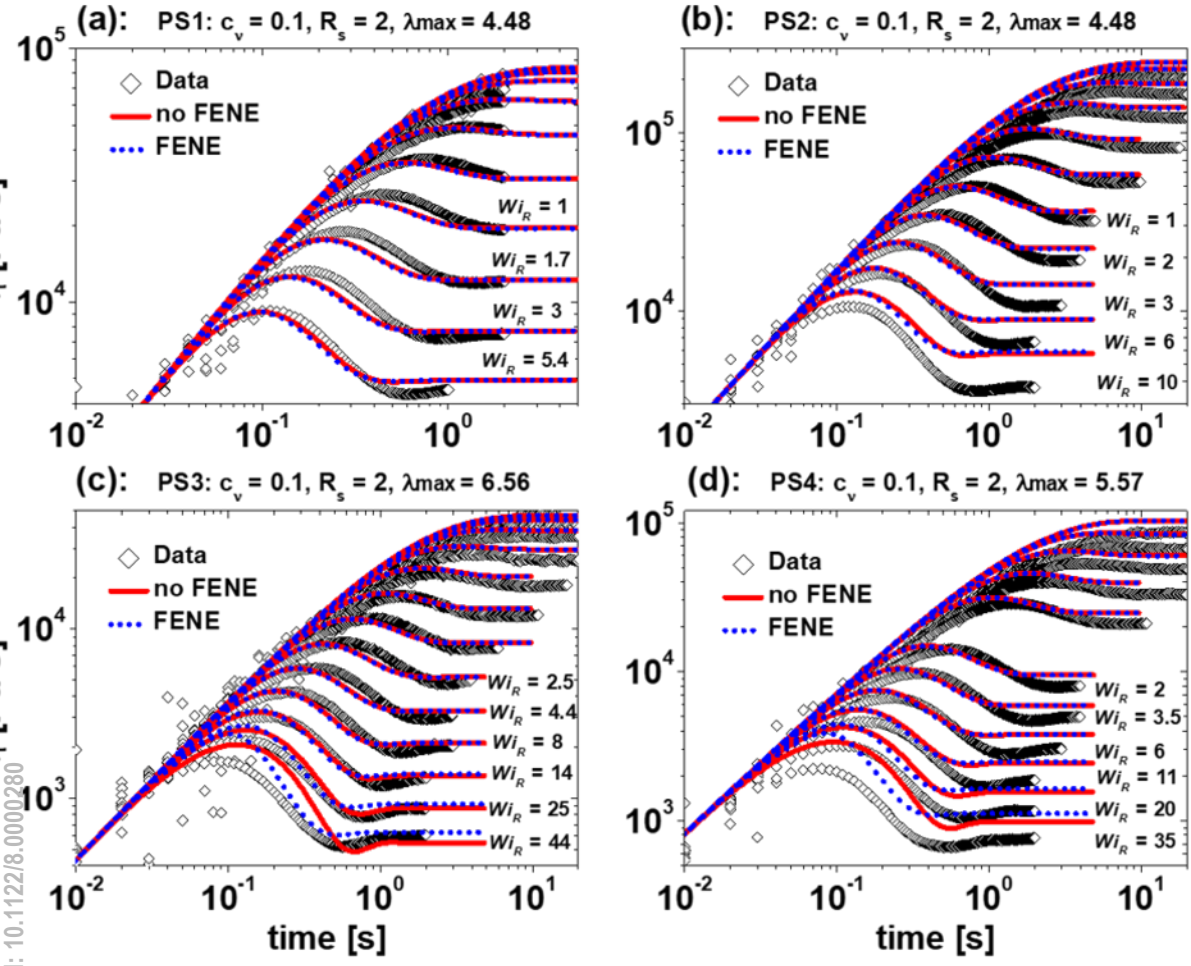

ACCEPTED MANUSCRIPT

Journal of Rheology

This is the author's peer reviewed, accepted manuscript. However, the online version of record will be different from this version once it has been copyedited and typeset.
PLEASE CITE THIS ARTICLE AS DOI: 10.1122/8.0000280

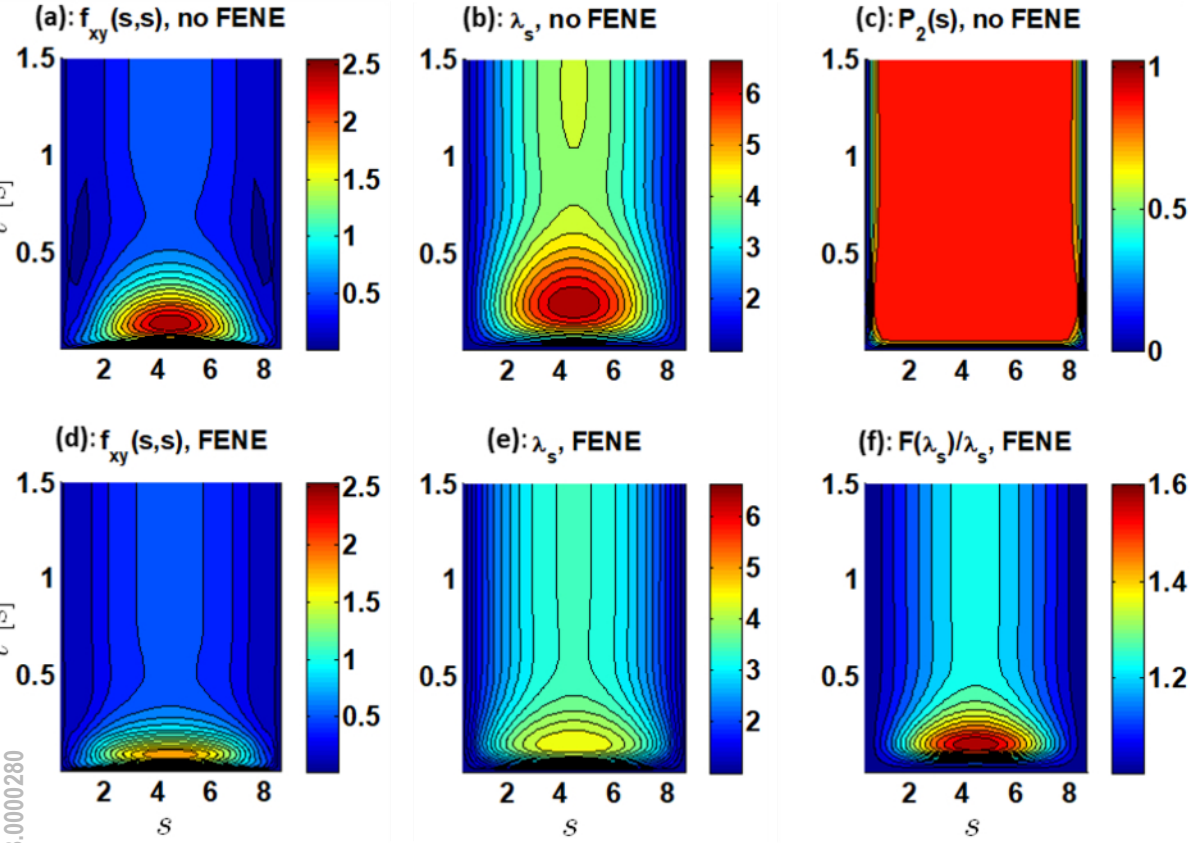

ACCEPTED MANUSCRIPT

Journal of Rheology

This is the author's peer reviewed, accepted manuscript. However, the online version of record will be different from this version once it has been copyedited and typeset.
PLEASE CITE THIS ARTICLE AS DOI: 10.1122/8.0000280

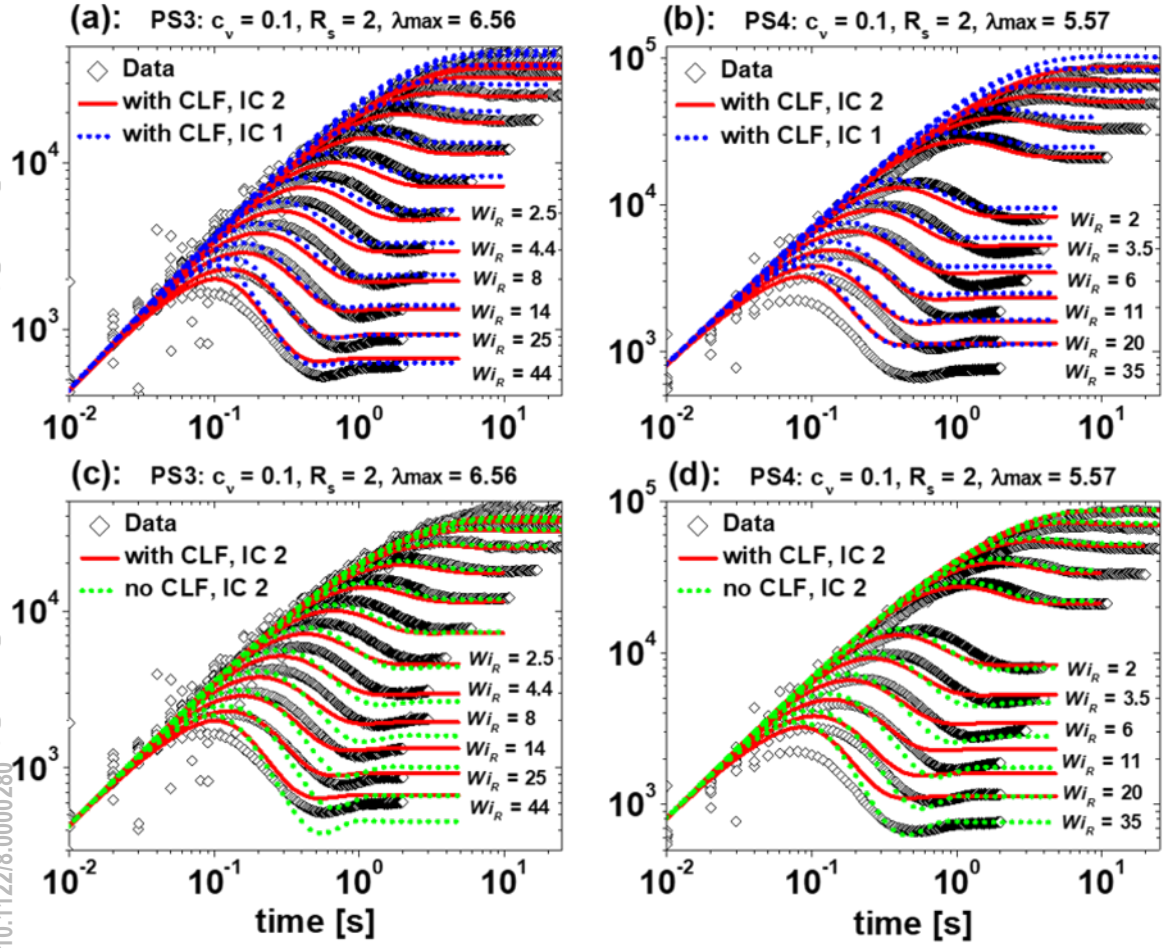

ACCEPTED MANUSCRIPT

Journal of Rheology

This is the author's peer reviewed, accepted manuscript. However, the online version of record will be different from this version once it has been copyedited and typeset.
PLEASE CITE THIS ARTICLE AS DOI: 10.1122/8.0000280

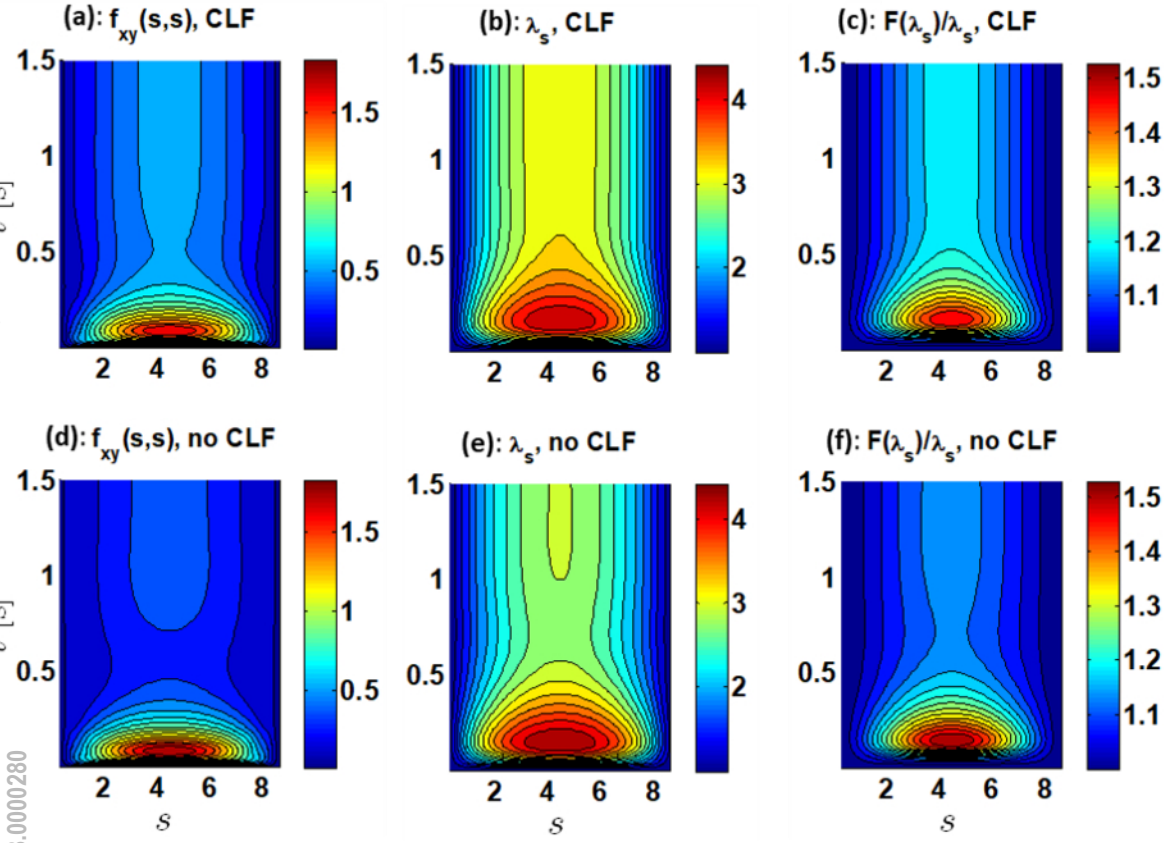

πάντα ῥεῖ

Journal of Rheology

ACCEPTED MANUSCRIPT

This is the author's peer reviewed, accepted manuscript. However, the online version of record will be different from this version once it has been copyedited and typeset.
PLEASE CITE THIS ARTICLE AS DOI: 10.1122/8.0000280

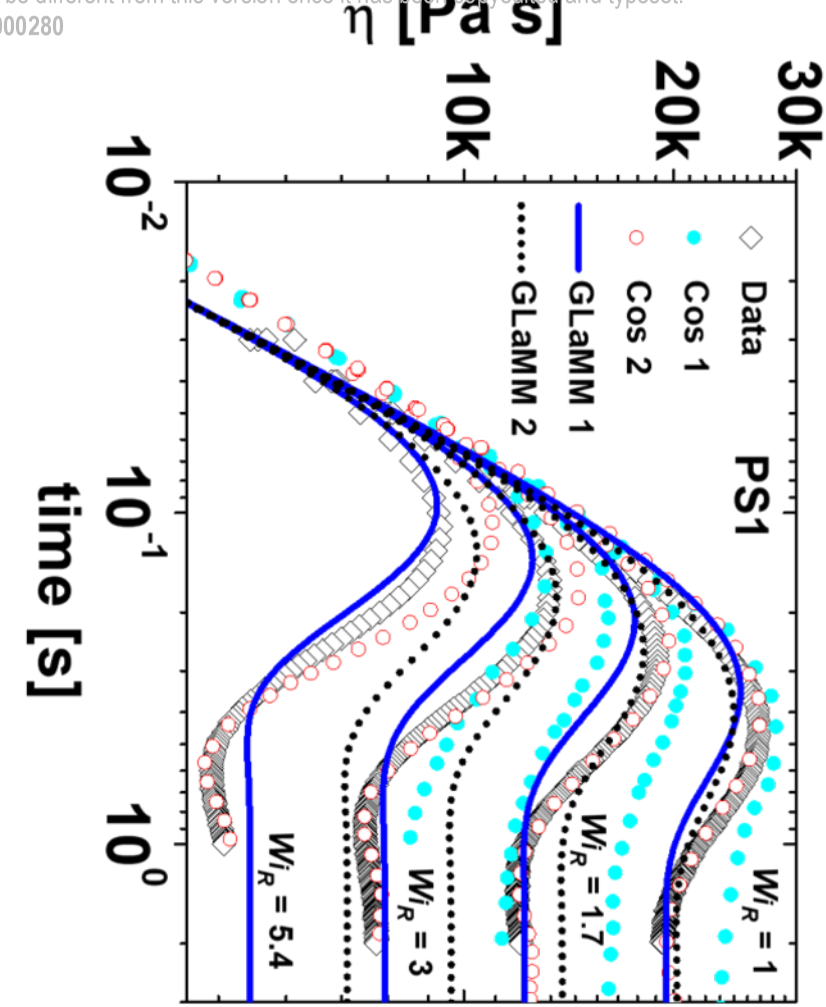

ACCEPTED MANUSCRIPT

Journal of Rheology

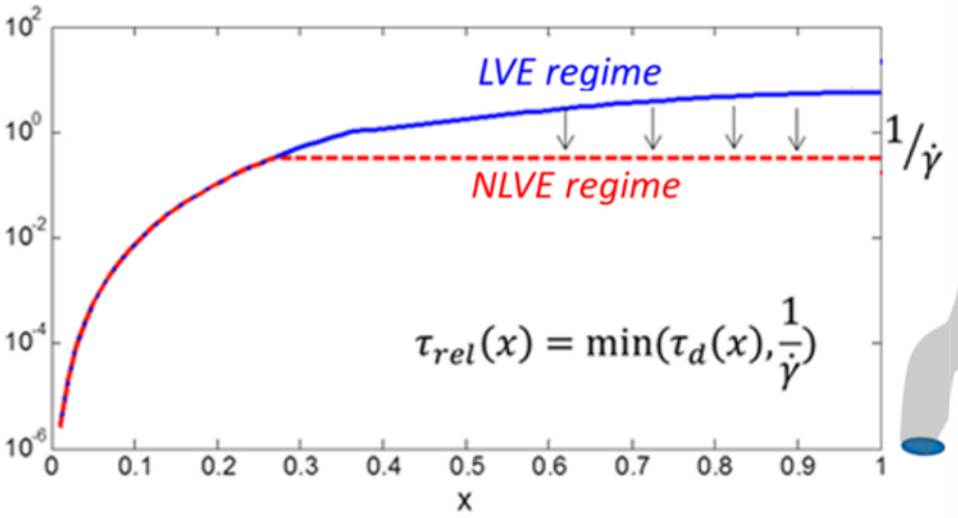

This is the author's peer reviewed, accepted manuscript. However, the online version of record will be different from this version once it has been copyedited and typeset.
PLEASE CITE THIS ARTICLE AS DOI: 10.1122/8.0000280

Journal of Rheology

ACCEPTED MANUSCRIPT

This is the author's peer reviewed, accepted manuscript. However, the online version of record will be different from this version once it has been copyedited and typeset.

PLEASE CITE THIS ARTICLE AS DOI: 10.1122/8.0000280

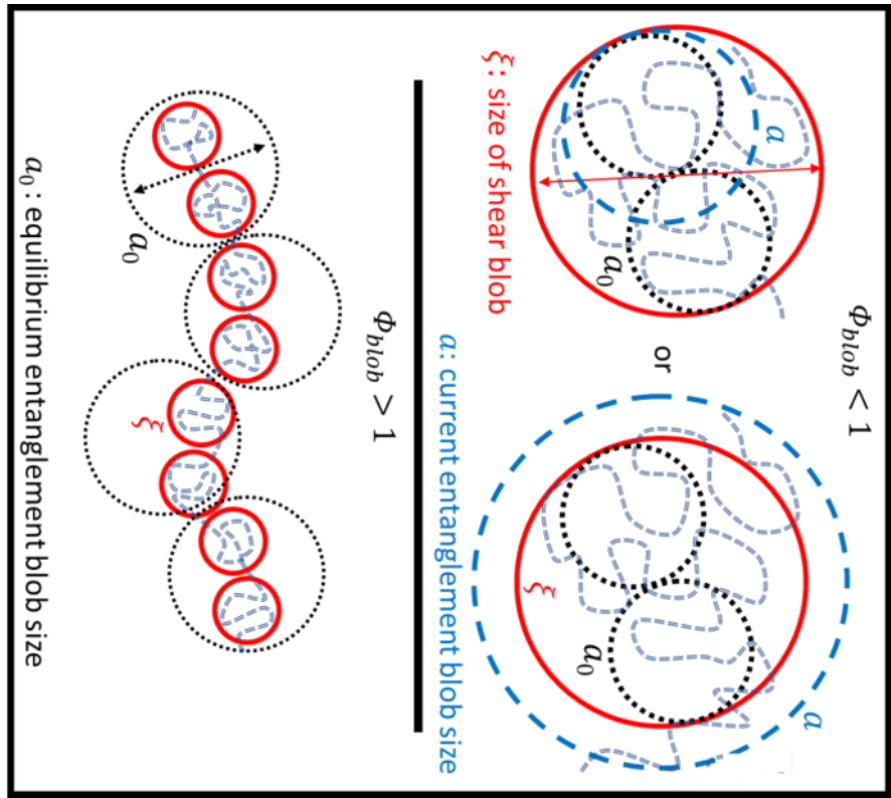

ACCEPTED MANUSCRIPT

Journal of Rheology

This is the author's peer reviewed, accepted manuscript. However, the online version of record will be different from this version once it has been copyedited and typeset.
PLEASE CITE THIS ARTICLE AS DOI: 10.1122/8.0000280